2-28-2018 4:45 PM

Examining Reverse Total Shoulder Arthroplasty Baseplate Fixation in Patients with E2-type Glenoid Erosion

Matthew D. Mahaffy, *The University of Western Ontario*

Supervisor: Johnson, James A., *The University of Western Ontario*

A thesis submitted in partial fulfillment of the requirements for the Master of Engineering Science degree in Biomedical Engineering

Abstract

Superior glenoid erosion of the shoulder joint is a result of humeral subluxation caused by rotator cuff tears, and can be addressed using implants, specifically reverse total shoulder arthroplasty. This thesis examined the regional variations of bone present in superiorly eroded glenoids, and using FEA, established a baseline for regular RTSA baseplate fixation and compared the effect of various baseplate geometries on implant fixation. The superiorly eroded glenoids demonstrated similar regional bone density variations as normal glenoids, and the superior and inferior regions of the glenoid demonstrated the densest and least dense cancellous bone, respectively. These regions also resulted in the most and least amounts of micromotion, respectively. The full-wedge and half-wedge baseplates resulted in more tangential micromotion, while the 6mm lateralized baseplate performed the worst overall. While the standard baseplate resulted in the best fixation outcomes, surgical limitations need to be accounted for when selecting the type of implant to be used.

Keywords

Reverse total shoulder arthroplasty, biomechanics, augmented implant, micromotion, bone density, E2 glenoid erosion

Co-Authorship Statement

Chapter 1: MD Mahaffy – sole author

Chapter 2: MD Mahaffy – study design, model generation, data collection, statistical analysis, wrote manuscript

N Knowles – study design

GS Athwal – study design, patient selection

JA Johnson – study design, reviewed manuscript

Chapter 3: MD Mahaffy – study design, data collection, statistical analysis, wrote manuscript

GDG Langohr – study design, reviewed manuscript

GS Athwal – study design

JA Johnson – study design, reviewed manuscript

Chapter 4: MD Mahaffy – study design, data collection, statistical analysis, wrote manuscript

GDG Langohr – study design

GS Athwal – study design

JA Johnson – study design, reviewed manuscript

Chapter 5: MD Mahaffy – sole author

Acknowledgments

I would like to begin by thanking my supervisor Dr. Jim Johnson for taking me on as a 4th year undergraduate, and providing the opportunity to continue research as a graduate student. Your knowledge and passion for orthopedic research has been an incredible motivation for this thesis, but I would like to thank you most of all for your patience with the progress of this work and for the confidence you have in all of your students. Were it not for you I often doubt that I would have accomplished what I have over the course of my Master's. I certainly could not have asked for a better supervisor.

Dr. George Athwal, thank you for your guidance and expertise. The passion you have for your work and the light-heartedness you bring to meetings truly allows for the best possible work and learning environment. I knew nothing about research before joining the lab for my 4th year thesis project and although difficult at first, I have been able to learn so much about shoulder orthopedics because of you.

To Dan Langohr, no words can express the impact you have on our lab, and I am grateful to have been able to work with you. I truly believe that you have an impact on everyone who passes through this lab. To the other students in the HULC lab, thank you for providing such a fun environment in which to work, and making the lab a great place to spend time.

Finally, thank you to my parents and my family away from home. It has not been easy living so far away from home and all the support and patience you have all had for me has allowed me to get to where I am today. There truly is no replacement for family.

Table of Contents

List of Tables

List of Figures

List of Appendices

Chapter 1

1 Introduction

OVERVIEW

This chapter serves to cover all the relevant background information regarding the anatomy of the glenohumeral joint, complications and uses of reverse total shoulder arthroplasty (RTSA), and examination of the available literature on glenoid erosion. At the end of this chapter the rationale, objectives, and hypothesis of this thesis are presented, as they pertain to RTSA and glenoid erosion.

1.1 Osseous Anatomy of the Shoulder

The shoulder is one of the most versatile joints in the body. It provides the arm with a large range of motion as well as allows for large amounts of force to be transmitted from the upper body to our arms and hands. The musculature surrounding this complex joint serves to maintain stability throughout its range of motion.

1.1.1 Bones

The three main bones found in the shoulder are the scapula, the humerus, and the clavicle (Figure 1-1). All bones are made up of cortical or cancellous bone tissue, and act as a structural base around which the rest of the body is built. The humerus and scapula form the glenouhumeral joint (GHJ) which is a shallow ball-and-socket joint that allows the arm to move through a large range of motion, while the clavicle and scapula form the acromioclavicular joint which acts as a secondary stabilizer for the scapula during arm movement.

The clavicle and humerus are both long bones and the scapula is a triangular, flat bone. Long bones are typically associated with strength and mobility within the body (*e.g.* The femur is the strongest bone in the body, while the humerus has the largest range of motion), while flat bones tend to be irregularly shaped and have large geometric variations based on their location and function. Since flat bones are very unique, they tend to have unique anatomic features, however long bones have 3 distinct regions. The diaphysis is the central portion of a long bone and contains primarily cortical bone. The metaphysis is a small transitional region between the epiphysis and diaphysis, which allows the bones to grow during childhood. The epiphysis is found at the ends of long bones, and is normally involved in joint articulation and muscle attachment. It contains cancellous bone, encased in a cortical shell as well as subchondral bone, which is the bone found underneath cartilage at joint articulations.[16]

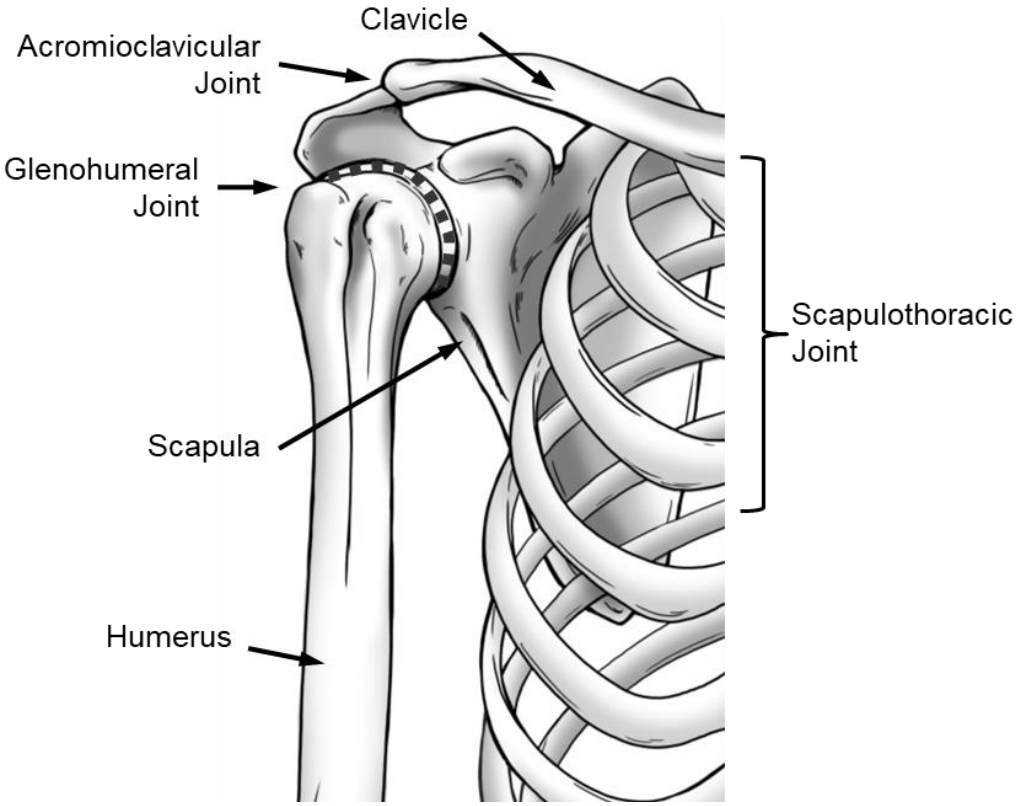

Figure 1-1 – Important osseous anatomy of the shoulder (retrieved from Langohr[26])

The shoulder is connected to the thorax via only the clavicle and certain musculature. The main shoulder joint, called the glenohumeral joint, is composed of the scapula and the humerus. More specifically, the proximal head of the humerus articulates with the glenoid of the scapula, creating a shallow ball-and-socket joint. Since shallow ball-and-socket joints are unstable, there is a large number of muscles and tendons that provide stabilization for the joint.

1.1.1.1 Humerus

As mentioned, the humerus is a long bone, and as such the diaphysis, metaphysis, and epiphysis each play key roles that allow the humerus to provide function to the musculoskeletal system. The GHJ involves articulation with the proximal end of the humerus, specifically, with the cartilage found on the head of the humerus which is located at the proximal epiphysis. Also, found in the proximal epiphyseal region of the humerus are the greater and lesser tubercles (Figure 1-2). These bony landmarks provide attachment sites for key stabilizer muscles in the shoulder. The greater tubercle provides attachments for 3 of the rotator cuff muscles, the supraspinatus, infraspinatus, and teres minor, and the lesser tubercle provides an attachment site for the 4th rotator cuff muscle, the subscapularis. The bicipital groove that runs between the tubercles is also important in humeral stabilization as the long tendon of the biceps runs through this groove and attaches to the scapula, providing a barrier from translation of the humerus and keeping it compressed against the scapula. The deltoid muscle, which provides function to the shoulder by controlling upper arm movement, also attaches to the humerus, but in the diaphyseal region.

1.1.1.2 Scapula

While the humerus performs a large range of circumduction and allows us to accomplish our tasks of daily living, the scapula is the base around which the GHJ joint is built. It is a flat, triangular bone, that sits on the posterior side of the thorax, and along with the clavicle, anchors the arm to the rest of the body (Figure 1-3). It contains attachment sites for the rotator cuff muscles, the triceps, biceps, back, neck, and a number of stabilizers muscles. The scapula glides in suspension over the thoracic cage with the help of all its attached muscles and can rotate to allow for stability and range of motion for a large variety of arm movements.

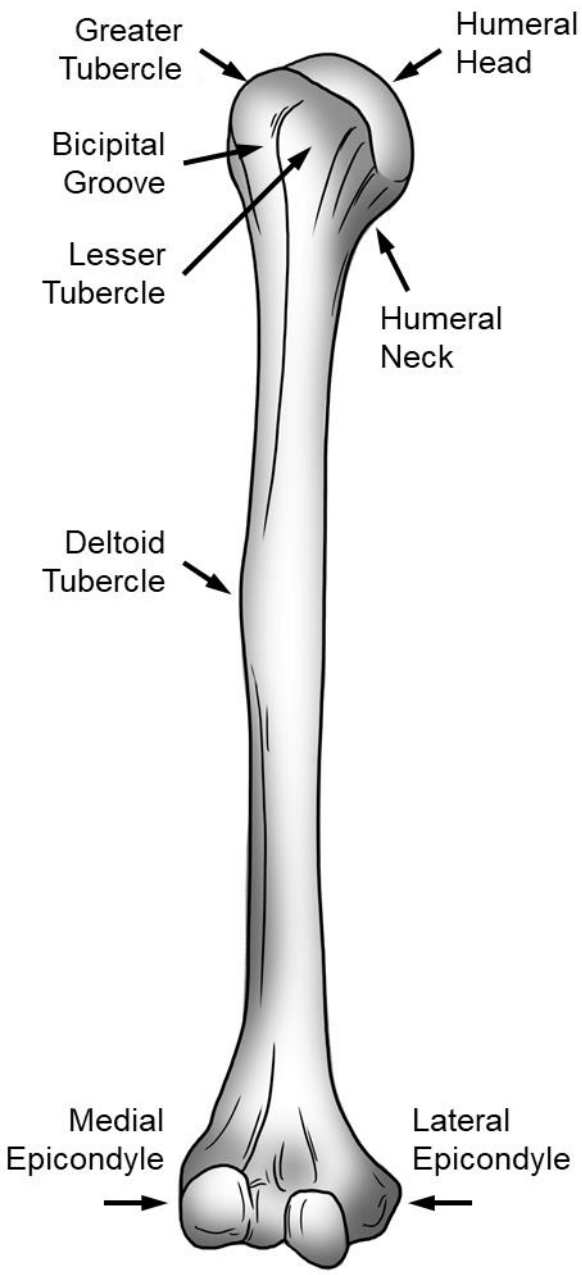

Figure 1-2 – Anatomic landmarks of the humerus (retrieved from Langohr[26])

The humeral head contains cartilaginous tissue which allows it to articulate with the glenoid of the scapula. The tubercles are important osseous landmarks or protrusions which serve as attachment sites for many of the shoulder's musculature.

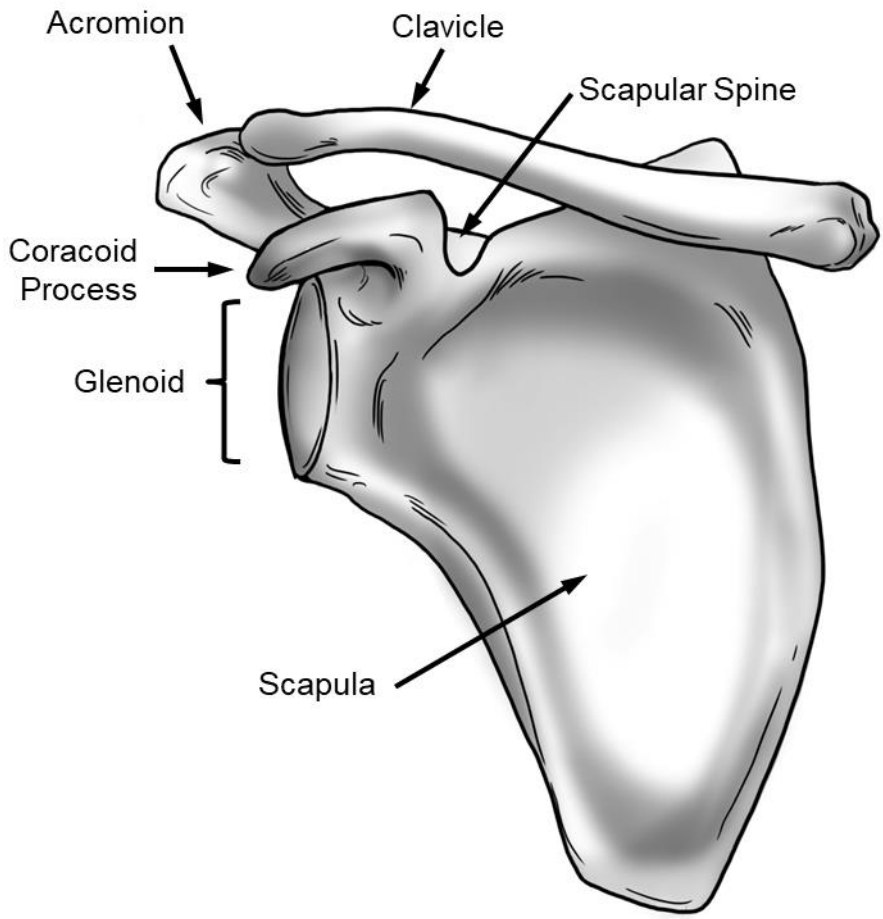

Figure 1-3 – Anatomic components of the scapula (retrieved from Langohr[26])

The acromion and coracoid process provide important attachment sites for ligamentous structures which stabilize the shoulder joint. However, the glenoid is the main articulation site for the glenohumeral joint.

Because of its complex functions, the scapula takes on a unique shape. Its large, flat surface provides space for the muscular attachments mentioned. It also has features that allow it to be useful in the GHJ. The medial border of the scapula, the inferior angle, and the scapular spine all play a role in muscular attachment. The coracoid process and the acromion contribute to muscular attachment and joint stability, physically preventing the humerus from translating. The glenoid fossa, or glenoid, is a shallow dish which and is the articular surface for the scapula in the GHJ. It is pear or oval shaped, longer vertically than horizontally to allow for rolling of the humerus within the joint, and also translation that occurs during abduction/adduction. As with any articular surface, the glenoid surface is covered in cartilage, but the rim of the glenoid is also surrounded by soft tissue called the glenoid labrum, which deepens the glenoid dish and is capable of providing suction on the humeral head to aid in stability. The glenoid fossa is connected to the scapula via the scapular neck, and within this scapular neck is where we find an important concentration of cancellous bone. This region of cancellous bone is referred to as the glenoid vault.

1.1.1.2.1 Morphology of the Glenoid

The relationship between the glenoid and the scapula is important for healthy joint mechanics. If any abnormalities or defects are present, it is possible that a person develops abnormal wear patterns in the joint and it has been shown that glenoid morphology can affect shoulder stability and health.[7,42] An important measure of normality in glenoids is its version and inclination (Figure 1-4). The scapula sits on the thoracic cage with the glenoid oriented anteriorly, or towards the front of the body. However, the glenoid is actually retroverted with respect to the scapula. A study by Churchill et al.[8] of 344 cadaveric scapulae of persons between the age of 20 and 30 found that the glenoid is actually slightly retroverted, or rear-facing, at around 1.23°, but can vary from 10° of anteversion to 10° of retroversion. They also found that glenoid inclination ranged from 6° of inferior tilt to 15.8° of superior tilt.[8] Although findings from other studies vary slightly, consensus in the literature is that the glenoid is more likely to be slightly retroverted and tilted superiorly. The shoulder has likely evolved this way to improve stability of the shoulder. The height of a healthy glenoid is longer than its width, and males are typically larger than females.[8]

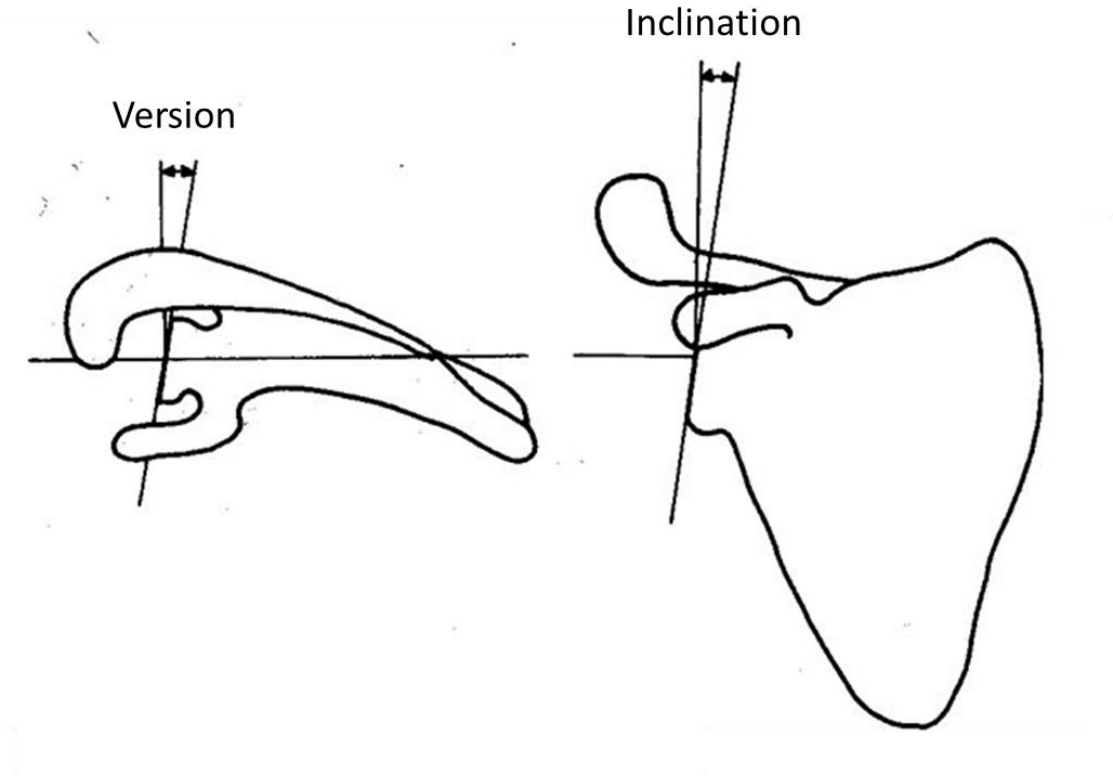

Figure 1-4 – Illustration demonstrating the measurement of glenoid version and inclination

The glenoid version (left) is measured from the sagittal plane to the plane of the glenoid, in the transverse plane. The glenoid inclination (right) is measured from the sagittal plane to the plane of the glenoid, in the coronal plane of the scapula (or scapular plane). (Image retrieved from an online slide deck.[2])

1.1.2 Rotator Cuff

The rotator cuff is a combination of muscles and ligaments that stabilize the shoulder joint and is crucial to maintaining a healthy shoulder over the course of our lifetime. The rotator cuff muscles include the supraspinatus, the infraspinatus, the subscapularis, and the teres minor (Figure 1-5). These muscles all serve to actively reduce, or maintain compression within the joint, and are incredibly important in joint stability. Wuelker et al.[43] found that reducing the force of the rotator cuff by 50% led to an increase in humeral translations of nearly 40% in a dynamic shoulder model. Other muscles that contribute to shoulder stability include teres major, latissimus dorsi, and pectoralis major.

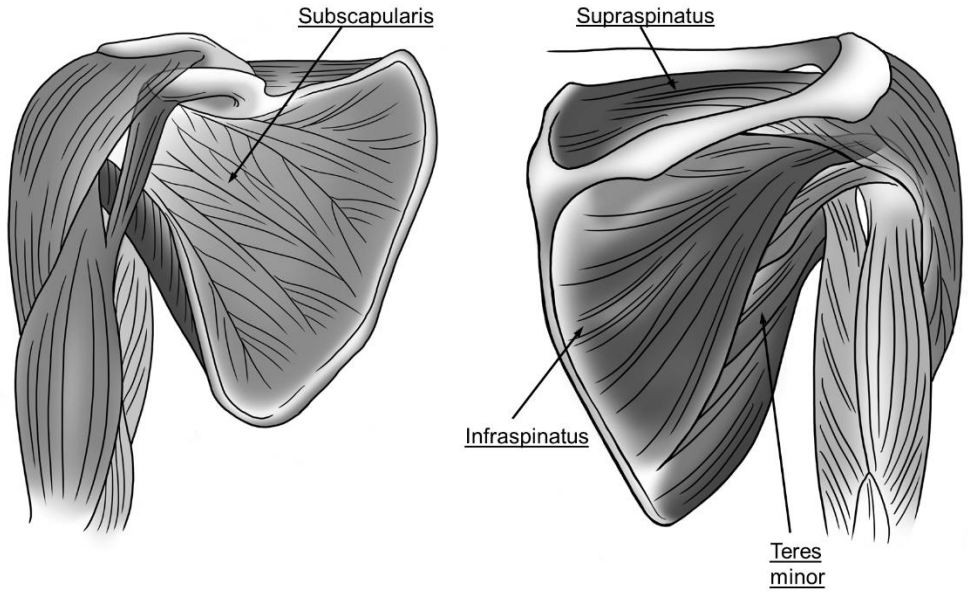

Figure 1-5 – Rotator cuff muscles (retrieved from Langohr[26])

The subscapularis, supraspinatus, infraspinatus, and teres minor are the four stabilizing muscles that are collectively referred to as the rotator cuff.

1.1.2.1 Rotator Cuff Arthropathy and Treatment

The rotator cuff may become damaged due to trauma, overuse, or bony deformities, and injury is more likely to result with an increase in age.[9,31,45] The extent of the damage, as well as the age, occupation, and lifestyle of the patient, are large factors in determining the type of treatment patients receive. While the term rotator cuff arthropathy may imply damage to any of the stabilizing structures, tears in the musculature, particularly the supraspinatus, are generally the main source of instability.[38,41] Damaged supraspinatus muscle fibers can lead to superior migration of the humeral head (Figure 1-6) which can lead to many complications such as nerve impingement, impingement of the supraspinatus muscle on the acromion, contact between the humerus and the acromion (which is a non-cartilaginous articulation and therefore leads to pain and osseous erosion), and irregular contact articulation between the humeral head and the glenoid fossa. Irregular articulation between bones damages cartilage and can potentially lead to osseous erosion.

Typically, small rotator cuff tears can be treated non-operatively, however when massive rotator cuff tears are present the treatment plan can vary greatly from patient to patient. Some tears are even considered irreparable. This may occur when the pathology of the injury is such that it is very likely to become a chronic issue, even in cases of smaller tears.[17] Non-operative treatment options include physical therapy and steroid injections, and they should always be attempted before proceeding with any surgical procedures. If rehabilitation does not provide significant pain relief, or should it fail to restore the patient's liveable range of motion, tendon repair is the next best option. This may include biceps tenotomy, suprascapular nerve release, or tendon and muscle transfers, all with the goal of either improving pain relief, shoulder range of motion, strength, or any combination of the three. The final option would be joint replacement. While joint replacement is typically used to address joint pain in patients with some form of arthritis, in the shoulder it can also be used to treat irreparable rotator cuff tears.[21]

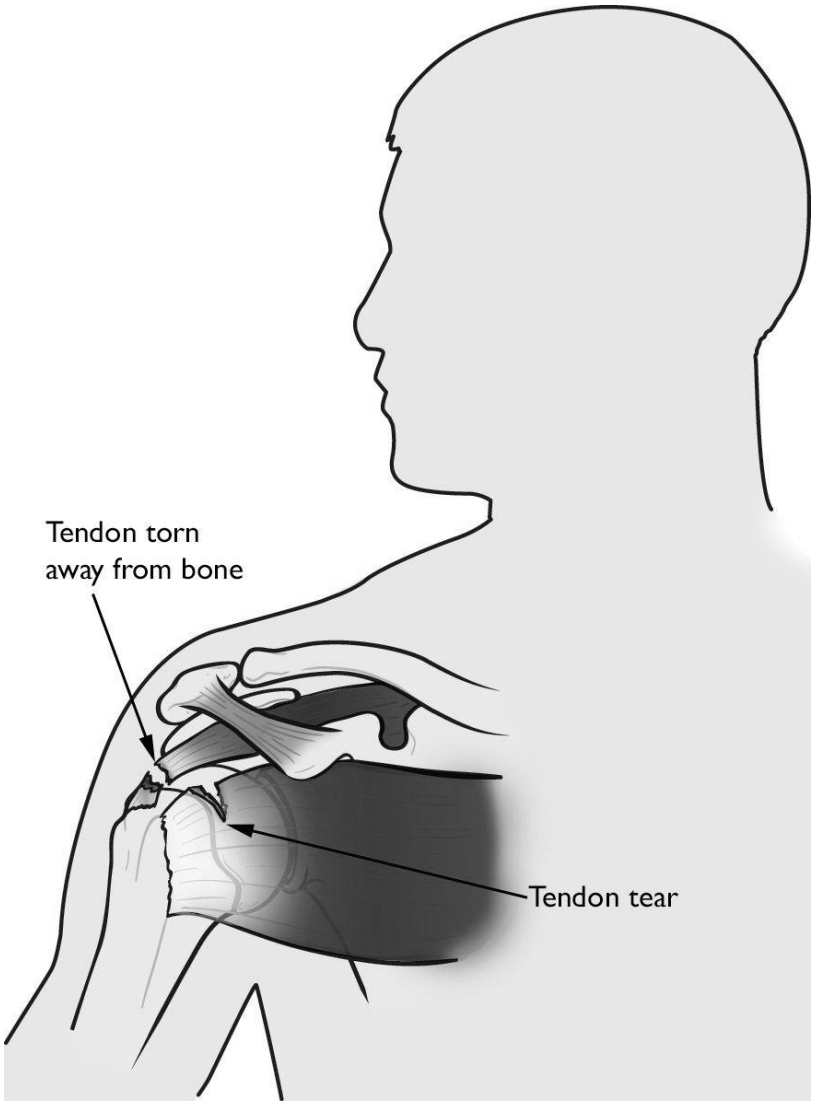

Figure 1-6 – Visualization of a rotator cuff tear

Tears in the tendon of the supraspinatus and the teres minor, both of which can lead to superior subluxation of the humeral head. (Image retrieved from the American Academy of Orthopaedic Surgeons information website).[46]

1.2 Shoulder Arthroplasty

Total shoulder arthroplasty, or TSA, is a surgical procedure involving the replacement of the articular surfaces of both the humeral head and the glenoid. It is typically required in patients who experience pain due to bone on bone contact. This occurs when the cartilage of the articular surface is worn, or damaged due to trauma. The resected humerus is replaced by a spherical, metal component, while a polyethylene insert is placed into the glenoid. Typically, this procedure succeeds in reducing pain, however patients with rotator cuff deficiencies continue to lack mobility in the shoulder leading to impaired daily living.

Reverse total shoulder arthroplasty (RTSA) addresses this issue by reversing the ball and socket relationship between the glenoid and the humerus, and by changing the anatomy of the joint to provide a mechanical advantage, increasing strength and range of motion (Figure 1-7).[30] By placing a spherical component on the glenoid, the center of rotation of the joint can be medialized relative to the native GHJ anatomy. This provides a larger moment arm upon which the deltoid may act. This moment arm allows the arm of the patient to be lifted more easily with less deltoid force due to mechanical advantage, compensating for loss of strength due to the rotator cuff tear.

RTSA is still a relatively new procedure and implant failure is a cause for concern. Implant loosening can occur with the glenoid baseplate due to medialization of the center of rotation of the joint as this can increase shear loading and moments. These can also be induced by improper implant placement or bony deformities and defects.

1.3 Glenoid Erosion and Shoulder Implants

Bony erosion can occur anywhere in the body, but it is particularly prevalent in joints and areas of inflammation. Patients suffering from rheumatoid arthritis and osteoarthritis are particularly susceptible to bone erosion.[13,35] Although it is normally reported as bone erosion, the true mechanism of bone loss is actually bone resorption. Osteoclasts and osteoblasts are types of cells that breakdown and create bone, respectively. Normal inflammation and damage in tissues leads to an increase in osteoclast activity so that bone

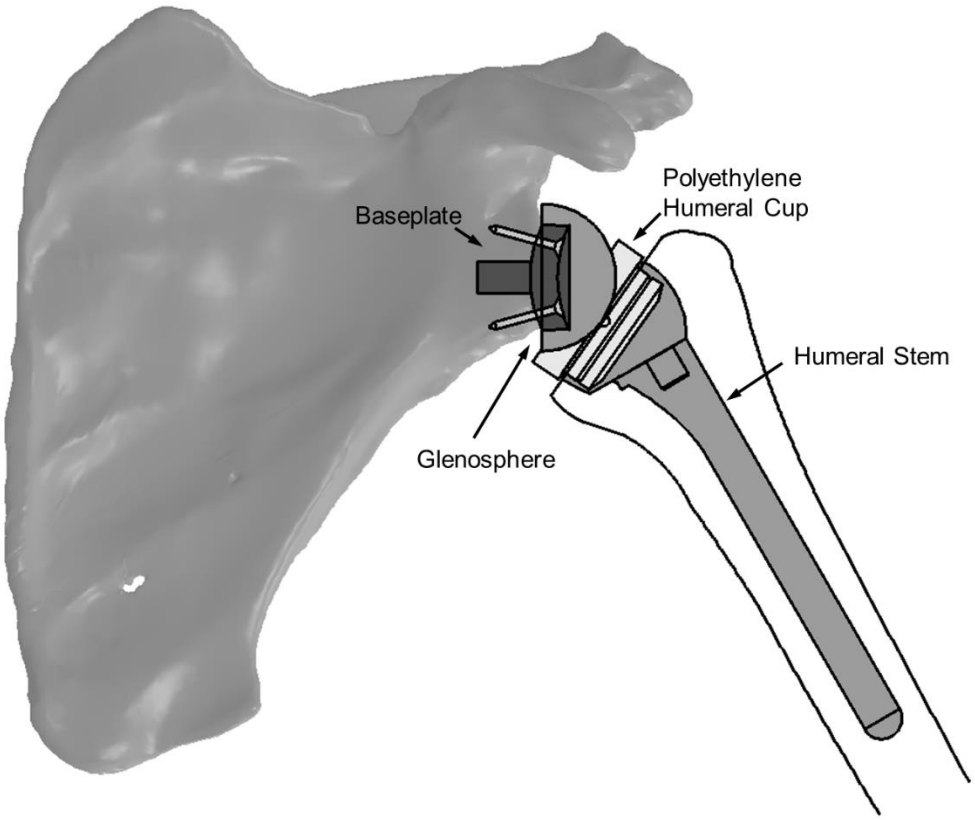

Figure 1-7 – Components of a reverse total shoulder arthroplasty prosthesis (retrieved from Langohr[26])

The humeral stem is cemented into the intermedullary canal of the humerus, which allows for fixation of the humeral cup. The baseplate (or metaglene) is fixed into the glenoid of the scapula via peripheral screws and a central peg, which is replaced with a central screw in some designs. The glenosphere fits onto the baseplate via a Morse taper, and medializes the center of rotation of the joint, providing shoulder function to patients with a non-functional rotator cuff.

repairing can occur. However, in cases of arthritis, osteoporosis, and similar diseases, osteoclasts outwork and outnumber osteoblasts. This results is an overall loss of bone in areas of high osteoclast concentration, and areas of high stress.[29]

As mentioned, osseous erosion is often a result of rotator cuff arthropathy. While sometimes unrelated to orthopaedics, literature on treatment of glenoid erosion is often associated with joint replacement. This is because joint replacement tends to be either the cause of, or the cure for erosion.

In shoulder hemi-arthroplasty, many factors can cause erosion. A study of 118 cases found that glenoid cysts, rheumatoid arthritis, loss of cartilage, and compromised rotator cuff muscles all led to higher risk of developing glenoid erosion.[20] They also found that implant positioning was an important factor affecting glenoid erosion, but implant size was not.[20] Since hemi-arthroplasty is a less invasive procedure, failure of hemi-arthroplasty typically requires revision surgery with either TSA or RTSA.[5,6] The consequences of this require that TSA and RTSA should be able to address any issues caused by hemi-arthroplasty while also addressing shoulder pain and dysfunction.

TSA is a potential solution to failed HA as it replaces the damaged glenoid surface, however TSA is only viable with an intact rotator cuff. TSA has been described as a solution to both anterior and posterior glenoid erosion, but often these solutions involve modifying the glenoid to accommodate the implant using techniques such as eccentric reaming or bone grafting.[27] While these methods may be customary, a main goal of orthopaedic surgery is to retain as much of the native bone as possible particularly, the glenoid vault bone.

If the rotator cuff is not intact and is irreparable, the only remaining option is RTSA. As noted above, the presence of a torn rotator cuff often leads to osseous erosion, and quite unique to RTSA in the presence of superior glenoid erosion. Although it is common, accounting for approximately 9% of glenoids in RTSA patients,[12] the literature on treatment of superior glenoid erosion is sparse. Even so, treatment must be administered and implants exist that attempt to address superior erosion while minimizing removal of bone or the necessity of performing bone grafts.

1.3.1 Types of Glenoid Erosion

In addition to superior glenoid erosion, there are other common types of erosion as well. An article titled "Classifications of glenoid dysplasia, glenoid bone loss and glenoid loosening: a review of the literature" by Jean[22] very nicely summarized different authors' classification of glenoid morphologies related to TSA and RTSA, and a number of these classification address the issue of glenoid erosion. Walch et al.[40] divided a cohort of 113 osteoarthritic shoulders into 3 categories. Type A glenoids which accounted for 59% of shoulders considered cases where the humeral head was centered on the glenoid, type B glenoids accounted for 32% of glenoids and related to posterior glenoid erosion due to humeral subluxation, and type C glenoids which accounted for 9% of the cohort was simply defined as any glenoids, with or without erosion, with more than 25° of retroversion. Each type is also often associated with a number indicating severity, with higher numbers indicating increasing severity (i.e. Type A2 is more sever than type A1). Habermeyer et al.[18] classified glenoids simply as Types 0 through 3 largely based on inferior tilt of the glenoid. A number of other authors describe glenoid erosion, wear, and implant related deformities as well,[1,25,28] and separately, Bigliani et al.[4] classified anterior rim defects as they more commonly relate to shoulder dislocation and traumatic fractures. Finally, Sirveaux et al.[36] studied 80 shoulders treated for massive irreparable cuff tears, and requiring RTSA, and loosely classified the glenoids based on superior erosion as shown in Figure 1-8.

1.3.2 Standard RTSA Treatments for Glenoid Erosion

Gilot[14] describes the methods used to address glenoid erosion using RTSA, including the using of bone grafting, eccentric or asymmetric reaming, and augmented implants. Asymmetric reaming involves reaming the glenoid medially to the depth of the erosion. This tactic has the advantage of simplicity. There is no extra monetary cost for the procedure and the surgery time is only slightly longer. However, the larger loss of bone and medialization of the joint can lead to complications. These include higher likelihood of scapular impingement, less contact area for implant fixation, and shorter penetration depths for the screws and central peg, which can all lead to implant failure.

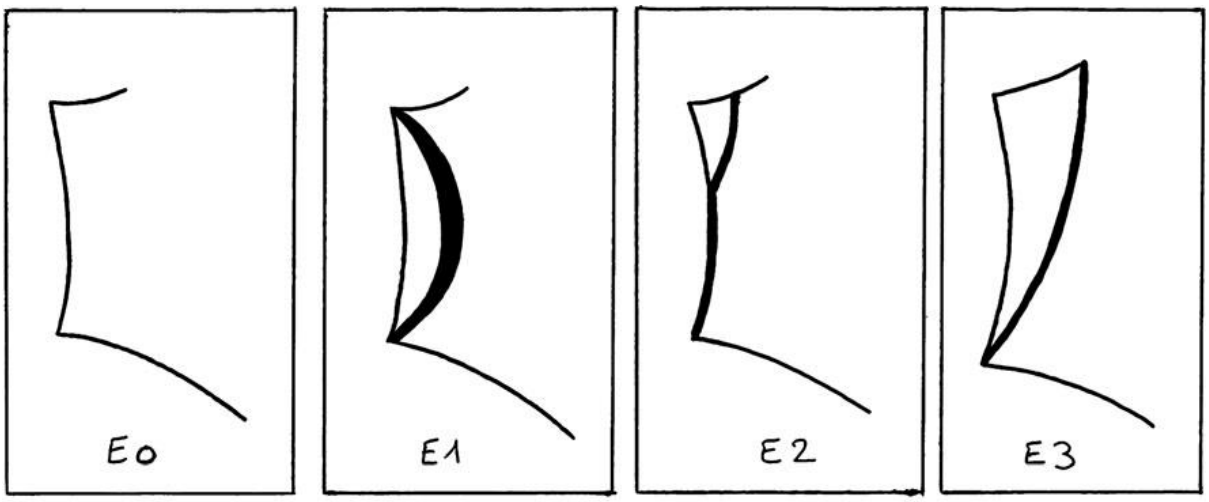

Figure 1-8 - E-Type glenoid classifications for shoulders with humeral subluxation due to cuff tear arthropathy, as classified by Sirveaux et al. (Image retrieved from Sirveaux et al.[36])

E0 *- Humeral subluxation without the presence of glenoid erosion*
E1 *-Slight humeral subluxation with global/centered glenoid erosion*
E2 *- Superior humeral subluxation with erosion of the glenoid not extending as far as the inferior glenoid rim*
E3 *- Superior glenoid erosion with little or no remaining articular bone*

Bone grafting is used for eroded glenoids that cannot afford to loss much more bone stock or glenoids where less than 80% of the baseplate is supported by glenoid bone. It increases the complexity of the procedure but allows the surgeon flexibility in changing the morphology of the glenoid. While many studies report successful integration of the bone graft, long term results are unsatisfactory or unknown with regards to RTSA, and implant loosening still occurs. Jones et al.[23] found that while augmented RTSA baseplates and bone-grafting both provided improved pain and function, 14.6% of bone grafts suffered from complications, and patients receiving bone grafts had a higher rate of scapular notching. Follow up for this study ranged from approximately 2 to 4 years. Steinmann and Cofield[37] reported 11% of bone-grafts with TSA implants were loose within 5 years, but a recent study by Ernstbrunner et al.[10] showed that even with 23% graft resorption and 30% scapular notching, baseplate fixation from 2 to 6 years follow up was not deemed to be at risk of loosening. The variation in success of bone grafting is apparent, and perhaps reveals

that its use remains situational, rather than a consistently successful method of treating glenoid erosions and defects.

1.3.3 Augmented RTSA Implants

Implants that address bony erosion are typically referred to as augmented implants and commercially available implants do exist (Figure 1-9). Exactech (Gainesville, Florida, US) offers a 10° superior augmented baseplate as well as an 18° posterior augmented baseplate and a 14.4°/7.7° superior/posterior augmented baseplate. They are oblong rather than circular like most baseplates, and the cage structured peg is located superiorly on the baseplate. Wright Medical Tornier (Warsaw, Indiana, US) offers a few different options. They offer a 35° half wedge augment, meaning the wedge portion of the implant covers half the implant while the other half remains flat, and a 15° full wedge implant. The augmented portion of these implants is made of a porous metal. This porous metal also covers the central peg of these implants. Biotechni (La Ciotat, France) offers a baseplate with 10° of superior inclination, but for the purpose of reducing scapular impingement of the humeral cup, rather than addressing glenoid deformities.

1.4 Finite Element Modeling of the Shoulder

Finite element analysis (FEA) can serve as a cost-effective way of testing orthopaedic implants without using physical resources such as cadavers, bone foams, implants, etc. It can also serve as validation for existing research, or be used in planning physical experiments. Finite element models are used to calculate stresses (mechanical, thermal, etc.) and strains in a material. Knowing these stresses allow us to make design decisions based on results such as high stress concentrations, localized contact pressure, and failure mechanisms.

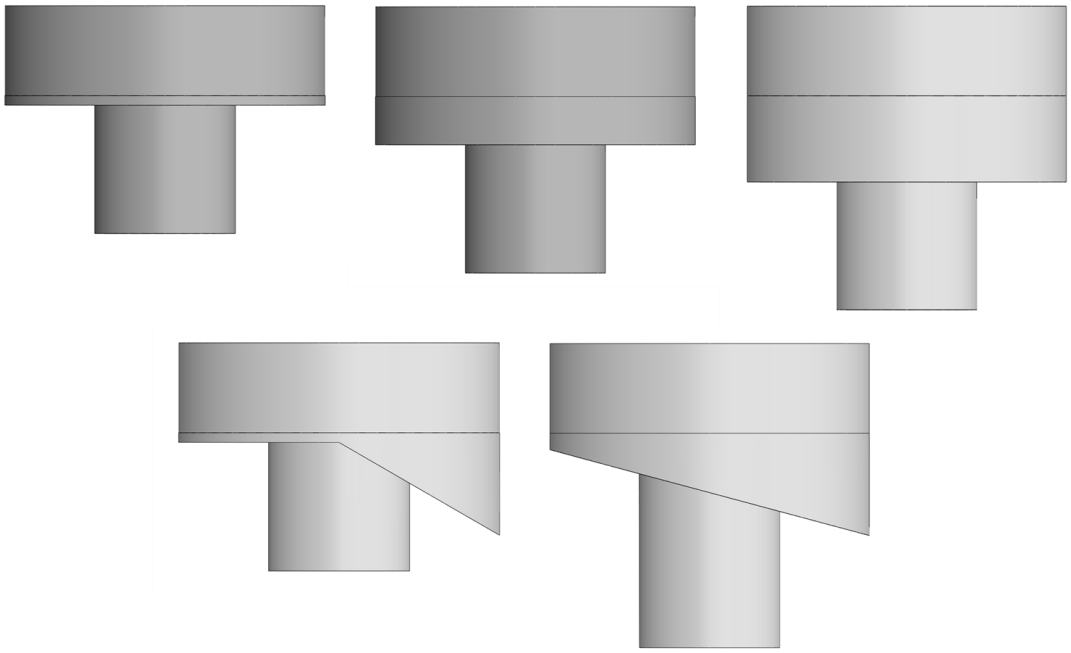

Figure 1-9 – Simplified geometry of augmented glenoid baseplates

While certain baseplates (as shown in the bottom row), provide changes in geometry to address glenoid erosion, others (top middle and right) simply aim to increase lateralization of the joint center of rotation to counteract the medialization of the joint required during reaming of the glenoid.

FEA functions by taking the object of study and rendering it into a finite number of elements using basic geometric shapes. These shapes can be two dimensional (2D) or three dimensional (3D) depending on the analysis being performed. Each of these individual elements are composed of nodes, which are connected to neighbouring elements via vertices and edges which act as the boundary for that element (Figure 1-10). When performing FEA on a model, the user determines many parameters including applicable loads and constraints, element size, and contact mechanics. Material properties of bone are typically heterogeneous,[44] but can be modeled by varying the spatial stiffness of bone using CT data. Due to the contact mechanics between bone and implant FEA of bone may require a non-linear model. In a non-linear model, the FEA software applies all the loading, boundary, contact, etc., conditions and iterates through equilibrium equations until the force required to balance the internal loads is sufficiently small. However, this iteration of equilibrium equations is only present in implicit, static models, which exclude the effect of mass inertia. Since all parameters are user defined there is always a possibility that the

model does not entirely represent the complexity of a real scenario and it is up to the user to ensure that results are reasonable.

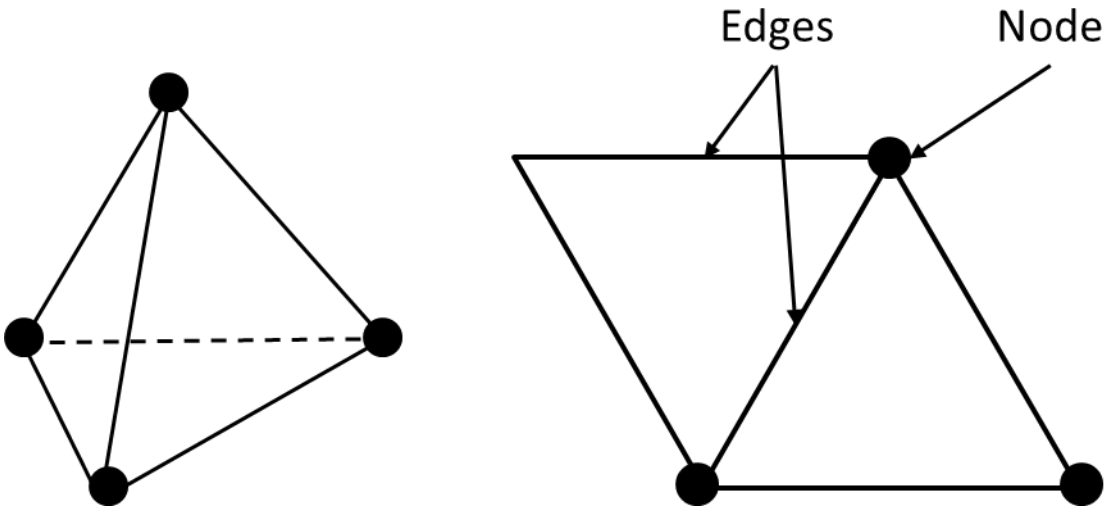

Figure 1-10 – Components of a finite tetrahedral element

A linear tetrahedral element (left) contains 4 nodes, 4 faces, and 6 vertices. Multiple elements are used to discretize simple and complex 3D structures.

Since models can be varied in many ways, multiple studies can be performed with the only expenses being computational run time and cost of the software license. However, in orthopaedics this can be more effective than cadaveric testing. It can provide more testing in a shorter time frame, and can help to potentially reduce or eliminate unnecessary experimental studies at later stages, saving on resources. In the shoulder, studies have been done to examine bone stress, implant stress, implant wear, joint biomechanics, as well as play a role in surgical planning and overall can lead to improved patient treatment.

1.4.1 FEA of Shoulder Implants

The applications of FEA in RTSA can be very useful due to the shoulder's complexity. The scapula is one of the most abnormally shaped bones in the human body, having no axes or planes of symmetry, nor is it able to be easily simplified into recognizable geometry (the long bones of the body for example can often be looked at as cylinders with spherical heads). The more complex the geometry, the more difficult it is to estimate stresses using first-order calculations. It also allows us to test implant designs quickly and efficiently. The

same specimen can be tested multiple times with different preparation, implants, and surgical approaches.

FEA studies involving shoulder arthroplasty dates back as far as the 1980s. Orr et al.[32] were among the first when analyzing the stress involved in the glenoid in TSA. Since then, the intricacy and availability of finite element software packages have increased and FEA studies have become more prevalent. This has lead to the ability to perform FEA studies for specific pathologies such as cuff tear arthropathy and glenoid erosion.

Terrier at al.[38] performed a finite element study on the importance of the supraspinatus in shoulder stability and strength. They found that without the supraspinatus, the humerus translated higher than normal within the GHJ and the contact point on the glenoid was more eccentric. This combination of altered joint mechanics can lead to abnormal articulation and erosion of the humerus or glenoid. They also reported that a lack of supraspinatus resulted in higher resultant muscle and joint forces, as well as superior migration of the humeral head on the glenoid.[38]

Finite element models can also be validated by experimental models. Virani et al.[39] examined the contact mechanics between the glenoid components of RTSA and bone using biomechanical and finite element models. They found a strong correlation between the results of the experimental testing and FEA. Hermida et al.,[19] on the other hand, studied the treatments mentioned in Section 1.3.1, solely using FEA with regards to posterior erosion for TSA, in an arthritic and normal scapula, concluding that TSA can be addressed using augmented implants in arthritic patients.

While to our knowledge very little amounts of literature currently exists on augmented RTSA models for glenoid erosion,[23,33] some early experimental studies using simple approaches do exist. In an experimental study by Roche et al.,[33] superior glenoid erosions were manually created in anatomically correct bone foam models, and they found no difference in fixation between reaming techniques or augmented implants over 10,000 cycles of simulated shoulder motion. The 10,000 cycles protocol was justified as being the amount of cycles involved during the crucial initial period where bony ingrowth and implant fixation occurs, but a much larger number of cycles can be simulated in a shorter

amount of time using FEA to determine long term implant outcomes. The bone foam materials are also typically homogeneous, which is inconsistent with bone which is highly anisotropic.

1.5 Motivation

As the body ages, it loses its ability to repair itself quickly, leading to breakdown of bones and joint, requiring the use of joint replacements. Although no statistics were available pertaining to Canadian shoulder arthroplasty, Schairer et al.[34] estimated that RTSA accounted for one third of all shoulder arthroplasties in the United States in 2011. Projections made by Statistics Canada[15] estimate the population aged >65 years to increase to nearly 25% by 2030 thereby increasing the potential number of shoulder joint replacements. RTSA is relatively new in the field of joint replacement, dating back to the 1970s,[24] and as such there are still complications preventing long-term success of RTSA.

Screw fixation, baseplate loosening and scapular notching are some of the main mechanical issues regarding RTSA.[3,11,30] However these issues have an important factor in common: quality of the osseous foundation. Joint arthritis has negative consequences on the quality of articular bone, therefore obtaining adequate implant fixation can be challenging. Frankle et al.[12] found that 37.5% of RTSA glenoids contained some level of osseous defect, and of those approximately 9% were superior glenoid erosion.

While superior glenoid erosion was only the second most common type of erosion found,[12] it is unique in that it primarily occurs due to rotator cuff tears, and humeral subluxation. Since the primary indication for RTSA is massive rotator cuff tears, the difficulties of implant fixation for superior glenoid erosion need to be addressed by RTSA.

Techniques have been described which attempt to address glenoid erosion, and commercially available implants can be used.[14] Unfortunately, the success of these implants and techniques, as well as the rationale behind there design, has been seldom discussed. Understanding the challenging osseous architecture involved in superior glenoid erosion may allow for appropriate implant design decisions to be made. It may also reveal

some insight into general mechanisms of glenoid erosions and glenoid component failure in RTSA.

1.6 Objectives and Hypothesis

Shoulder mobility is extremely important in determining the quality of day-to-day life, and having implants available to address a number of shoulder complications is necessary. However, poor understanding of the causes and effects of erosion may lead to poor implant designs, which can have drastic effects on a patient's wellbeing, putting them at an increased risk for further health complications. The objective of this thesis was therefore to expand the orthopaedic community's understanding of osseous erosion as it pertains to shoulder implant design and fixation.

This thesis consists of 3 studies as given in Chapter 2, 3 and 4. The specific objectives of this thesis are to:

Ch2: Quantify the bone density of the E2-type glenoid in various regions, at various depths. The regional variations of cortical and cancellous bone density will be quantified by the region of the glenoid in which the bone is found, as well as the depth within the glenoid at which the bone is found. A secondary objective was to determine the volume ratio of cortical to cancellous bone in each region.

Ch3: Establish a baseline for RTSA baseplate fixation in patient's with E2 glenoids using standard RTSA guidelines (*i.e.* in the absence of any special techniques), and examine the ability of a standard baseplate to transfer forces from the implant to the bone.

Ch4: Examine the fixation of several augmented implant designs and analyze potential design factors affecting fixation, including implant geometry and baseplate-bone load transfer area.

The respective hypothesis for each of these objectives is as follows:

Ch2: Regions of the E2-type erosion will contain denser bone as a result of increased stress-induced bone remodeling, however it will contain a lower volume of cancellous bone due to the intensity of the stresses. A shift of the joint articulation due to humeral subluxation

may also cause decreased-bone response in areas opposite of the erosion site, therefore resulting in less dense bone. At the erosion site, bone density will also likely be affected at a further depth.

Ch3: A standard RTSA baseplate will be able to achieve good fixation due to requirements of standard RTSA procedures (such as full baseplate backside contact and neutral implant inclination). Higher shear loads are expected to cause more micromotion. Load transfer area should be acceptable due to full backside contact and neutral implant inclination requirements.

Ch4: Baseplates with backside geometries at inclinations parallel or near parallel to the load vector will result in large shearing or tangential motion, while implants with more lateralized joint centers of rotation will result in larger amounts of liftoff from the bone. As a result, any implants that approach either of these undesired extremes will also suffer from poor load transfer mechanics from the baseplate to the bone.

1.7 Thesis Overview

To begin, Chapter 2 focuses on examining the morphology and density of patients with E2-type glenoids. This consists of examining the anterior, inferior, posterior and superior regions of the glenoid, up to a depth of 10mm into the glenoid. Using patient data, trends for locations of greater and lesser bone densities will be established, as well as any significant differences between any of the regions of interest. The results will be related to the visible geometry of the E2-type erosion. Next, Chapter 3 will use a subset of the patient data from Chapter 2 to examine the fixation of a standard, simplified RTSA baseplate. The baseplate will not model screw fixation in the interest of analyzing the effect of baseplate geometry. Relative micromotion between the baseplate and the bone will be examined under quasi-physiologic loads, and load transfer area between the baseplate and the implant will be recorded. Chapter 4, employs the same subset of patient data and will be used to examine the baseplate-bone micromotion of a full-wedge, half-wedge, 3mm lateralized, and 6mm lateralized implant as they compare to each other, and to the standard baseplate that was used in Chapter 3. Finally, Chapter 5 will summarize the results of the previous chapters and attempt to establish potential links between the quality of the osseous

foundation in E2 glenoids and the positive and negative outcomes of the tested implant designs. It will also be used to critically analyze the successes and failures of these studies, and to suggest future directions for this work to be expanded upon.

1.8 References

1. Antuna SA, Sperling JW, Cofield RH, Rowland CM. Glenoid revision surgery after total shoulder arthroplasty. J. Shoulder Elbow Surg. 2001;10(3):217–224. doi:10.1067/mse.2001.113961

2. Bartron A. The Shoulder Complex. - ppt download [Internet]. [cited 2017 Dec 19];Available from: http://slideplayer.com/slide/1663856/

3. Berliner JL, Regalado-Magdos A, Ma CB, Feeley BT. Biomechanics of reverse total shoulder arthroplasty. J. Shoulder Elbow Surg. 2015 Jan;24(1):150–160. doi:10.1016/j.jse.2014.08.003

4. Bigliani LU, Newton PM, Steinmann SP, Connor PM, McIlveen SJ. Glenoid Rim Lesions Associated with Recurrent Anterior Dislocation of the Shoulder. Am. J. Sports Med. 1998;26(1):41–45. doi:10.1177/03635465980260012301

5. Boileau P, Sinnerton RJ, Chuinard C, Walch G. Arthroplasty of the shoulder. J. Bone Joint Surg. Br. 2006 May 1;88–B(5):562–575. doi:10.1302/0301-620X.88B5.16466

6. Boileau P, Watkinson D, Hatzidakis AM, Hovorka I. Neer Award 2005: The Grammont reverse shoulder prosthesis: Results in cuff tear arthritis, fracture sequelae, and revision arthroplasty. J. Shoulder Elbow Surg. 2006 Sep;15(5):527–540. doi:10.1016/j.jse.2006.01.003

7. Brewer BJ, Wubben RC, Carrera GF. Excessive retroversion of the glenoid cavity. A cause of non-traumatic posterior instability of the shoulder. J. Bone Joint Surg. Am. 68(5):724–731.

8. Churchill RS, Brems JJ, Kotschi H. Glenoid size, inclination, and version: An anatomic study. J. Shoulder Elbow Surg. 2001 Jul;10(4):327–332. doi:10.1067/mse.2001.115269

9. Ecklund KJ, Lee TQ, Tibone J, Gupta R. Rotator cuff tear arthropathy. J. Am. Acad. Orthop. Surg. 2007;15(6):340–349.

10. Ernstbrunner L, Werthel J-D, Wagner E, Hatta T, Sperling JW, Cofield RH. Glenoid bone grafting in primary reverse total shoulder arthroplasty. J. Shoulder Elbow Surg. 2017 Aug;26(8):1441–1447. doi:10.1016/j.jse.2017.01.011

11. Farshad M, Gerber C. Reverse total shoulder arthroplasty—from the most to the least common complication. Int. Orthop. 2010 Dec;34(8):1075–1082. doi:10.1007/s00264-010-1125-2

12. Frankle MA, Teramoto A, Luo Z-P, Levy JC, Pupello D. Glenoid morphology in reverse shoulder arthroplasty: Classification and surgical implications. J. Shoulder Elbow Surg. 2009 Nov;18(6):874–885. doi:10.1016/j.jse.2009.02.013

13. Friedman RJ, Hawthorne KB, Genez BM. The use of computerized tomography in the measurement of glenoid version. J. Bone Jt. Surg. 1992 Aug 1;74(7):1032–1037.

14. Gilot GJ. Addressing glenoid erosion in reverse total shoulder arthroplasty. Bull. Hosp. Jt. Dis. 2013. 2013;71 Suppl 2:S51-53.

15. Government of Canada SC. The Daily — Population projections: Canada, the provinces and territories, 2013 to 2063 [Internet]. 2014 Sep 17 [cited 2015 Oct 9];Available from: http://www.statcan.gc.ca/daily-quotidien/140917/dq140917a-eng.htm

16. Gray H. Anatomy of the human body. Lea & Febiger; 1918.

17. Gulotta LV, Craig EV, editors. Massive Rotator Cuff Tears [Internet]. Boston, MA: Springer US; 2015 [cited 2015 Nov 16]. Available from: http://link.springer.com/10.1007/978-1-4899-7494-5

18. Habermeyer P, Magosch P, Luz V, Lichtenberg S. Three-dimensional glenoid deformity in patients with osteoarthritis: a radiographic analysis. JBJS. 2006;88(6):1301–1307.

19. Hermida JC, Flores-Hernandez C, Hoenecke HR, D'Lima DD. Augmented wedge-shaped glenoid component for the correction of glenoid retroversion: a finite element analysis. J. Shoulder Elbow Surg. 2014 Mar;23(3):347–354. doi:10.1016/j.jse.2013.06.008

20. Herschel R, Wieser K, Morrey ME, Ramos CH, Gerber C, Meyer DC. Risk factors for glenoid erosion in patients with shoulder hemiarthroplasty: an analysis of 118 cases. J. Shoulder Elbow Surg. 2017 Feb;26(2):246–252. doi:10.1016/j.jse.2016.06.004

21. Hyun YS, Huri G, Garbis NG, McFarland EG. Uncommon Indications for Reverse Total Shoulder Arthroplasty. Clin. Orthop. Surg. 2013 Dec;5(4):243–255. doi:10.4055/cios.2013.5.4.243

22. Jean K. Classifications of glenoid dysplasia, glenoid bone loss and glenoid loosening: a review of the literature. Eur. J. Orthop. Surg. Traumatol. 2013 Apr;23(3):301–310. doi:10.1007/s00590-012-1119-4

23. Jones RB, Wright TW, Roche CP. Bone Grafting the Glenoid Versus Use of Augmented Glenoid Baseplates with Reverse Shoulder Arthroplasty. Bull. Hosp. Jt. Dis. 2013. 2015 Dec;73 Suppl 1:S129-135.

24. Katz D, O'Toole G, Cogswell L, Sauzieres P, Valenti P. A history of the reverse shoulder prosthesis. Int. J. Shoulder Surg. 2007 Oct 1;1(4):108. doi:10.4103/0973-6042.37113

25. Katz DC, Sauzières P, Valenti P, Kany J. The case for the metal-backed glenoid design in total anatomical shoulder arthroplasty. Eur. J. Orthop. Surg. Traumatol. 2012 Jan 1;22(1):9–16. doi:10.1007/s00590-011-0796-8

26. Langohr GD. Fundamentals of the Biomechanical Characteristics Related to the Loading of Reverse Total Shoulder Arthroplasty Implants and the Development of a Wear Simulation Strategy. Electron. Thesis Diss. Repos. [Internet]. 2015 Nov 25;Available from: https://ir.lib.uwo.ca/etd/3436

27. Lenart BA, Namdari S, Williams GR. Total shoulder arthroplasty with an augmented component for anterior glenoid bone deficiency. J. Shoulder Elbow Surg. 2016 Mar;25(3):398–405. doi:10.1016/j.jse.2015.08.012

28. Lévigne C, Franceschi JP. Rheumatoid Arthritis of the Shoulder: Radiological Presentation and Results of Arthroplasty [Internet]. In: Shoulder Arthroplasty. Springer, Berlin, Heidelberg; 1999 [cited 2017 Oct 20]. p. 221–230.Available from: https://link-springer-com.proxy1.lib.uwo.ca/chapter/10.1007/978-3-642-58365-0_24

29. Manolagas SC, Jilka RL. Bone Marrow, Cytokines, and Bone Remodeling — Emerging Insights into the Pathophysiology of Osteoporosis. N. Engl. J. Med. 1995 Feb 2;332(5):305–311. doi:10.1056/NEJM199502023320506

30. Matsen FA, Boileau P, Walch G, Gerber C, Bicknell RT. The Reverse Total Shoulder Arthroplasty. J Bone Jt. Surg Am. 2007 Mar 1;89(3):660–667.

31. Milgrom C, Schaffler M, Gilbert S, van Holsbeeck M. Rotator-cuff changes in asymptomatic adults. The effect of age, hand dominance and gender. J. Bone Joint Surg. Br. 1995 Mar;77(2):296–298.

32. Orr TE, Carter DR, Schurman DJ. Stress analyses of glenoid component designs. Clin. Orthop. 1988;232:217–224.

33. Roche CP, Stroud NJ, Martin BL, Steiler CA, Flurin P-H, Wright TW, et al. Achieving fixation in glenoids with superior wear using reverse shoulder arthroplasty. J. Shoulder Elbow Surg. 2013 Dec;22(12):1695–1701. doi:10.1016/j.jse.2013.03.008

34. Schairer WW, Nwachukwu BU, Lyman S, Craig EV, Gulotta LV. National utilization of reverse total shoulder arthroplasty in the United States. J. Shoulder Elbow Surg. 2015 Jan;24(1):91–97. doi:10.1016/j.jse.2014.08.026

35. Schett G, Gravallese E. Bone erosion in rheumatoid arthritis: mechanisms, diagnosis and treatment. Nat. Rev. Rheumatol. 2012 Nov;8(11):656–664. doi:10.1038/nrrheum.2012.153

36. Sirveaux F, Favard L, Oudet D, Huquet D, Walch G, Mole D. Grammont inverted total shoulder arthroplasty in the treatment of glenohumeral osteoarthritis with massive rupture of the cuff RESULTS OF A MULTICENTRE STUDY OF 80 SHOULDERS. J. Bone Joint Surg. Br. 2004;86(3):388–395.

37. Steinmann SP, Cofield RH. Bone grafting for glenoid deficiency in total shoulder replacement. J. Shoulder Elbow Surg. 2000;9(5):361–367. doi:10.1067/mse.2000.106921

38. Terrier A, Reist A, Vogel A, Farron A. Effect of supraspinatus deficiency on humerus translation and glenohumeral contact force during abduction. Clin. Biomech. 2007 Jul;22(6):645–651. doi:10.1016/j.clinbiomech.2007.01.015

39. Virani NA, Harman M, Li K, Levy J, Pupello DR, Frankle MA. In vitro and finite element analysis of glenoid bone/baseplate interaction in the reverse shoulder design. J. Shoulder Elbow Surg. 2008 May;17(3):509–521. doi:10.1016/j.jse.2007.11.003

40. Walch G, Badet R, Boulahia A, Khoury A. Morphologic study of the glenoid in primary glenohumeral osteoarthritis. J. Arthroplasty. 1999;14(6):756–760.

41. Wening JD, Hollis RF, Hughes RE, Kuhn JE. Quantitative morphology of full thickness rotator cuff tears. Clin. Anat. 2002 Jan;15(1):18–22. doi:10.1002/ca.1086

42. Wong AS, Gallo L, Kuhn JE, Carpenter JE, Hughes RE. The effect of glenoid inclination on superior humeral head migration. J. Shoulder Elbow Surg. 2003 Jul 1;12(4):360–364. doi:10.1016/S1058-2746(03)00026-0

43. Wuelker N, Korell M, Thren K. Dynamic glenohumeral joint stability. J. Shoulder Elb. Surg. Am. Shoulder Elb. Surg. Al. 1998 Feb;7(1):43–52.

44. Zannoni C, Mantovani R, Viceconti M. Material properties assignment to finite element models of bone structures: a new method. Med. Eng. Phys. 1999;20(10):735–740.

45. Zingg PO. Clinical and Structural Outcomes of Nonoperative Management of Massive Rotator Cuff Tears. J. Bone Jt. Surg. Am. 2007 Sep 1;89(9):1928. doi:10.2106/JBJS.F.01073

46. Rotator Cuff Tears - OrthoInfo - AAOS [Internet]. [cited 2017 Dec 19];Available from: https://orthoinfo.aaos.org/en/diseases--conditions/rotator-cuff-tears/

Chapter 2

2 Morphology and Density of the E2 Glenoid

OVERVIEW

Glenoid bone density, strength, and morphology has been well established in the literature for healthy and arthritic patients, however the literature describing these characteristics of bone in patients with osseous defects is sparse. This chapter will examine the cortical and cancellous bone density and its distribution in E2-type patients.

(Some aspects of the Introduction and Methods have been covered in Chapter 1, but are repeated here due to the "Integrated Article" format of this thesis, to ensure that this chapter can stand alone as a publishable paper.)

2.1 Introduction

As documented in the previous chapter, reverse total shoulder arthroplasty (RTSA) has been successful in treating patients with rotator cuff tears and degenerative arthritis in the shoulder. Unfortunately, there are still cases of implant failure due to a variety of causes such as trauma, bone fracture, aseptic loosening, and mechanical failure.[4,5,8] In situations of loosening or mechanical failure, it is often important to understand the mechanics involved in joint and implant loading, particularly regarding the osseous foundation used for implant fixation. Evaluation of the bony foundation can potentially determine the viability of joint replacement and can have a profound effect on long-term implant success. Patients with abnormal morphologies due to erosion are particularly susceptible to implant failure.[9,10,13,15,27]

Although numerous studies have examined properties of healthy bone,[2,17,22,23] these properties may not be reflective of bone found in patients who have progressed to the point of requiring joint replacement. In the case of erosion, which is often found in patients requiring arthroplasty, abnormal bone morphology increases the complexity of procedures.[11,19]

Treatment options for these patients typically follows one of two approaches. More severe erosions may result in insufficient bone and hence require bone grafts, while less severe cases may be treated using modified reaming techniques to allow for proper contact between the glenoid surface and the implant. However, the effectiveness of each method has been the subject of debate and neither have been proven to be conclusively more effective than the other.[13,15,16,19,25] Regardless of the method used, it is important to understand the osseous morphology and properties of erosion patterns to provide groundwork which supports and promotes surgical and implant design decisions.

Total shoulder arthroplasty (TSA) has been used to treat posterior and anterior glenoid erosions, and literature exists describing its ability to do so.[21,24] However superior glenoid erosion is more often treated with RTSA. Patients requiring RTSA typically suffer from rotator cuff arthropathy, which causes instability in the shoulder. The non-functional rotator cuff becomes incapable of stabilizing the joint and activation of the deltoid muscle

fibers causes the humeral head to subluxate superiorly on the glenoid. Over time this subluxation changes the location of articulation within the joint, and combined with osteoarthritis this creates erosion in the superior portion of the glenoid. Sirveaux et al.[29] classified glenoids with superior erosion based on humeral position and glenoid wear (Figure 1-8). E2-type erosion has clear erosion into the superior aspect of the glenoid, but maintains some volume of native glenoid bone near the inferior rim of the glenoid. Since the progression of E2 is apparent, but there is still evidence of native glenoid bone, we can assume that E2-type erosions represent a moderate level osseous defect. This is ideal for studying the morphology of this defect.

The objective of this study was to examine the bone quality of patients with E2-type erosion. It is hypothesized that the eroded region contains denser bone, as well as a higher volume of cortical bone relative to cancellous bone when compared to non-eroded regions. A secondary objective was to quantify inclination and retroversion of E2 type glenoids.

2.2 Methods and Materials

Clinical computed tomography (CT) scans were obtained from 23 shoulders, 13 females and 10 males, that had undergone RTSA and were classified as having E2-type erosions (mean age 72.5, ranging from 56-83). E2-type erosions were classified as any glenoid that showed superior erosion not extending as far as the inferior glenoid rim (Figure 1-8). All CT scans used were the most recently available scans pre-operation.

2.2.1 Model Creation

The CT images were compiled in Mimics imaging processing software (Materialise, Belgium) and scapulae were isolated from other bony structures through a combination of bone thresholding via Hounsfield units (HU) and manual separation of bones, similar to the method used by Bryce et al.[6] Manual separation was required where contact between the humerus, and the acromion and/or glenoid occurred. The minimum threshold for cancellous bone was chosen to be 100 HU[28] and anything above 600 HU[1] was considered to be cortical bone. Once the scapula was isolated, the acromion and coracoid were removed to decrease computational time in later steps. The coracoid was removed because the anterior and superior measurement regions could potentially overlap with the coracoid

in smaller scapula (Figure 2-1). This was done by removing all coracoid bone that was above the superior rim of the glenoid, and in front of the anterior rim, when viewed in the sagittal scapular plane, at 'zero' glenoid version. (this removal was inspected and approved by a board-certified orthopaedic surgeon).

2.2.2 Region Definition and Setup

To create consistent coordinate systems between patients, a method previously described by Frankle et al[10] was used, with slight modifications, to establish scapular reference planes (Figure 2-2). First, the scapular plane was created using points at the center of the glenoid, the medial angle of the scapula, and the inferior most point of the inferior angle (Figure 2-3). Next, the line connecting the glenoid center and medial angle was chosen as the normal vector for the scapular sagittal plane (also called the transverse axis), and finally, the transverse plane was created perpendicular to the other 2 planes. All planes intersect at the glenoid center point.

Typical methods of finding the glenoid center were unavailable in most patients, due to erosion and osteophytes, therefore the glenoid center was defined as the center of the circle of best fit passing through the most inferior, posterior, and anterior points of the glenoid rim (Figure 2-4). The glenoid center point was placed on the surface of the glenoid using the center of the previously mentioned circle of best fit and moving it along the transverse axis until it came into contact with the glenoid surface.

Bone density measurements were taken from 4 different quadrants (30mm x 30mm) at 2mm depth increments, from 0-10mm in depth medially, with 0mm starting at the glenoid center (Figure 2-5). All the bone lateral to the glenoid center was considered as a separate region and excluded from the study. The size of the regions was chosen to be large enough to cover all patient sizes.

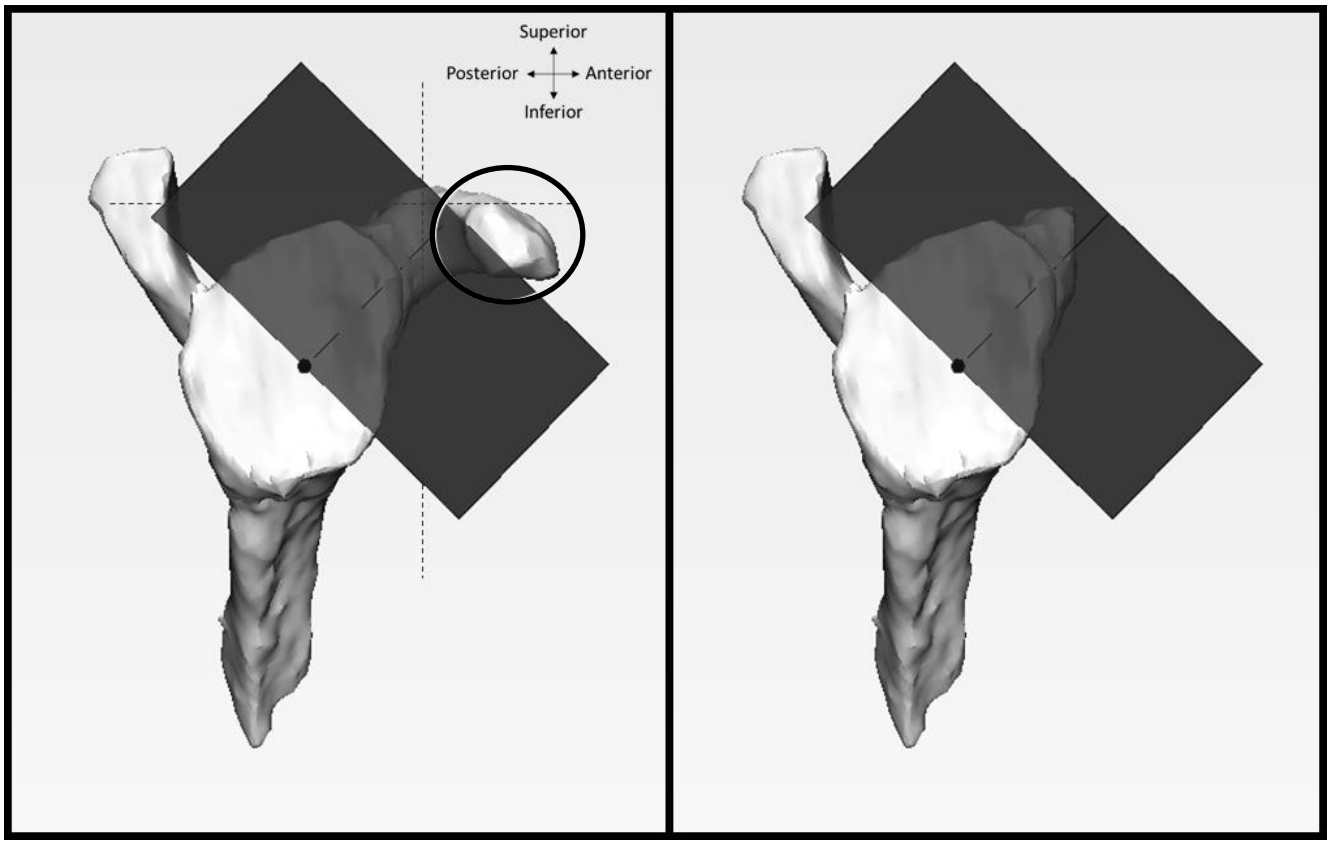

Figure 2-1 - Removal of the coracoid

Left: *A small section of the coracoid (circled) in some patients may reach into the anterior and superior quadrants.* ***Right:*** *Post-removal of the majority of the coracoid by using the transverse and scapular plane as reference. The base of the coracoid was generally deeper than any measurements taken and therefore did not affect results.*

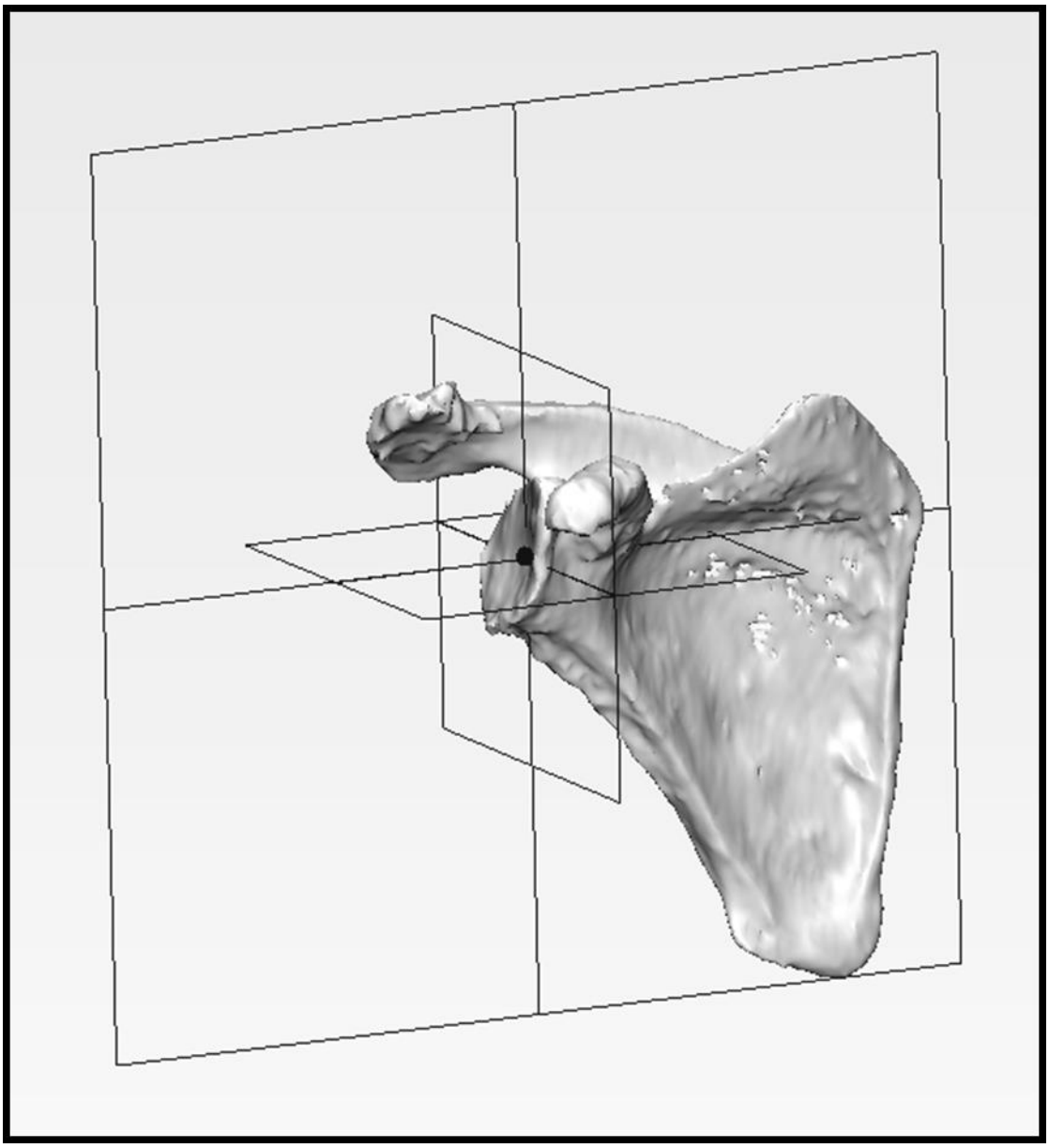

Figure 2-2 – Scapular, transverse, and sagittal reference planes.

The transverse axis, defined as the line passing through the glenoid center and trigonum spinae are the main anatomic landmarks used to establish the planes of the scapula. The methods used are based on a study by Frankle et al.[10]

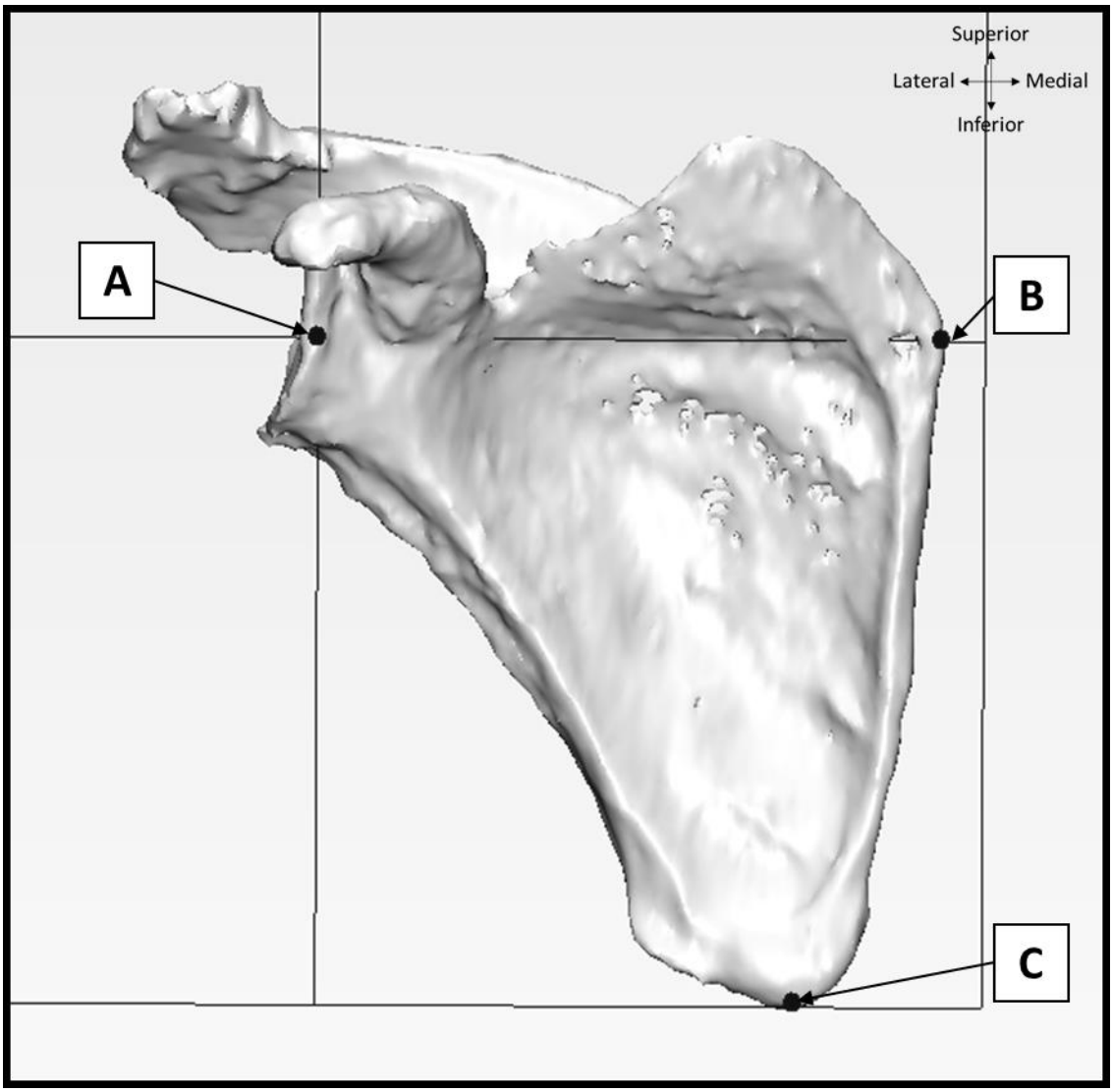

Figure 2-3 – The 3 anatomic landmarks used to create the scapular plane.

A) The glenoid center point
B) The trigonum spinae
C) *The inferior angle of the scapula*

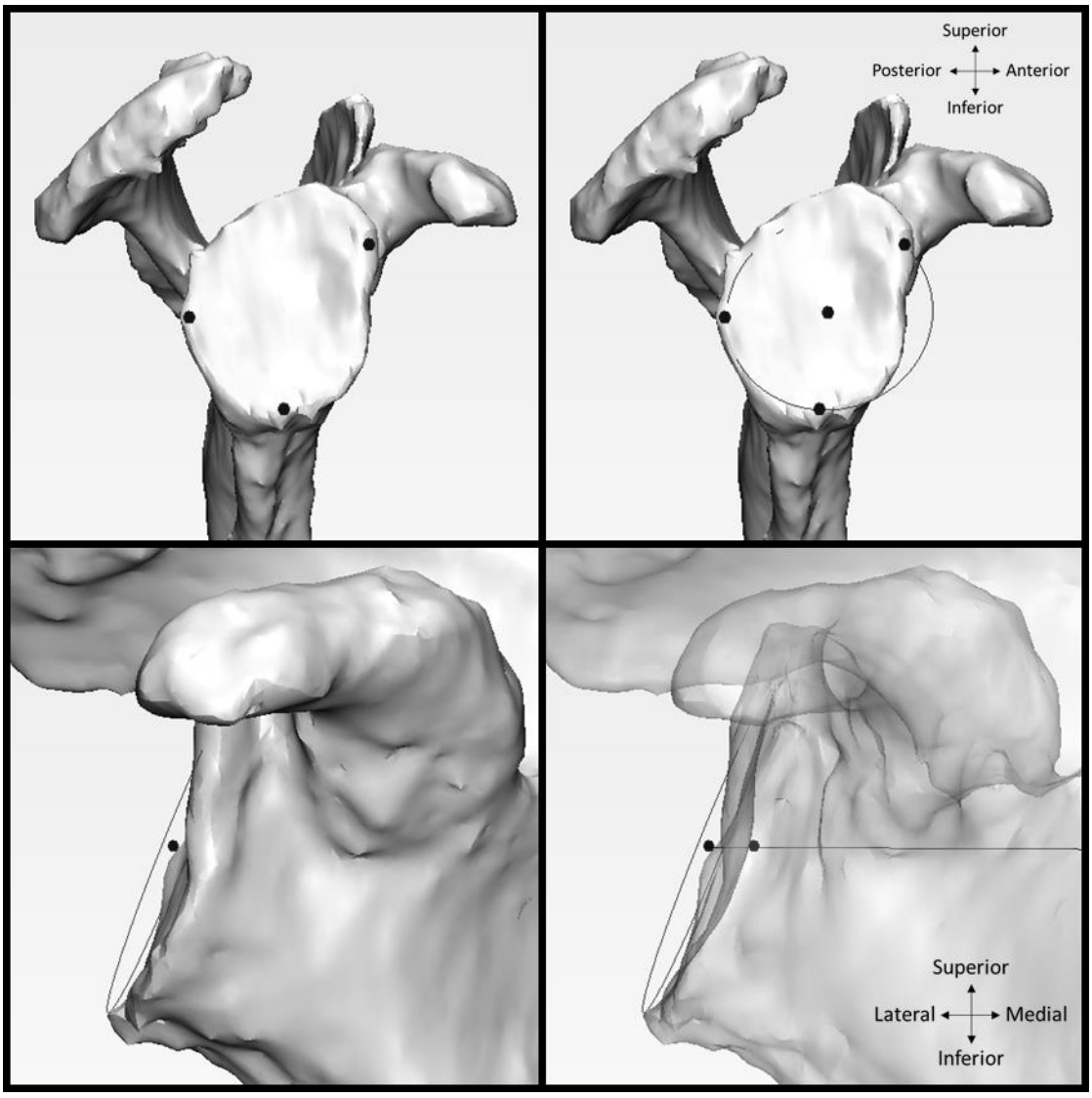

Figure 2-4 – Creating the glenoid center point in patients with superior erosion

Top: *Due to erosion of the superior portion of the glenoid, the glenoid center was defined using a circle of best fit through the most anterior, posterior, and inferior points on the glenoid rim.* ***Bottom:*** *The center of the circle of best fit did not lie on the surface of the glenoid, therefore the center point of the circle was translated towards the trigonum spinae until this point reached the glenoid surface, at which point it becomes the glenoid center point.*

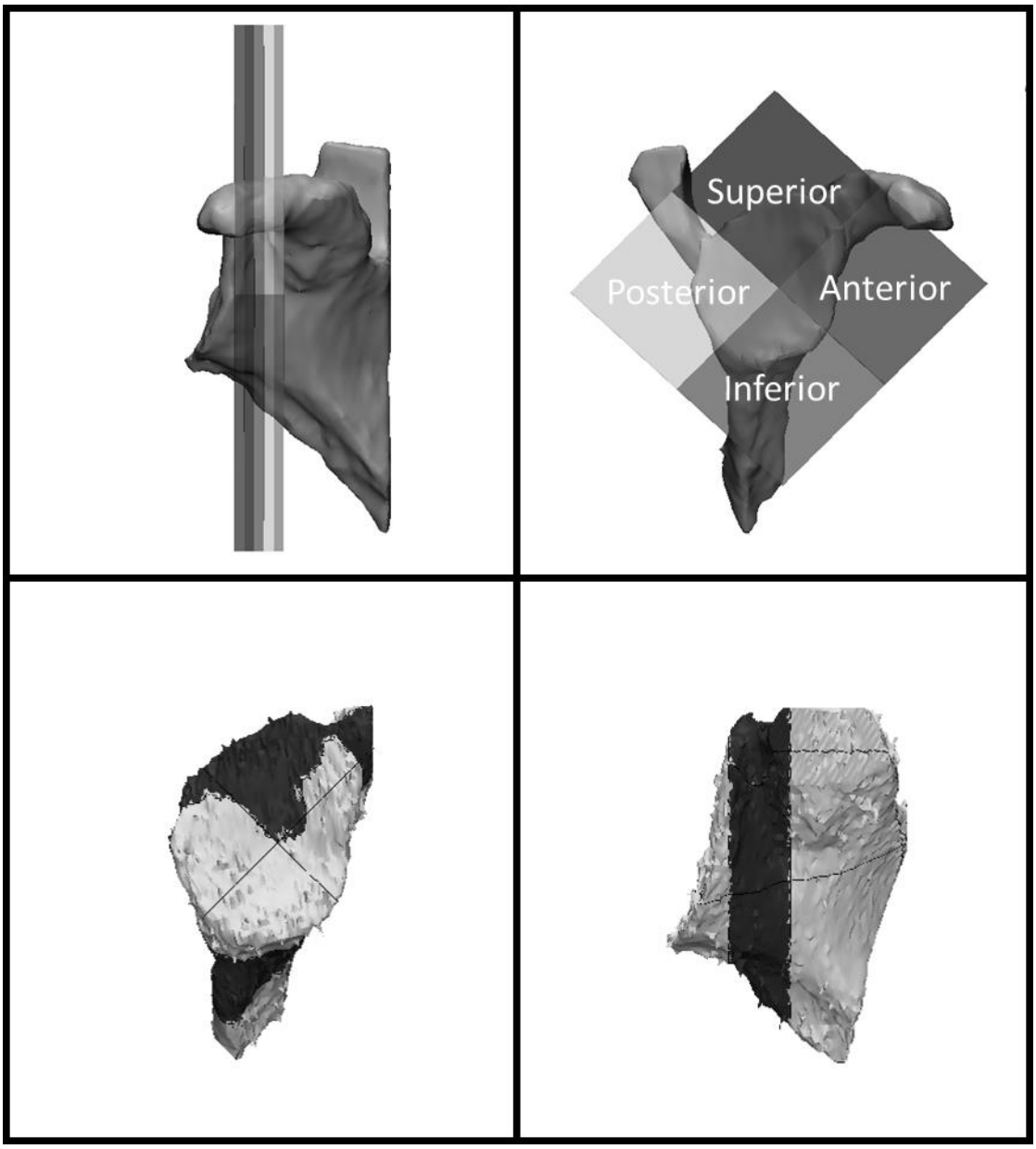

Figure 2-5 – Images illustrating the measurement regions

Top Left: *Depth regions in 2mm increments, beginning at 0mm at the glenoid center point.*
Top Right: *The four quadrants of interest (anterior, inferior, posterior, and superior).*
Bottom: *Medial-lateral and anterior-posterior views of the glenoid with acromion and coracoid removed. The region in black illustrates the entire region of measurement.*

2.2.3 Density Analysis and Statistics

To calculate the average density for each region, the density value associated with each voxel found within the boundaries of said region was averaged. Glenoid inclination and version were measured using Glenosys (Imascap, France), a non-clinical, preoperative, surgical planning software which has been shown to provide reproducible glenoid measurements accurate enough for use in glenoid component positioning.[26,30]

A repeated-measures multiple analysis of variance (MANOVA) was performed using SPSS statistical software to compare differences between mean densities for each depth, quadrant, and gender, as well as any interactions between them. Ratios of mean cortical to cancellous bone volume were analyzed for effects of gender and quadrant of the glenoid using a two-way repeated-measures analysis of variance (RM-ANOVA). Significance was set at $p < 0.05$.

2.3 Results

Statistical analysis showed that the within subject factors (quadrant and depth) had significant multivariate main effects ($p<0.001$ for both), and the interaction between quadrant and depth was also a significant factor in determining bone density ($p<0.001$). Any interactions involving gender, did not have significant main effects with regards to bone density ($p=0.8$), and examining the between subject main effects of gender was also insignificant for determining both cortical and cancellous bone densities ($p=0.483$ and $p=0.306$ respectively).

For univariate main effects, quadrant, depth, and the interaction between the quadrant and depth showed significance for cortical bone ($p=0.013$, $p=0.001$, $p<0.001$) and cancellous bone ($p<0.001$, $p=0.015$, $p<0.001$).

Table 2-1 outlines the means and standard deviations for each gender, quadrant, and depth level.

Table 2-1 - Mean(±SD) bone density of cortical and cancellous bone for each within- and between-subject factor

Bone type		Cortical [HU]	Cancellous [HU]
Gender	Male	853(±92)	336(±60)
	Female	870(±83)	356(±50)
Quadrant	Anterior	871(±75)	339(±53)
	Inferior	831(±71)	302(±53)
	Posterior	844(±93)	371(±47)
	Superior	894(±97)	368(±44)
Depth	0-2mm	891(±88)	351(±51)
	2-4mm	851(±87)	349(±60)
	4-6mm	837(±87)	349(±63)
	6-8mm	851(±86)	341(±58)
	8-10mm	872(±84)	335(±49)
Overall		860(±88)	345(±57)

2.3.1 Glenoid Bone Density

2.3.1.1 Quadrant Density

As shown in Table 2-1 and Figure 2-6, the quadrant containing the least dense cortical and cancellous bone was the inferior quadrant. The only significant difference between cortical bone densities in each quadrant was between the posterior and superior quadrants ($p=0.006$). In cancellous bone however, the inferior quadrant was significantly less dense than all other quadrants ($p<0.005$). The anterior quadrant was significantly less dense than the posterior ($p=0.01$) and superior ($p=0.007$) quadrants as well, while the superior quadrant was denser than the anterior ($p=0.007$) quadrant.

2.3.1.2 Depth Measurements

When examining bone density as it relates to depth, it was found that cortical bone is least dense in the center (4-6 mm), and increases in both directions, with the glenoid surface (0-2 mm) containing the densest cortical bone (Figure 2-7). The cortical bone at the glenoid surface was significantly denser than cortical bone at depths of 2-4 mm ($p=0.013$), 4-6 mm ($p=0.001$), and 6-8 mm ($p=0.033$). While the 4-6mm depth was the least dense overall, it

was only significantly less dense than the glenoid surface (mentioned above), and the 8-10mm depth (p=0.009).

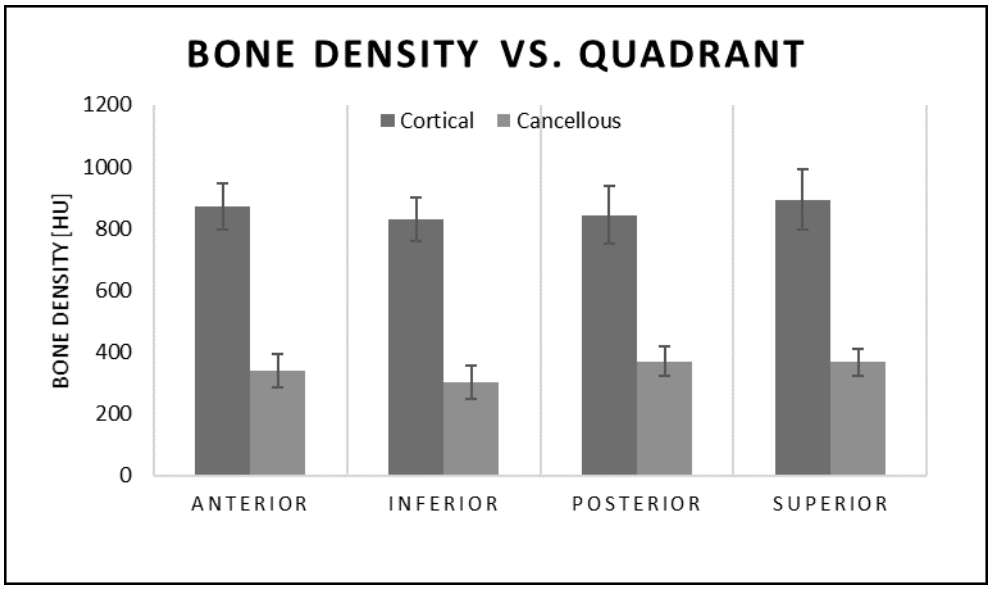

Figure 2-6 – Cortical and cancellous bone density of each quadrant of the glenoid (Mean±SD)

Cancellous bone was the densest at the glenoid surface, however it was found to be only significantly denser than at 8-10mm in depth (p=0.025), and was found to decrease with increasing depth. The cancellous bone at 8-10mm from the glenoid center was also significantly less dense than at 2-4mm (p=0.005), and 4-6mm (p=0.021) in depth.

2.3.1.3 Quadrant-Depth Interaction

When comparing quadrants, there was no significant difference found between the cortical bone density of any of the 4 quadrants at depths ranging from 6 to 10 mm (Figure 2-8). The inferior quadrant was found to be significantly less dense at a depth of 0 to 2 mm when compared to anterior (p<0.001), posterior (p=0.002), and superior (p<0.001) quadrants, and the superior quadrant was significantly denser than the inferior and posterior quadrants at depths of 0 to 2mm (p<0.001 and p=0.002) and 2 to 4 mm (p=0.005 and p<0.001). For cancellous bone, the inferior quadrant was significantly less dense than all quadrants from the glenoid surface up to 6mm in depth (p<0.039), and was less dense than the posterior

and superior quadrants across all depths ($p<0.032$) (Figure 2-9). The anterior quadrant was also significantly less dense than the posterior quadrant across all depths except the glenoid surface ($p<0.049$). Considering the interaction between depths of measurement and quadrant, the superior quadrant again demonstrated that it contained the densest cancellous bone overall. It was significantly denser than the anterior quadrant ($p<0.014$) from 2-8mm, and was denser than the inferior quadrants for the entire depth range of measurement ($p<0.032$).

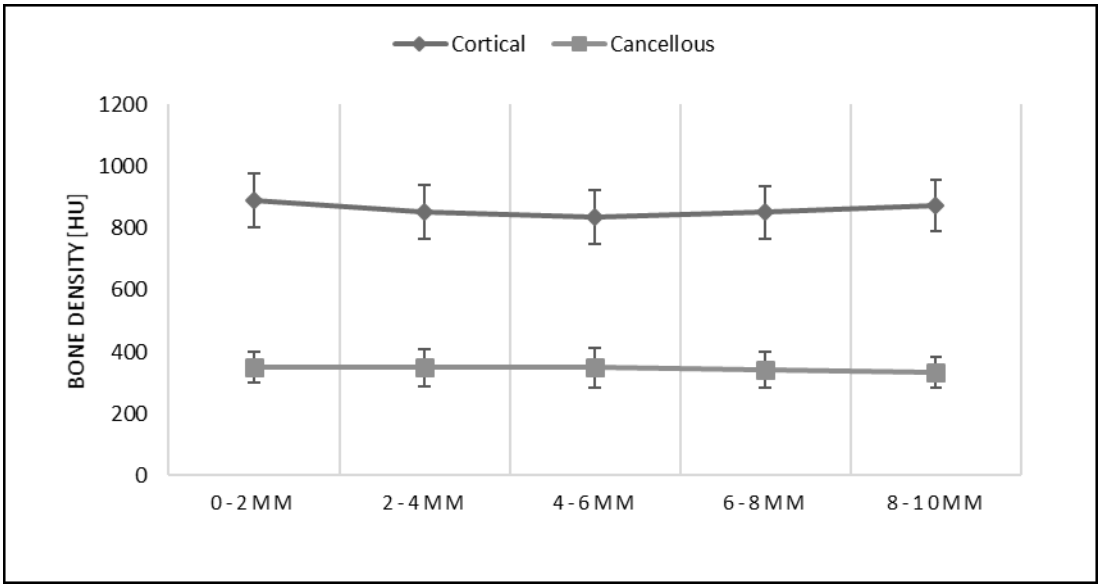

Figure 2-7 - Cortical and cancellous bone density as a function of increasing depth, or increase in distance medially from the glenoid center (Mean±SD)

Within each individual quadrant, there was also little significance found in the difference in cortical bone density between any depth increments from 0 to 10 mm in the anterior and posterior quadrants. The superior quadrant was significantly denser from 0-2 mm than from 4-6mm ($p=0.005$), 6-8 mm ($p<0.001$) and 8-10 mm ($p<0.001$), and the inferior quadrant was significantly denser from 8-10mm in depth than any other depth ($p<0.028$). In cancellous bone, there was no significant difference found between depths in inferior, and posterior quadrants. In the superior quadrant, bone density at a depth of 8-10mm was found to be significantly lower than at all other depths $p<0.008$. The inferior quadrant had less dense cancellous bone at 8-10mm than at the glenoid surface (0-4mm, $p<0.02$).

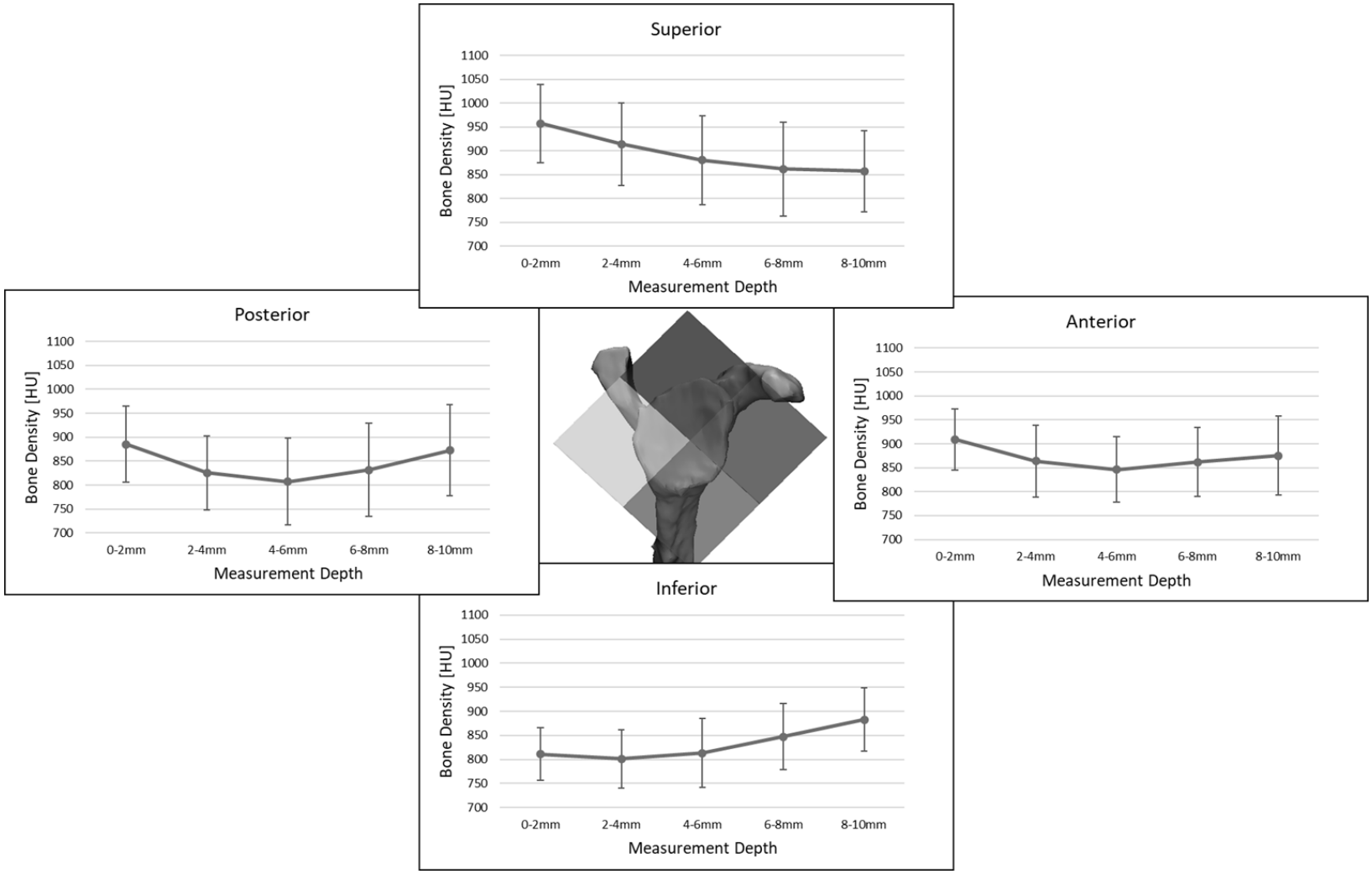

Figure 2-8 - Cortical bone density for each quadrant as a function of depth (Mean±SD).

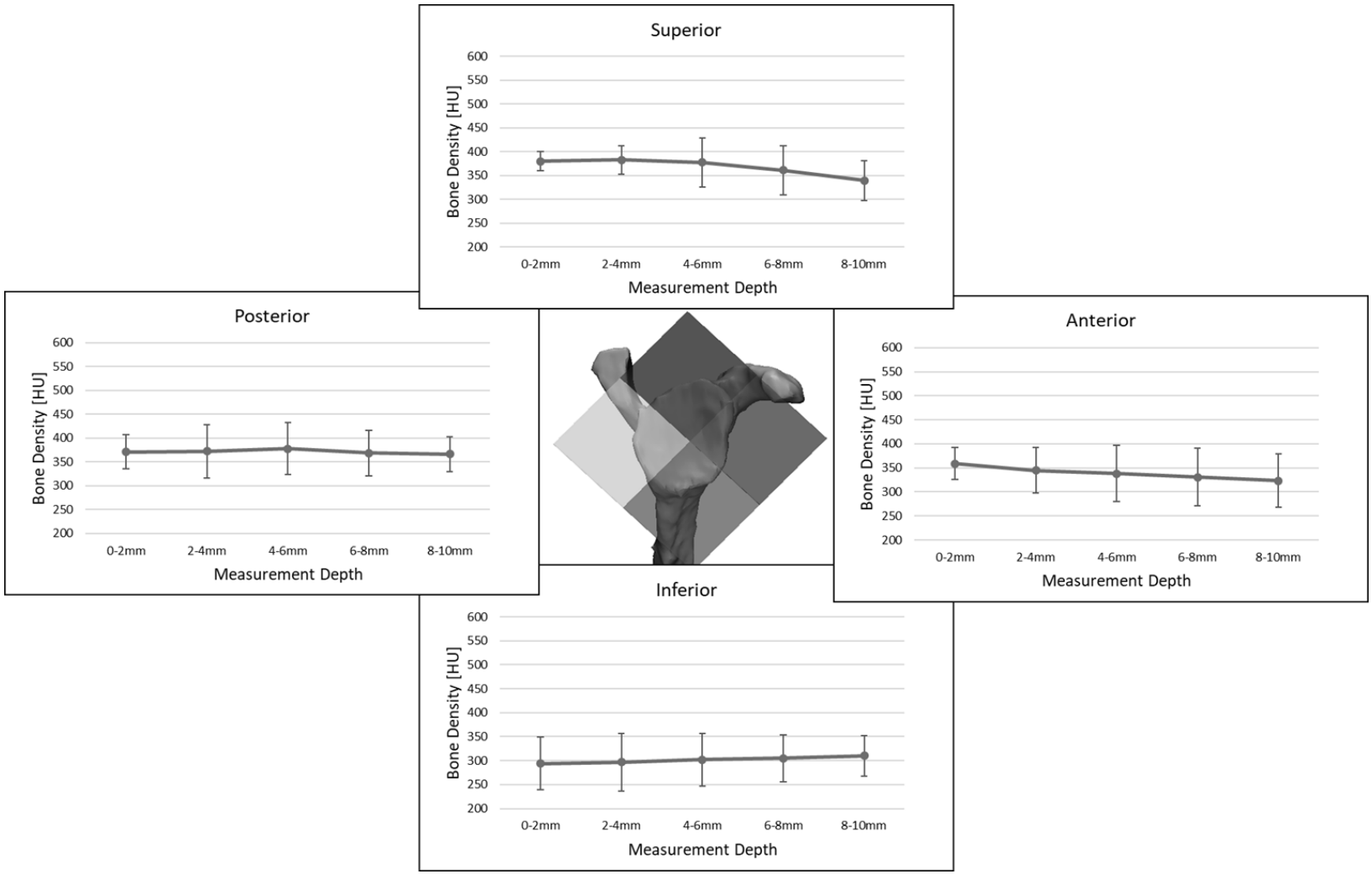

Figure 2-9 - Cancellous bone density for each quadrant as a function of depth (Mean±SD)

2.3.2 Cortical to Cancellous Bone Volume Fraction

The volume fraction of cortical to cancellous bone was found to be 0.71±0.45 for males and 0.82±0.51 for females, however no significant effects from gender were found ($p=0.312$). Differences in volume fraction between quadrants were very significant ($p<0.001$). The region with the highest volume of cortical bone relative to cancellous bone was found in the superior quadrant (1.06±0.48), which was significantly higher than the volume fractions determined for the anterior (0.74±0.40, $p=0.021$) and inferior quadrants (0.33±0.25, $p<0.001$). The posterior (0.92±0.45) and anterior quadrants, also had significantly higher cortical to cancellous volume fraction than the inferior quadrant ($p<0.001$ for all).

2.4 Discussion

As per Wolff's law,[12] bone subjected to varying levels of strain will adapt to support that strain. Subluxation of the humeral head into the erosion site reduces the area of articular contact in the joint, hence increasing bone stresses and strains in the eroded region.

Our results showed that the superoposterior region, which is typically the loading direction of joint loads, was found to have denser cancellous bone. We also found that the inferior quadrant had the least dense cortical and cancellous bone, indicating that lack of routine microstrains in that region of bone may cause a reduction in bone density. The most significant differences in density were found near the glenoid surface (i.e. Typically 0-2mm medially from the glenoid center), however this region of bone is likely to be reamed away when preparing for shoulder arthroplasty. Our sample also showed that gender played no role in determining bone density or cortical to cancellous bone volume fraction.

There was little effect overall of depth increases on cancellous bone, whereas cortical bone was mostly stiffest near the glenoid surface and deep in the glenoid vault. Interestingly, this coincides with the desired entry and exit points of cortical screws when fixing an RTSA baseplate to the glenoid.

Comparing quadrants and depths showed that the density of any cortical bone deeper than 6mm did not differ between quadrants. However, the inferior quadrant was less dense than other quadrants, up to 2mm. For cancellous bone, it was shown that the inferior quadrant was less dense than all other quadrants up to a depth of at least 6 mm, and the superior quadrant again contained the densest bone, especially with relation to the inferior and anterior quadrants. The trend of differences in bone density across depths for each individual quadrant was similar to the overall trend mentioned above for measurements at different depths.

Examining volume fractions of cortical to cancellous bone revealed that the inferior quadrant contained significantly lower volume of cortical bone than cancellous bone. Since the articulation site of an E2 glenoid is likely to have shifted superiorly, cortical bone in the inferior region is likely to have undergone resorption due to reduced mechanical stresses. The scapular pillar is also known to be a good location for peripheral RTSA screw fixation,[10,14] likely due to high volume of cancellous bone. Higher volumes of cancellous bone with higher levels of cortical bone resorption likely lead to the results reported here.

Although previous studies have examined density of normal and arthritic glenoid bone,[2,7,17,22,23] using both mechanical and image based methods, there has been a lack of studies examining bone that has undergone morphologic changes such as E2 erosion. In these cases, it is necessary to understand what mechanical changes have occurred within the bone so patient treatment can be adjusted accordingly.

Lehtinen et al.[23] examined bone mineral density of cortical and cancellous bone in normal glenoids and found that anterior and posterior regions only differed significantly in density for cancellous bone. However, the superior and inferior regions differed in both cortical and cancellous bone. These results are in agreement with what was found in our study. Couteau et al.[7] also found that, in arthritic patients, the superior and inferior regions, and the anterior and posterior regions demonstrated significantly different densities.

While most studies agrees that the posterior region showed more dense bone than the anterior region of the glenoid,[7,17,20,23] the present study, along with Lehtinen et al.,[23] found that this did not apply to cortical bone. There was also general agreement that the superior

region provides more dense bone than the inferior region. Studies that reported glenoid bone density in Hounsfield Units showed that glenoid bone density can range anywhere from approximately 200HU to 1000HU, and our data fell within this range.[7,20,22]

This study has some implications with regard to hardware placement. Cortical bone deeper into the glenoid vault is important for bicortical, peripheral screw fixation, and our findings shows that density is not affected by the region in which cortical bone density is measured. Therefore, the regions in which bicortical fixation screws exit the bone can be chosen without regard for the location of the densest cortical bone. This means that limited screw angles and preservation of important extraosseous anatomic structures remain the primary limiting factors in screw placement. However, since our measurement regions did not extend far inferiorly, we are unaware of any changes in density in the scapular pillar that may affect fixation of an inferiorly directed peripheral screw.

There were a few limitations in this study related to image processing and standardization of measurements. When creating a 3D representation of patient anatomy based on CT images, image quality can impact the end results. There is often noise in the image and it is possible that voxels superfluous to the actual anatomy of the glenoid are included in the data. However, this likely affects a very small thickness of bone at the boundaries of the scapula, and as such only affects measurements of cortical bone to a very small degree. We also need to consider that smaller patients are going to possess a smaller glenoid vault relative to larger patients, therefore while bone at a depth of 10 mm may represent a moderate portion of the glenoid vault in a larger patient, in smaller patients 10mm may represent the entirety, or more, of the glenoid vault. Bicknell et al.[2] found that the glenoid vault is of different sizes between males and females, and while discussing implant design, Kirchner et al.[18] found that a maximum of only about 20mm of glenoid vault depth is available for fixation of a 10mm prosthesis peg (averaged for a number of patient sizes). For future studies, standardizing the measurements by examining depth regions as a percentage of the total depth of each individual's glenoid vault should be considered. This can also be applied when examining quadrants, by normalizing the data to the total surface area of each quadrant.

To our knowledge, this is the first study of the osseous foundation found in patients with E-type erosion. Many studies have examined healthy and arthritic bone properties, and some studies have investigated the bone found in patients with anterior or posterior erosion, both of which are more commonly issues treated using TSA, but no studies have been published quantifying the quality of bone density in E-type glenoids. Studies that do examine bone properties of the glenoid, typically do so at depths of less than 5mm, and as such we provide a rare insight into bone properties moderately deep into the glenoid vault. Our data also falls within the range of values found within the literature, and our investigation benefits from studying patient data, rather than cadaveric. This allows us to potentially examine the outcomes of the applied treatment against predictions based on our theoretical data. Each patient was also documented as having received RTSA which supports that joint failure leading to RTSA is the same mechanism causing E2-type erosions.

It is concerning that implant designs attempting to address glenoid erosion exist with sparse data available in supporting literature. The present study provided an insight into the morphological variations of bone density in E2-type glenoid erosion, and showed that although density variations occurred, likely due to bone remodeling, cortical and cancellous bone densities remain within what is seen in the literature. With this information, studies can perhaps focus on addressing biomechanical limitations of performing RTSA as they pertain to functional patient outcomes and long-term implant fixation.

In summary, this study showed that the density and morphology of the E2 eroded glenoid demonstrates many of the same trends that are reported for normal and arthritic glenoids. The superior quadrant contained the densest cancellous bone, and the inferior quadrant the least. We also found that the superior quadrant contained the highest volume of cortical bone relative to cancellous bone. With an understanding of these characteristics of bone density for E2-type glenoids, implant designs and surgical procedures can be modified to better compliment the osseous foundation in patients with these bone defects.

2.5 References

1. Aamodt A, Kvistad KA, Andersen E, Lund-Larsen J, Eine J, Benum P, et al. Determination of the Hounsfield value for CT-based design of custom femoral stems. J. Bone Jt. Surg. 1999 Jan 1;81(1):143–147. doi:10.1302/0301-620X.81B1.8880

2. Anglin C, Tolhurst P, Wyss UP, Pichora DR. Glenoid cancellous bone strength and modulus. J. Biomech. 1999 Oct;32(10):1091–1097. doi:10.1016/S0021-9290(99)00087-1

3. Bicknell RT, Patterson SD, King GJW, Chess DG, Johnson JA. Glenoid vault endosteal dimensions: An anthropometric study with special interest in implant design. J. Shoulder Elbow Surg. 2007 May;16(3):S96–S101. doi:10.1016/j.jse.2006.03.008

4. Boileau P, Watkinson DJ, Hatzidakis AM, Balg F. Grammont reverse prosthesis: Design, rationale, and biomechanics. J. Shoulder Elbow Surg. 2005 Jan;14(1, Supplement):S147–S161. doi:10.1016/j.jse.2004.10.006

5. Bonnevialle N, Melis B, Neyton L, Favard L, Molé D, Walch G, et al. Aseptic glenoid loosening or failure in total shoulder arthroplasty: revision with glenoid reimplantation. J. Shoulder Elbow Surg. 2013 Jun;22(6):745–751. doi:10.1016/j.jse.2012.08.009

6. Bryce CD, Pennypacker JL, Kulkarni N, Paul EM, Hollenbeak CS, Mosher TJ, et al. Validation of three-dimensional models of in situ scapulae. J. Shoulder Elbow Surg. 2008 Sep 1;17(5):825–832. doi:10.1016/j.jse.2008.01.141

7. Couteau B, Mansat P, Mansat M, Darmana R, Egan J. In vivo characterization of glenoid with use of computed tomography. J. Shoulder Elbow Surg. 2001 Mar 1;10(2):116–122. doi:10.1067/mse.2001.112884

8. Farshad M, Gerber C. Reverse total shoulder arthroplasty—from the most to the least common complication. Int. Orthop. 2010 Dec;34(8):1075–1082. doi:10.1007/s00264-010-1125-2

9. Formaini NT, Everding NG, Levy JC, Santoni BG, Nayak AN, Wilson C, et al. The effect of glenoid bone loss on reverse shoulder arthroplasty baseplate fixation. J. Shoulder Elbow Surg. 24(11):e312–e319. doi:10.1016/j.jse.2015.05.045

10. Frankle MA, Teramoto A, Luo Z-P, Levy JC, Pupello D. Glenoid morphology in reverse shoulder arthroplasty: Classification and surgical implications. J. Shoulder Elbow Surg. 2009 Nov;18(6):874–885. doi:10.1016/j.jse.2009.02.013

11. Friedman R, Stroud N, Glattke K, Flurin P-H, Wright TW, Zuckerman JD, et al. The Impact of Posterior Wear on Reverse Shoulder Glenoid Fixation. Bull. Hosp. Jt. Dis. 2013. 2015 Dec;73 Suppl 1:S15-20.

12. Frost HM. Wolff's Law and bone's structural adaptations to mechanical usage: an overview for clinicians. Angle Orthod. 1994 Jun 1;64(3):175–188. doi:10.1043/0003-3219(1994)064<0175:WLABSA>2.0.CO;2

13. Gilot GJ. Addressing glenoid erosion in reverse total shoulder arthroplasty. Bull. Hosp. Jt. Dis. 2013. 2013;71 Suppl 2:S51-53.

14. Hart ND, Clark JC, Wade Krause FR, Kissenberth MJ, Bragg WE, Hawkins RJ. Glenoid screw position in the Encore Reverse Shoulder Prosthesis: an anatomic dissection study of screw relationship to surrounding structures. J. Shoulder Elbow Surg. 2013 Jun;22(6):814–820. doi:10.1016/j.jse.2012.08.013

15. Jones RB, Wright TW, Roche CP. Bone Grafting the Glenoid Versus Use of Augmented Glenoid Baseplates with Reverse Shoulder Arthroplasty. Bull. Hosp. Jt. Dis. 2013. 2015 Dec;73 Suppl 1:S129-135.

16. Jones RB, Wright TW, Zuckerman JD. Reverse total shoulder arthroplasty with structural bone grafting of large glenoid defects. J. Shoulder Elbow Surg. 2016 Sep;25(9):1425–1432. doi:10.1016/j.jse.2016.01.016

17. Kalouche I, Crépin J, Abdelmoumen S, Mitton D, Guillot G, Gagey O. Mechanical properties of glenoid cancellous bone. Clin. Biomech. 2010 May;25(4):292–298. doi:10.1016/j.clinbiomech.2009.12.009

18. Kircher J, Bittersohl B, Zilkens C, Hedtmann A, Krauspe R. Biometrical analysis of the shoulder joint regarding glenoid implant dimensions for arthroplasty. Surg. Radiol. Anat. 2014 May;36(4):321–325. doi:10.1007/s00276-013-1197-y

19. Klein SM, Dunning P, Mulieri P, Pupello D, Downes K, Frankle MA. Effects of Acquired Glenoid Bone Defects on Surgical Technique and Clinical Outcomes in Reverse Shoulder Arthroplasty. J Bone Jt. Surg Am. 2010 May 1;92(5):1144–1154. doi:10.2106/JBJS.I.00778

20. Knowles NK, Athwal GS, Keener JD, Ferreira LM. Regional bone density variations in osteoarthritic glenoids: a comparison of symmetric to asymmetric (type B2) erosion patterns. J. Shoulder Elbow Surg. 2015 Mar;24(3):425–432. doi:10.1016/j.jse.2014.07.004

21. Knowles NK, Ferreira LM, Athwal GS. The arthritic glenoid: anatomy and arthroplasty designs. Curr. Rev. Musculoskelet. Med. 2016 Mar;9(1):23–29. doi:10.1007/s12178-016-9314-2

22. Kraljević M, Zumstein V, Wirz D, Hügli R, Müller-Gerbl M. Mineralisation and mechanical strength of the glenoid cavity subchondral bone plate. Int. Orthop. 2011;35(12):1813–1819. doi:10.1007/s00264-011-1308-5

23. Lehtinen JT, Tingart MJ, Apreleva M, Warner JJP. Total, trabecular, and cortical bone mineral density in different regions of the glenoid. J. Shoulder Elbow Surg. 2004;13(3):344–348. doi:10.1016/j.jse.2004.01.012

24. Lenart BA, Namdari S, Williams GR. Total shoulder arthroplasty with an augmented component for anterior glenoid bone deficiency. J. Shoulder Elbow Surg. 2016 Mar;25(3):398–405. doi:10.1016/j.jse.2015.08.012

25. Mizuno N, Denard PJ, Raiss P, Walch G. Reverse Total Shoulder Arthroplasty for Primary Glenohumeral Osteoarthritis in Patients with a Biconcave Glenoid. J Bone Jt. Surg Am. 2013 Jul 17;95(14):1297–1304. doi:10.2106/JBJS.L.00820

26. Moineau G, Levigne C, Boileau P, Young A, Walch G. Three-dimensional measurement method of arthritic glenoid cavity morphology: Feasibility and reproducibility. Orthop. Traumatol. Surg. Res. 2012 Oct;98(6):S139–S145. doi:10.1016/j.otsr.2012.06.007

27. Neyton L, Boileau P, Nové-Josserand L, Edwards TB, Walch G. Glenoid bone grafting with a reverse design prosthesis. J. Shoulder Elbow Surg. 2007 May;16(3, Supplement):S71–S78. doi:10.1016/j.jse.2006.02.002

28. Schreiber JJ, Anderson PA, Hsu WK. Use of computed tomography for assessing bone mineral density. Neurosurg. Focus. 2014;37(1):E4.

29. Sirveaux F, Favard L, Oudet D, Huquet D, Walch G, Mole D. Grammont inverted total shoulder arthroplasty in the treatment of glenohumeral osteoarthritis with massive rupture of the cuff RESULTS OF A MULTICENTRE STUDY OF 80 SHOULDERS. J. Bone Joint Surg. Br. 2004;86(3):388–395.

30. Walch G, Vezeridis PS, Boileau P, Deransart P, Chaoui J. Three-dimensional planning and use of patient-specific guides improve glenoid component position: an in vitro study. J. Shoulder Elbow Surg. 2015 Feb;24(2):302–309. doi:10.1016/j.jse.2014.05.029

Chapter 3

3 Micromotion of a Standard Glenoid Baseplate in the Presence of E2 Erosion

OVERVIEW

Due to the lack of literature on E2-type glenoid erosions, there has been little discussing the success and flaws of implant design for augmented implants. An important aspect of discussing novel implant designs is comparing them to previous designs. In this chapter, we will examine the fixation of a standard RTSA implant to establish a baseline for baseplate performance in E2-type glenoids.

(Some aspects of the Introduction and Methods have been covered in Chapters 1 & 2, but are repeated here due to the "Integrated Article" format of this thesis, to ensure that this chapter stands alone as a publishable paper.)

3.1 Introduction

Surgical outcomes of reverse total shoulder arthroplasty (RTSA) are evaluated based on patient satisfaction regarding improvements in shoulder function, strength, mobility and pain. While the risk and frequency of complications, failure, or revision surgery can be estimated, the ultimate goal should be to understand and prevent complications rather than address them as they come along. Experimental research into failure mechanisms can allow us to do just that.

RTSA can be employed to treat various shoulder pathologies, but was designed to treat patients who have a combination of glenohumeral arthritis and irreparable rotator cuff tear.[22] Rotator cuff tears cause the shoulder to become unstable and suffer a loss of strength and function.[6] Often, this causes the humeral head to migrate superiorly resulting in unnatural joint articulation, and osseous erosion can occur due to the glenohumeral arthritis. Frankle et al.[7] found that approximately 37.5% of patients requiring RTSA will have some type of erosion, leading to increased surgical complexity. Of these, 9% are classified as superior or E-type glenoid erosions caused by the aforementioned humeral head migration. This classification of glenoid erosion was described by Sirveaux et al.,[25] and the E2-type glenoids, which is a moderate level of E-type erosion, most accurately represents the mechanism or erosion described above.

Gilot[9] describes how erosion in the presence of RTSA can be treated through different reaming techniques, the use of bone grafts, or the use of augmented implants. While these methods are currently used to treat glenoid erosion, their success and failures are in the initial stages of documentation, and decisions on the best method of treatment are inconclusive. In addition, the results are all reported based on true patient outcomes rather than predictor experiments, however experimental outcomes can be vital in understanding causes of failure or success.

Implant fixation is a primary concern when trying to predict the success of glenoid implants, and an important variable that can affect glenoid component fixation is micromotion at the bone-implant interface. Glenoid components are notorious for loosening in both TSA and RTSA,[3,4,8,16] and research has shown that good initial implant

fixation can lead to better implant outcomes. Implants are often coated with a porous material that promotes bone ingrowth. Pilliar et al.[24] were the first to identify that a threshold level of implant-bone micromotion >150µm resulted in poor or dysfunctional bone ingrowth and implant fixation due to the formation of dense fibrous tissues. However, studies by Pilliar et al.[24] and Jasty et al.,[14,15] have shown that micromotion <60µm can achieve bone ingrowth even though there is still formation of fibrous tissue. More recently, Harman et al.[12] examined the level of micromotion in commercial RTSA glenoid baseplates and found that the baseplates with <150µm reported good short-term outcomes in the literature.

In this finite element study, we established a baseline for micromotion that occurs with the use of a standard RTSA baseplate in patients with superiorly eroded glenoids. We quantified the tangential motion of the baseplate, and the liftoff of the baseplate from the glenoid. We will also examine the effective load transfer area (ELTA) of the standard baseplate, that is the total backside contact of the baseplate participating in load transfer.

3.2 Methods and Materials

Seven patient CT scans, (mean age 68.8 ranging from 56 to 78, with E2 glenoid inclinations ranging from 10° to 19°) for patients scheduled to undergo RTSA, were used to create 3D finite element models. All CT scans used were the most recently available scans pre-operation.

3.2.1 Scapula Model Generation

The CT images were compiled in Mimics imaging processing software (Materialise, Belgium), and scapula were isolated from other bony structures through a combination of bone thresholding via Hounsfield units (HU) and manual separation of bones, similar to the method used by Bryce et al.[5] Manual separation was required where contact between the humerus, and the acromion and/or glenoid occurred. The complete three-dimensional scapula model was then smoothed to reduce noise from the CT images. The scapula was exported as a stereolithography (STL) file into MeshLab (Visual Computing Lab – ISTI – CNR, Italy) which was used to reduce the number of faces on the scapula to 10 000, which

allows for manipulation of the models in Solidworks (SOLIDWORKS Corp - Dassault Systemes, USA).

Each scapula was imported into Solidworks, and the coronal, sagittal, and transverse scapular planes were used to position and align a simplified glenoid RTSA baseplate (Figure 3-1). The glenoid baseplate diameter was either 25mm or 29mm based on patients' shoulder size, and consisted of a solid titanium alloy core with a 0.75mm layer of porous titanium alloy on the backside and central peg of the baseplate. In all cases, the baseplates were implanted with 0° version and inclination. The baseplates were medialized in 0.25mm increments until full backside contact was achieved and were then positioned as inferiorly as possible, to simulate avoidance of scapular impingement. The average amount of medialization to achieve full backside contact was 5.61±1.46mm (4.25-7.75mm). Screw fixation was not included in this study in an effort to examine only the effects of baseplate geometry.

With the implant in position, the scapula model was "reamed" using a larger diameter baseplate. The positioned implant was exported as a STEP214 file to preserve implant positioning relative to the scapula, and the scapula was exported as a STL file.

3.2.2 Finite Element Modeling

The reamed scapula and the glenoid baseplate were imported into ABAQUS (SIMULIA – Dassault Systemes, USA) computer-aided engineering (CAE) software to be meshed. All models and testing were done under static, implicit analysis. Linear solid tetrahedral elements (C3D4) were used on the scapula to model its complex geometry, and on the implant to provide some level of mesh congruency between the implant and the reamed glenoid surface. A mesh convergence analysis was performed and a 0.75mm mesh was used for the entirety of the baseplate and for the surfaces of the scapula in contact with the baseplate. From these surfaces, the mesh size was gradually increased up to 2mm as the elements move medially towards the edge of the scapula. These volumetric, scapular meshes were saved and exported as ABAQUS input files. The total model size was approximately 75 000 elements for the baseplates, and up to 392 000 elements for the scapula.

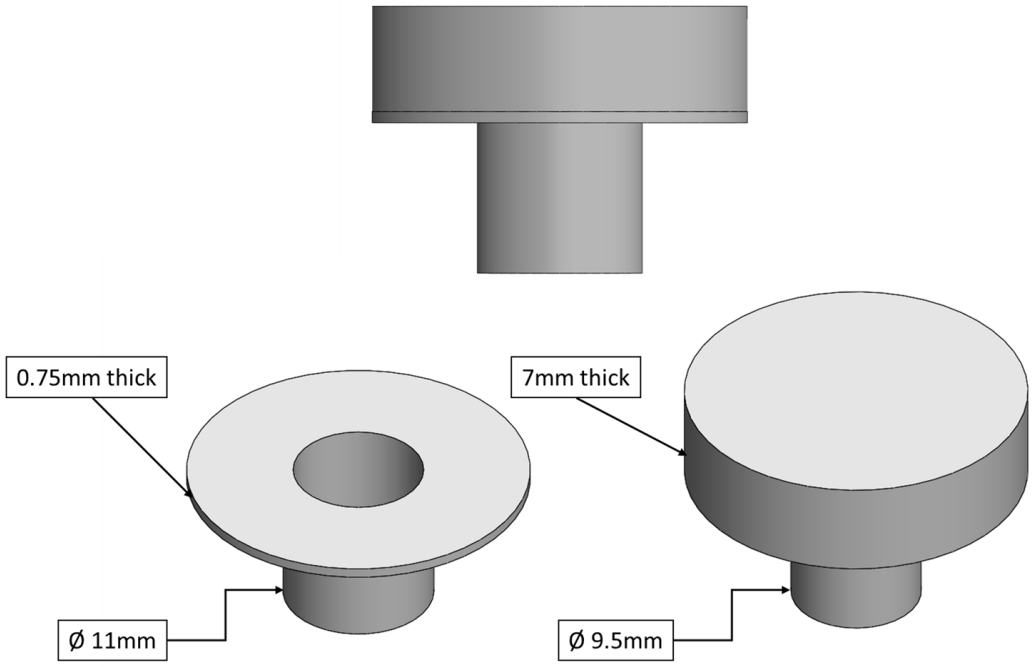

Figure 3-1 – Simplified CAD model of a standard glenoid baseplate

Diameter of the baseplate was 25mm (shown above) or 29mm depending on the patient's size. Shown on the left is the porous metal layer that covers the back of the implant. Notice that it increases the diameter of the central peg by 1.5mm.

Using these input files, material properties were applied to the scapular mesh using Mimics image processing software. Density was calculated linearly based on CT scan Hounsfield units and Young's modulus was calculated using the relationship:

$$E = 8920\rho_{app}^{1.83} \qquad \text{Equation 3-1}$$

from Morgan et al.,[23] where ρ_{app} is the apparent density of bone. The conversion from Hounsfield units to density can vary based upon CT scan settings. However, the settings for this study were the same for all specimens. The implant was assigned uniform material properties of Ti-6Al-4V-ELI, and the porous coating was given a compressive young's modulus of 2.3GPa, and Poisson's ratio of 0.34. No gap between the baseplate and bone was modeled. Friction at the baseplate-bone interface was assigned a value of 0.88[10] for a

penalty contact model. The scapulae were fixed at the medial edge of the scapula to simulate typical experimental test setup.

3.2.3 Testing Protocol and Outcome Variables

The implant was loaded to simulate abduction 15° to 90°, at 15° intervals, such that the applied force passed through the center of rotation of the glenosphere (Figure 3-2 and Table 3-1). Applied loads were based on a previous *in-vitro* cadaveric study, which used an instrumented RTSA to measure joint reaction forces.[19]

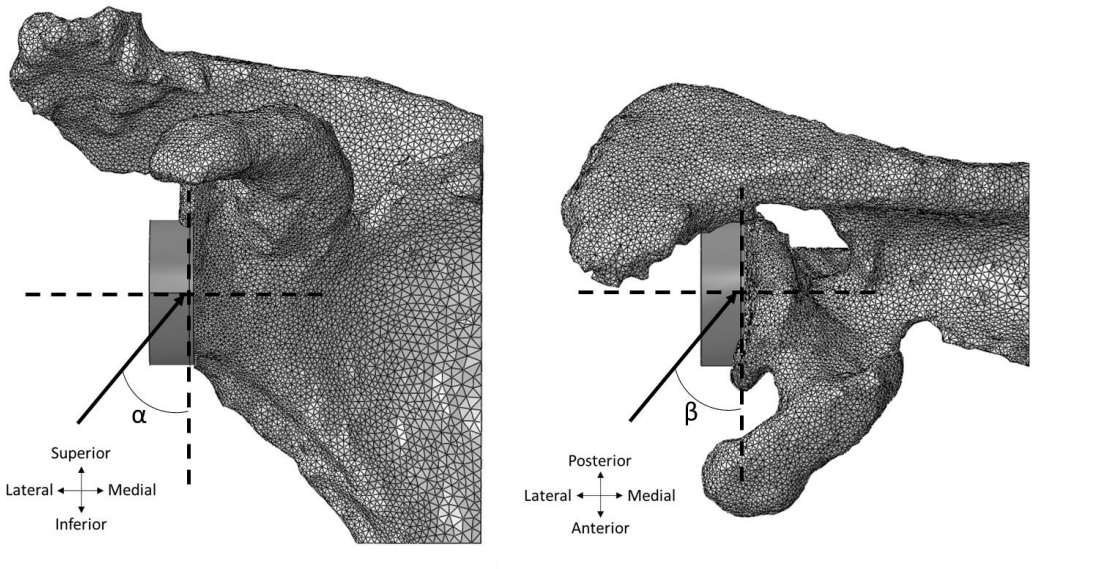

Figure 3-2 - Visualization of the resultant load direction

Implant load vector illustrating the angles in the sagittal plane (α), and in the transverse plane (β). Resultant load magnitude and angles as a function of abduction shown in Table 1.

Table 3-1 - Load profile as a function of abduction angle (Figure 3-2)

Abduction Angle [deg]	Load [N]	α [deg]	β [deg]
15	185	47	25
30	311	48	27
45	346	51	24
60	376	57	21
75	398	64	16
90	394	73	12

All outcome variables were extracted from the ABAQUS data files using python macros, and the resulting data sets were manipulated and interpreted using MATLAB (MathWorks, USA). The top and bottom 0.5% of data for all outcome variables was trimmed to remove the effect of any singular values of extreme maximums or minimums on the outcomes measured. Maximum micromotion was defined as the maximum relative motion between the implant and the glenoid surfaces, and mean micromotion was defined as the mean relative motion between the implant and glenoid for all points on the baseplate backside surface. Effective load transfer area (ELTA) of the baseplate, was calculated as shown in Equation 3-2. A two-way repeated-measures analysis of variance (RM-ANOVA) was performed for tangential and normal micromotion (Figure 3-3) and a one-way RM-ANOVA was performed for effective load transfer area.

$$ELTA = \frac{Load\ Transfer\ Area}{Total\ Backside\ Contact\ Area} * 100\% \qquad \textbf{Equation 3-2}$$

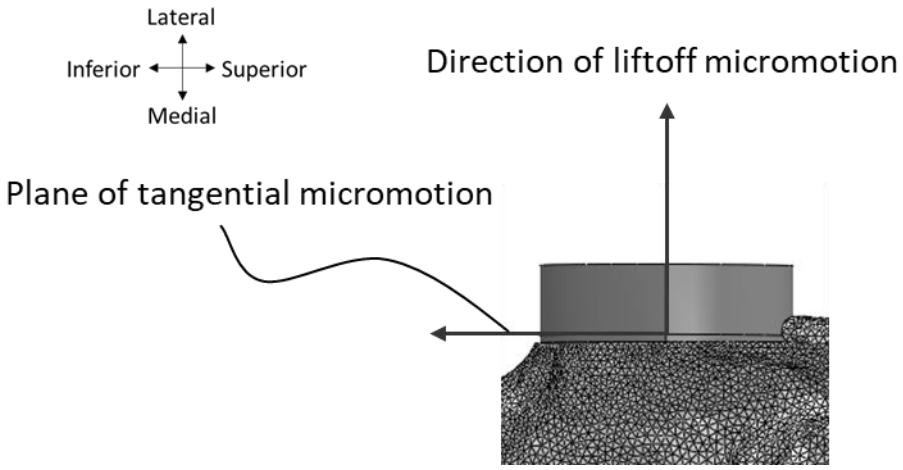

Figure 3-3 – Illustration of the direction and plane of micromotion measurements

*The above image illustrates the positive direction of the normal micromotion outcome measures (referred to as liftoff micromotion), as well as the plane within which acts the tangential micromotion (always parallel to the reamed surface/surfaces). The direction of tangential micromotion was not calculated because tangential micromotion was defined as the resultant tangential micromotion of the x-axis (out of the page) and the y-axis (to the right, in the plane of the page). This study was not concerned with directionality of tangential micromotion however it assumed to generally be in the direction of loading (*Table 3-1*).*

3.3 Results

Normal and tangential micromotion was found to be significantly affected by the quadrant where micromotion was measured, as well as abduction ($p<0.047$). While tangential micromotion resulted in very significant main effects for both parameters ($p<0.006$, observed power>0.928), the effect of quadrants on normal micromotion is more likely to provide a type II error based on the sample size used in this study ($p<0.047$, observed power<0.601). However, a larger sample size may improve the accuracy of findings pertaining to the effect of quadrants on normal micromotion.

3.3.1 Normal Micromotion

The mean normal micromotion for the anterior, inferior, posterior, and superior quadrants was 4.1±4.4μm, 4.5±3.5μm, 0.8±0.6μm, and 0.4±0.6μm respectively, and no significant differences were detected between quadrants ($p>0.099$) (Figure 3-4). Micromotion was greatest at 30° (4.1±3.0μm) of abduction compared to 45° (3.6±3.0μm, $p=0.001$), 60° (2.6±2.6μm, $p=0.009$), and 75° (1.3±1.8μm, $p=0.048$) of abduction. The largest mean normal micromotion (8.0±5.1μm) was found in the inferior quadrant at 30° of abduction. The inferior quadrant was found to contain larger mean normal micromotion than all other quadrants at all levels of abduction except, 75° and 90°, however significance was only found between the inferior and superior quadrants at 15° ($p=0.046$) and 30° ($p=0.046$) of abduction.

The maximum normal micromotion for the anterior, inferior, posterior, and superior quadrants was 7.1±6.4μm, 7.5±6.4μm, 3.2±2.0μm, and 2.9±3.0μm respectively, and no significant differences were detected between quadrants ($p>0.152$) (Figure 3-5). Micromotion was greatest at 30° (8.2±5.6μm) of abduction compared to 45° (7.4±5.7μm, $p=0.009$), 60° (5.7±5.2μm, $p=0.014$), and 75° (3.3±3.9μm, $p=0.044$) of abduction. The largest maximum normal micromotion (12.1±8.4μm) was found in the inferior quadrant at 30° of abduction. The inferior quadrant was found to contain larger maximum normal micromotion than all other quadrants at all levels of abduction except, 75° and 90°, however significance was only found between the inferior and anterior quadrants at 30° ($p=0.033$) of abduction.

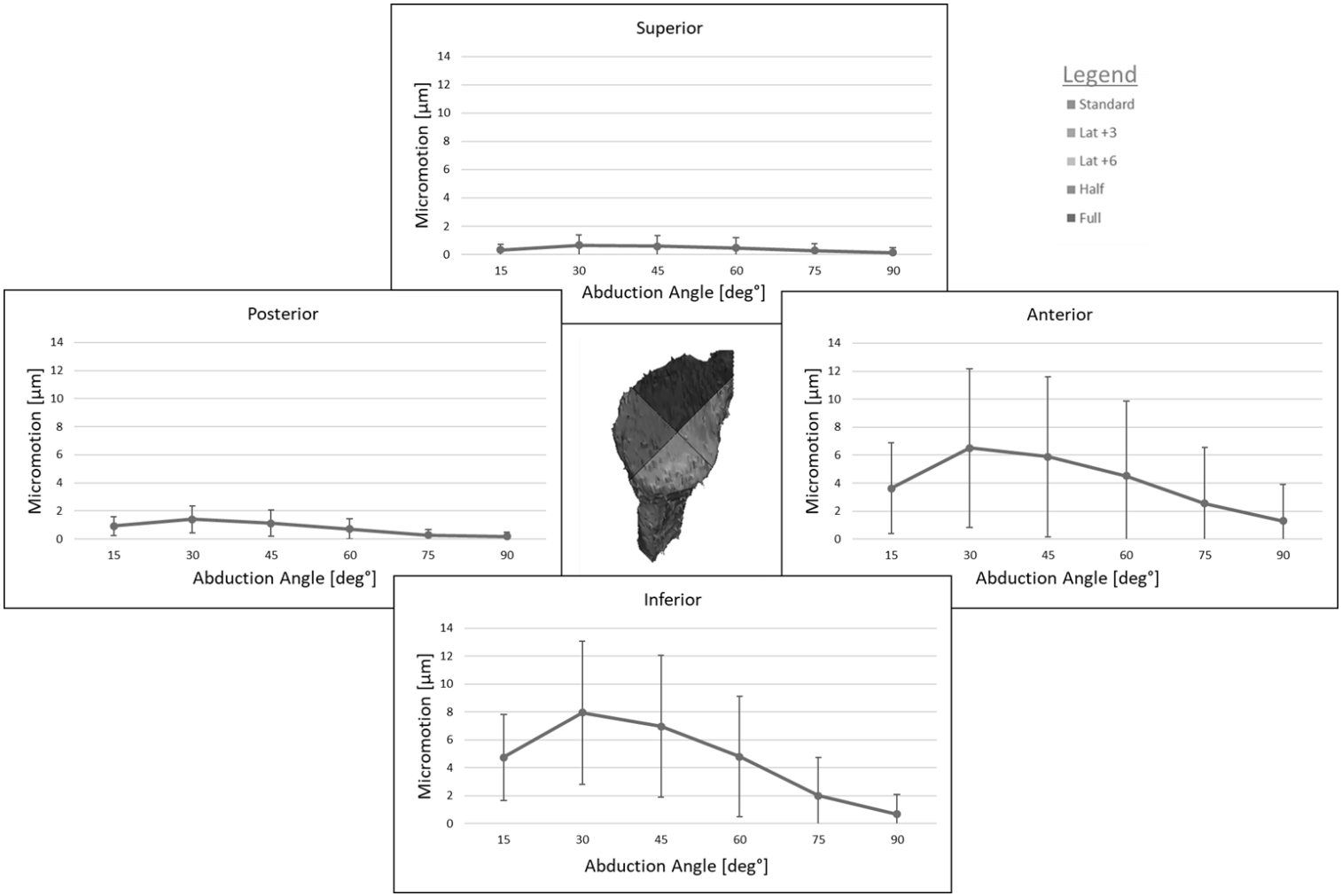

Figure 3-4 – Mean normal micromotion [µm] for various abduction angle [deg°], by quadrant of the glenoid (mean±SD)

Since we are only concerned with lift off micromotion, error bars were cut off at 0µm.

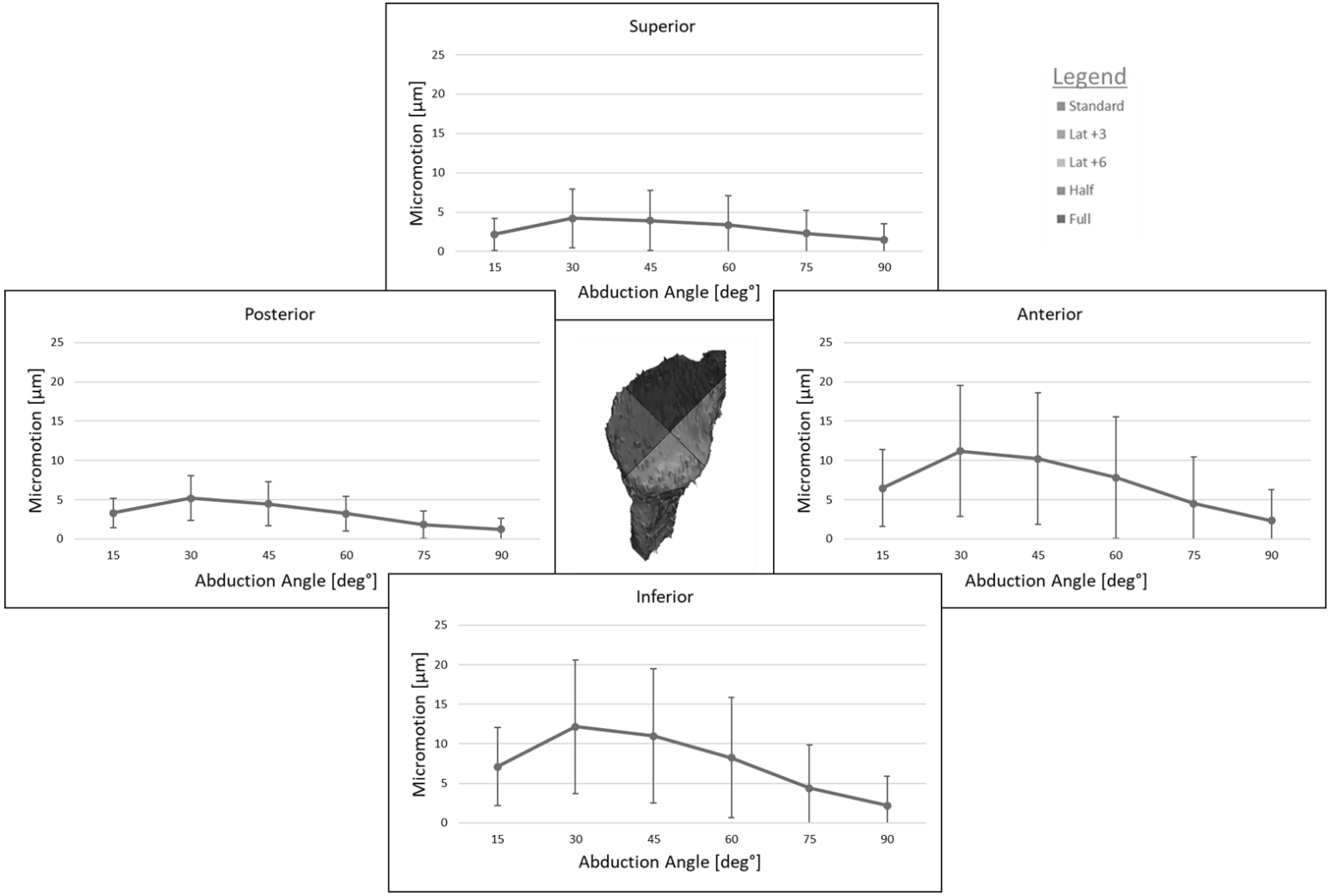

Figure 3-5 – Maximum normal micromotion [µm] for various abduction angle [deg°], by quadrant of the glenoid (mean±SD)

Since we are only concerned with lift off type normal micromotion, error bars were cut off at 0µm.

3.3.2 Tangential Micromotion

The mean tangential micromotion for the anterior, inferior, posterior, and superior quadrants was 5.1±3.0μm, 8.1±4.1μm, 4.4±1.9μm, and 2.3±1.1μm respectively (Figure 3-6). The inferior quadrant had significantly greater micromotion than anterior (p=0.011), posterior (p=0.048), and superior (p=0.022) quadrants, and micromotion in the posterior quadrant was significantly greater (p=0.008) than in the superior quadrant. Micromotion was greatest at 30° (6.2±2.8μm) and 45° (6.1±3.0μm) of abduction compared to 60° (5.5±2.9μm, p=0.03/0.017), 75° (4.5±2.6μm, p=0.015/0.023), and 90° (3.8±2.2, p=0.019/0.03) of abduction. The largest mean tangential micromotions (10.1±4.6μm and 10.0±4.8μm) were found in the inferior quadrant at 30° and 45° of abduction, respectively. The inferior quadrant was found to have significantly higher mean tangential micromotion than all other quadrants at 15° (p=0.009 to 0.024), 30° (p=0.008 to 0.028), and 45° (p=0.011 to 0.035), and was significantly higher than the anterior quadrant for all levels of abduction (p=0.008 to 0.018).

The maximum tangential micromotion for the anterior, inferior, posterior, and superior quadrants was 7.2±3.8μm, 9.3±4.8μm, 8.6±4.8μm, and 4.5±2.5μm respectively (Figure 3-7). The inferior quadrant had significantly greater micromotion than anterior (p=0.034), posterior (p=0.032), and superior (p=0.028) quadrants. Micromotion at 30° of abduction (9.0±4.3μm) was significantly higher than 15° (5.5±2.5μm, p=0.049), 75° (6.7±4.1μm, p=0.026), and 90° (5.9±3.8μm, p=0.026) of abduction. The largest maximum tangential micromotions (11.4±5.3μm and 11.3±5.6μm) were found in the inferior quadrant at 30° and 45° of abduction, respectively. The inferior quadrant was found to have significantly higher maximum tangential micromotion than all other quadrants at 15° (p=0.016 to 0.033), 30° (p=0.017 to 0.04), 45° (p=0.021 to 0.043), and 60° (p=0.029 to 0.047), whereas no significant difference was found at 75° and 90° of abduction.

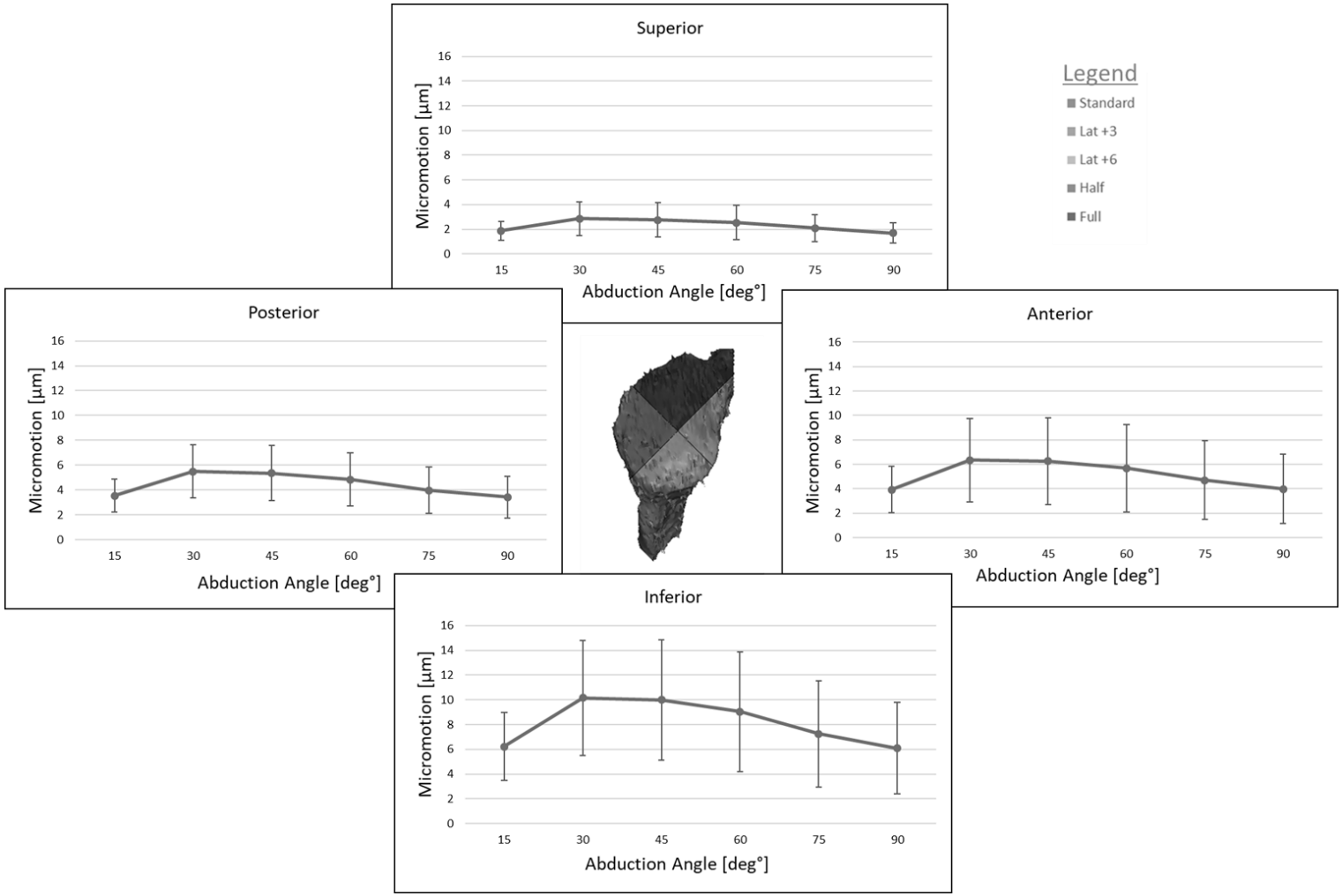

Figure 3-6 – Mean tangential micromotion [µm] for various abduction angles [deg°], by quadrant of the glenoid (mean±SD)

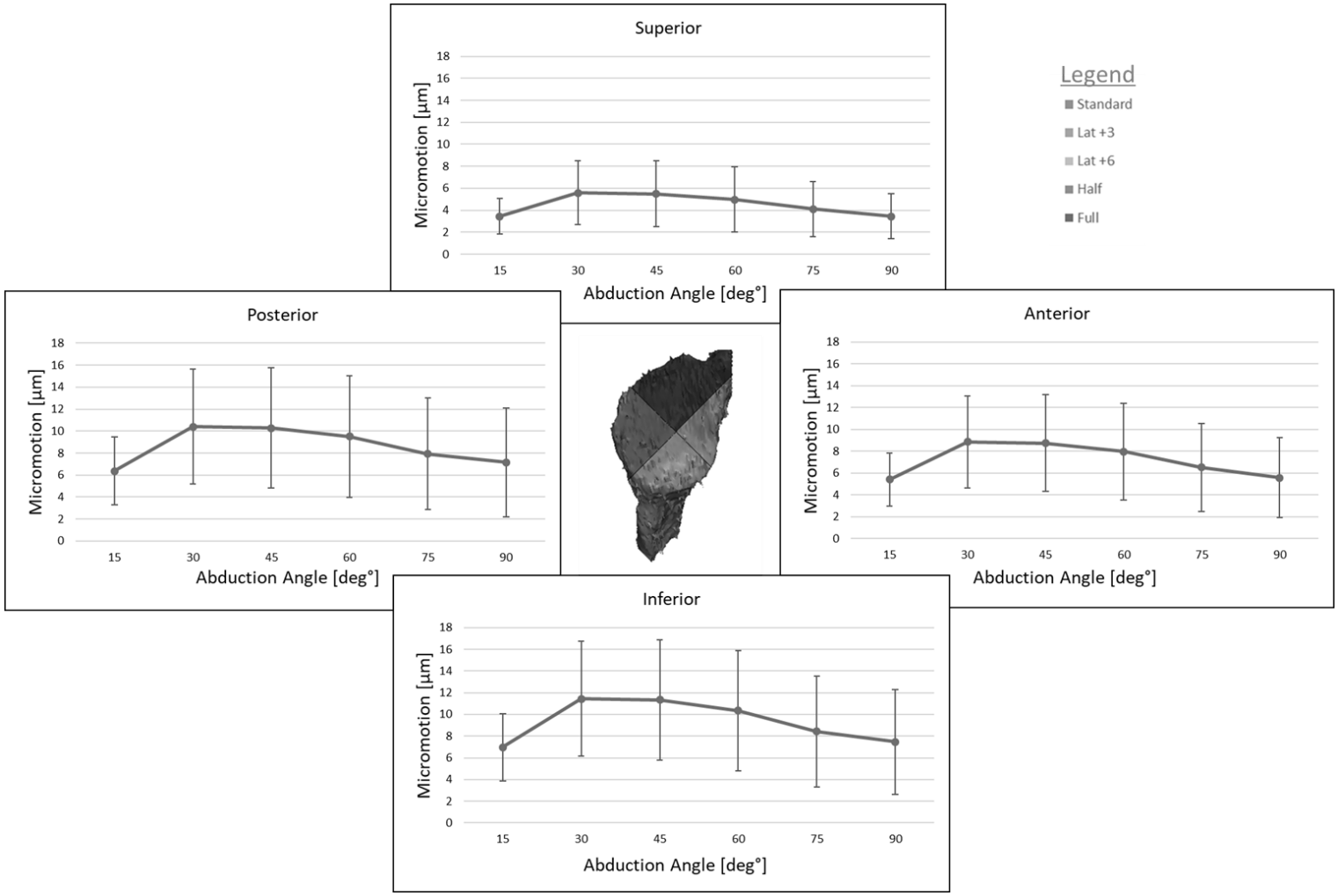

Figure 3-7 – Maximum tangential micromotion [µm] for various abduction angles [deg°], by quadrant of the glenoid (mean±SD)

3.3.3 Effective Area of Load Transfer

The effective load transfer area (ELTA) was assessed by comparing the maximum possible area of baseplate contact (excluding the central peg) against the contact area transferring load between the implant and the glenoid for each angle of abduction. As shown in Figure 3-8**,** it was found that the percentage of baseplate contact increased with increasing abduction, however the only significant difference between levels of abduction was between 75° and 90° of abduction (p=0.037).

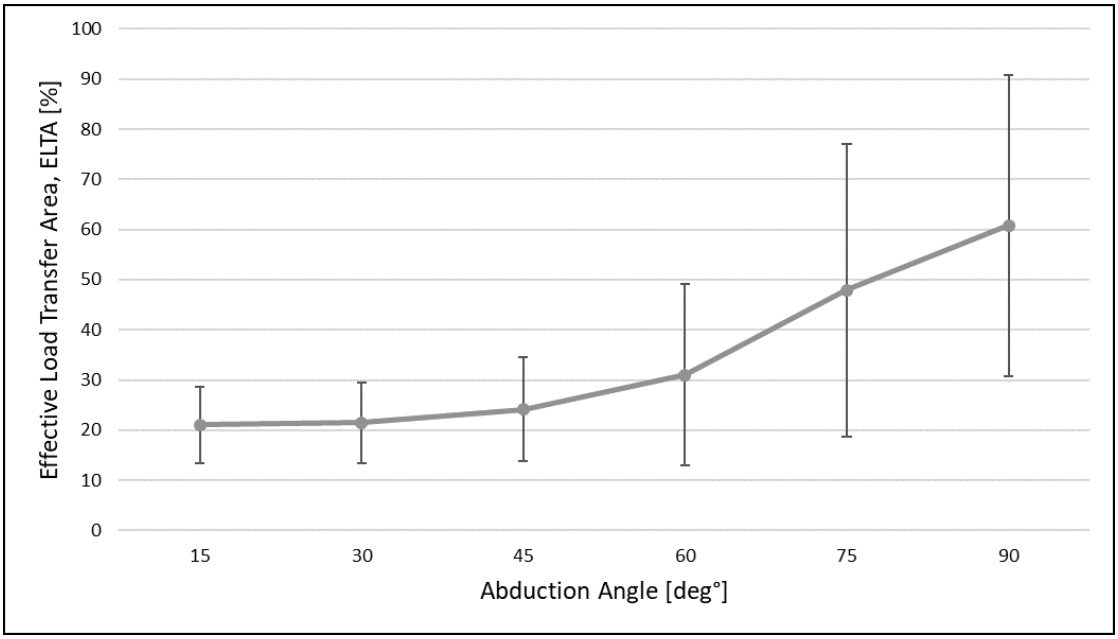

Figure 3-8 - Percentage of effective load transfer area, ELTA [%] (Mean±SD) for various abduction angles [deg°]

ELTA is defined as the percentage of area of the underside of the baseplate that participated in load transfer to the glenoid. It was not adjusted to account for differences in unloaded contact area due to differing glenoid sizes and amounts of reaming.

3.4 Discussion

The objective of this work was to establish a baseline for the performance of a standard baseplate used in patients with E2-type glenoid erosions. Studies have shown that obtaining early bone ingrowth onto the implant is important in increasing the odds of successful implant fixation.[12,14,15,24] Bony ingrowth depends on micromotion between the bone and the implant, and in this study, we quantified which regions and levels of abduction produced the highest levels of micromotion.

While the inferior quadrant generally produced the highest level of micromotion, both in terms of implant lift-off and tangential motion, significance was found mostly for tangential motion. Normal micromotion generally had lower levels of micromotion and higher standard deviation influencing the significance of the results. It is possible that this occurred because any significant lift off micromotion was occurring near the edge of the implant and therefore large motion was localised to the edges. On the other hand, tangential motion affects the baseplate more uniformly and so resulted in less deviation between patients. As far as the overall magnitudes of micromotion, more baseplate liftoff allows for higher levels of tangential motion, arising from the decrease in frictional forces. That said, the highest value of micromotion found was 12.1±8.4μm for liftoff in the inferior quadrant.

The general trend for abduction as it was simulated from 15° to 90°, showed that 30° of abduction always resulted in the most micromotion. A study by Gutierrez et al.[11] showed similar results, with baseplate motion peaking at 30° of abduction, however their study stopped at 60° abduction. Increasing abduction resulted in decreasing micromotion, except for the change from 15° to 30° of abduction. If we consider micromotion as a function of abduction, there are two factors to account for: magnitude of the joint reaction force, and ELTA. In our study, at 15° abduction, ELTA is at its lowest, which would result in more micromotion, however since the loads are small, it does not result in peak micromotion values. At 30° abduction, the load increases significantly and still has low ELTA, therefore resulting in more micromotion. The magnitude of joint force can affect the overall magnitude of the micromotion, while the ELTA affects micromotion by improving the ability of the implant to distribute stress into the osseous foundation. Although we did not provide a statistical relationship between the magnitude of the joint reaction force and

ELTA, there seems to be an important interaction between them and it should be studied further. It should also be noted that not all baseplates were able to achieve full baseplate contact during implantation due to small scapula, or reduction in cross-sectional area of the scapular neck with medialization of the implant. This was not of any concern because the portions of the baseplate with no glenoid coverage and the areas of load transfer were exclusive, but it remains an area of improvement for future studies.

Gutierrez et al.[11] examined glenosphere motion for various implant positions, and in neutral, found that micromotion peaked at 30° abduction, as in our study. However, Kwon et al.[18] studied joint loads and micromotion in cadaveric specimen and found micromotion for 4 different standard RTSA implants peaked at 60° of abduction. This was based on the loads found in their study which only simulated deltoid loads, within the scapular plane. However, if we compare the load profile of our study to the load profile used by Kwon et al.,[18] we find that in their study the direction of load vectors at 60° were similar to the load direction in the present study at 30°, indicating that our measurements of micromotion peaked at the same load vector angle rather than the same level of abduction. Kwon et al.[18] also examined normal micromotion by quadrants and, contrary to our study, found the highest levels of micromotion in the superior and posterior quadrants.

In the previous chapter, which examined the morphology of E2-type glenoids, we found that the inferior quadrant contained significantly less dense cortical and cancellous bone than all other quadrants. Results for the anterior and posterior quadrant varied slightly as to which region was denser, but the superior quadrant was found to be the densest. Other studies have also shown that these regions contain the densest bone,[17,20] even in glenoids without defects, and others still have shown that these regions of bone tend to be the stiffest.[1,17] These results are in agreement with the regional differences in micromotion found in the current study, showing that the regions with the densest bone resulted in the least amount of micromotion. This can partially be explained by tilting of the baseplate produced by loading of the arm during abduction. The baseplate tilts and compresses the superior aspect of the glenoid, while the inferior portion of the baseplate lifts off from the glenoid surface. The denser bone in the superior aspect of the glenoid resists compression from the baseplate, however the inferior aspect undergoes liftoff so the bone in the inferior

region does not contribute to resisting baseplate motion. If fixation screws were introduced, the inferior aspect of the baseplate may be more capable of resisting liftoff micromotion.

Our loads also differed from other studies in terms of magnitude and direction, which may explain why our reported micromotion was smaller than what has been found in the literature. The loading protocol based on Anglin et al.[2,28] is often used to assess glenoid baseplate fixation and involves a 756N compressive force, followed by a cyclic shear force which in some cases is cycled up to 756N, all applied in the scapular plane. This results in peak resultant loads of greater than 1000N whereas our resultant loads never exceeded 400N, was non-cyclic, and was not restricted to the scapular plane. Micromotion for Anglin-type loading is generally reported to start around 50μm, and can reach as high as 200μm.[12,13,27] Others have achieved drastically different results, reporting as little as 8μm and well upwards of 250μm, using very similar loading protocols, as well as using identical bone foams in place of cadavers.[21,26] One main difference between our loading and Anglin-type loading is that Anglin-type loading was designed for loosening of TSA glenoid components. Loading described in past studies also only load the joint at load vector angles of between 45° and 60° maximum, which is less than what was tested here.[2,12,13,21,27]

The E-2 type glenoids provide a challenge for proper fixation of RTSA baseplates, and put patients at an increased risk of early implant loosening. Although treatment tends to address the defect in the superior portion of the glenoid, there may also be other ways of improving baseplate fixation in these patients. The inferior region of the glenoid is a potential weak link for baseplate fixation, and focus on good fixation in this area may improve implant outcomes. Focusing on the defect region however should not be ignored. Improved stability of the superior portion of the glenoid-baseplate interface may reduce liftoff occurring in the inferior region, due to the “rocking horse” phenomenon,[8] also resulting in better fixation.

This study was limited in its ability to draw comparison to pre-existing literature. Only a few studies have examined the effect of superior bone defects on glenoid fixation for RTSA and none have been performed on cadavers or accurate patient models. In addition, our model parameters such as screw fixation and applied loads differed from those in previous

studies. Our sample size of 7 patients may have also been too small to allow us to draw statistical conclusions from the variations in liftoff micromotion between quadrants.

This study also has significant strengths. As far as we are aware we are the first to study implant fixation for superior glenoid defects using accurate patient models. Our loads are physiologically based and, as such they are more representative of *in vivo* mechanics than would be a generalized loading procedure. In addition, excluding the use of fixation screws reduced the complexity of the finite element model. Also, we used a repeated-measures approach on seven specimens which is more robust than a variety of other finite element studies that are confined to one specimen or model.

Suggestions for future work include modifying implant design to improve micromotion in the inferior quadrant, improve stability in the superior quadrant, while taking into account realistic surgical limitations such as bone removal and maintaining appropriate medialization of the baseplate. Examining the interaction between the ELTA and load magnitudes as a function of abduction will also be of interest for baseplate fixation in all RTSA patients.

3.5 References

1. Anglin C, Tolhurst P, Wyss UP, Pichora DR. Glenoid cancellous bone strength and modulus. J. Biomech. 1999 Oct;32(10):1091–1097. doi:10.1016/S0021-9290(99)00087-1

2. Anglin C, Wyss UP, Pichora DR. Glenohumeral contact forces. Proc. Inst. Mech. Eng. [H]. 2000 Jun 1;214(6):637–644. doi:10.1243/0954411001535660

3. Boileau P, Avidor C, Krishnan SG, Walch G, Kempf J-F, Molé D. Cemented polyethylene versus uncemented metal-backed glenoid components in total shoulder arthroplasty: A prospective, double-blind, randomized study. J. Shoulder Elbow Surg. 2002 Jul;11(4):351–359. doi:10.1067/mse.2002.125807

4. Bonnevialle N, Melis B, Neyton L, Favard L, Molé D, Walch G, et al. Aseptic glenoid loosening or failure in total shoulder arthroplasty: revision with glenoid reimplantation. J. Shoulder Elbow Surg. 2013 Jun;22(6):745–751. doi:10.1016/j.jse.2012.08.009

5. Bryce CD, Pennypacker JL, Kulkarni N, Paul EM, Hollenbeak CS, Mosher TJ, et al. Validation of three-dimensional models of in situ scapulae. J. Shoulder Elbow Surg. 2008 Sep 1;17(5):825–832. doi:10.1016/j.jse.2008.01.141

6. Ecklund KJ, Lee TQ, Tibone J, Gupta R. Rotator cuff tear arthropathy. J. Am. Acad. Orthop. Surg. 2007;15(6):340–349.

7. Frankle MA, Teramoto A, Luo Z-P, Levy JC, Pupello D. Glenoid morphology in reverse shoulder arthroplasty: Classification and surgical implications. J. Shoulder Elbow Surg. 2009 Nov;18(6):874–885. doi:10.1016/j.jse.2009.02.013

8. Franklin JL, Barrett WP, Jackins SE, Matsen III FA. Glenoid loosening in total shoulder arthroplasty: Association with rotator cuff deficiency. J. Arthroplasty. 1988;3(1):39–46. doi:10.1016/S0883-5403(88)80051-2

9. Gilot GJ. Addressing glenoid erosion in reverse total shoulder arthroplasty. Bull. Hosp. Jt. Dis. 2013. 2013;71 Suppl 2:S51-53.

10. Grant JA, Bishop NE, Götzen N, Sprecher C, Honl M, Morlock MM. Artificial composite bone as a model of human trabecular bone: The implant–bone interface. J. Biomech. 2007 Jan;40(5):1158–1164. doi:10.1016/j.jbiomech.2006.04.007

11. Gutiérrez S, Greiwe RM, Frankle MA, Siegal S, Lee III WE. Biomechanical comparison of component position and hardware failure in the reverse shoulder prosthesis. J. Shoulder Elbow Surg. 2007 May;16(3, Supplement):S9–S12. doi:10.1016/j.jse.2005.11.008

12. Harman M, Frankle M, Vasey M, Banks S. Initial glenoid component fixation in "reverse" total shoulder arthroplasty: A biomechanical evaluation. J. Shoulder Elbow Surg. 2005 Jan;14(1, Supplement):S162–S167. doi:10.1016/j.jse.2004.09.030

13. Hopkins AR, Hansen UN, Bull AMJ, Emery R, Amis AA. Fixation of the reversed shoulder prosthesis. J. Shoulder Elbow Surg. 2008 Nov;17(6):974–980. doi:10.1016/j.jse.2008.04.012

14. Jasty M, Bragdon C, Burke D, O'Connor D, Lowenstein J, Harris WH. In vivo skeletal responses to porous-surfaced implants subjected to small induced motions. J. Bone Joint Surg. Am. 1997 May;79(5):707–714.

15. Jasty M, Bragdon CR, Zalenski E, O'Connor D, Page A, Harris WH. Enhanced stability of uncemented canine femoral components by bone ingrowth into the porous coatings. J. Arthroplasty. 1997 Jan;12(1):106–113.

16. Jean K. Classifications of glenoid dysplasia, glenoid bone loss and glenoid loosening: a review of the literature. Eur. J. Orthop. Surg. Traumatol. 2013 Apr;23(3):301–310. doi:10.1007/s00590-012-1119-4

17. Kalouche I, Crépin J, Abdelmoumen S, Mitton D, Guillot G, Gagey O. Mechanical properties of glenoid cancellous bone. Clin. Biomech. 2010 May;25(4):292–298. doi:10.1016/j.clinbiomech.2009.12.009

18. Kwon YW, Forman RE, Walker PS, Zuckerman JD. Analysis of reverse total shoulder joint forces and glenoid fixation. Bull. NYU Hosp. Jt. Dis. 2010 Oct;68(4):273.

19. Langohr GDG, Giles JW, Athwal GS, Johnson JA. The effect of glenosphere diameter in reverse shoulder arthroplasty on muscle force, joint load, and range of motion. J. Shoulder Elbow Surg. 2015 Jun;24(6):972–979. doi:10.1016/j.jse.2014.10.018

20. Lehtinen JT, Tingart MJ, Apreleva M, Warner JJP. Total, trabecular, and cortical bone mineral density in different regions of the glenoid. J. Shoulder Elbow Surg. 2004;13(3):344–348. doi:10.1016/j.jse.2004.01.012

21. Martin EJ, Duquin TR, Ehrensberger MT. Reverse total shoulder glenoid baseplate stability with superior glenoid bone loss. J. Shoulder Elbow Surg. 2017 Oct;26(10):1748–1755. doi:10.1016/j.jse.2017.04.020

22. Matsen FA, Boileau P, Walch G, Gerber C, Bicknell RT. The Reverse Total Shoulder Arthroplasty. J Bone Jt. Surg Am. 2007 Mar 1;89(3):660–667.

23. Morgan EF, Bayraktar HH, Keaveny TM. Trabecular bone modulus–density relationships depend on anatomic site. J. Biomech. 2003 Jul 1;36(7):897–904. doi:10.1016/S0021-9290(03)00071-X

24. Pilliar RM, Lee JM, Maniatopoulos C. Observations on the effect of movement on bone ingrowth into porous-surfaced implants. Clin. Orthop. 1986 Jul;(208):108–113.

25. Sirveaux F, Favard L, Oudet D, Huquet D, Walch G, Mole D. Grammont inverted total shoulder arthroplasty in the treatment of glenohumeral osteoarthritis with massive rupture of the cuff RESULTS OF A MULTICENTRE STUDY OF 80 SHOULDERS. J. Bone Joint Surg. Br. 2004;86(3):388–395.

26. Stroud NJ, DiPaola MJ, Martin BL, Steiler CA, Flurin P-H, Wright TW, et al. Initial glenoid fixation using two different reverse shoulder designs with an equivalent center of rotation in a low-density and high-density bone substitute. J. Shoulder Elbow Surg. 2013 Nov;22(11):1573–1579. doi:10.1016/j.jse.2013.01.037

27. Virani NA, Harman M, Li K, Levy J, Pupello DR, Frankle MA. In vitro and finite element analysis of glenoid bone/baseplate interaction in the reverse shoulder design. J. Shoulder Elbow Surg. 2008 May;17(3):509–521. doi:10.1016/j.jse.2007.11.003

28. ASTM F2028-14 Standard Test Methods for Dynamic Evaluation of Glenoid Loosening or Disassociation, ASTM International, West Conshohocken, PA, 2014, https://doi-org.proxy1.lib.uwo.ca/10.1520/F2028-14

Chapter 4

4 Micromotion of Augmented and Lateralized Glenoid Baseplates in the Presence of E2 Erosion

OVERVIEW

As previously documented, glenoid erosion can be particularly debilitating in the everyday functions of the shoulder. To address erosion in the glenoid, modified glenoid reaming techniques, bone grafting, lateralized implants, and augmented implants have been used, however a lack of literature exists on the successes and failures of these methods. Now that a baseline has been established for the performance of a standard RTSA baseplate, this study examines the fixation of augmented and lateralized baseplates in E2-type glenoids.

(Some aspect of the Introduction and Methods have been covered in Chapters 1, 2, & 3, but are repeated here due to the "Integrated Article" format of this thesis, to ensure that this chapter stands alone as a publishable paper.)

4.1 Introduction

As previously documented, the presence of glenoid defects increases the difficulty required to achieve positive outcomes in shoulder arthroplasty,[16] and patients suffering from arthritis are more susceptible to osseous erosion occurring from bone on bone contact and irregular joint articulations.[5,22]

Treatment of glenoid erosion depends on the severity of the erosion, and can differ between surgeons, however, minimizing the amount of bone removal while achieving good implant fixation is generally the desired outcome.[18] The use of bone grafts in combination with regular implants has been documented but results seem to be inconclusive with regard to its effectiveness.[14,16,26] Eccentric or off-axis reaming has been described as another potential method to correct for excessive glenoid inclination or version.[4,6,13,21] Unfortunately, eccentric reaming removes a more than ideal amount of bone, while off-axis reaming does not correct for version or inclination without the aid of a modified implant.

When implants are modified to address osseous defects, they are referred to as augmented implants. Augmented implants for glenoid defects are currently available, but the clinical outcomes of these implants, particularly for reverse total shoulder arthroplasty (RTSA), are still considered short-term.[14,27] In addition, most of the literature reports solely on the functional outcome of the implant. There are however a few studies that do examine augmented implant fixation for RTSA.[4,21]

A particular type of glenoid erosion prevalent in patients requiring RTSA is superior glenoid erosion[3]. Sirveaux et al.[23] classified superior glenoid erosion into types E0, E1, E2, and E3, where E2-type glenoids represents a mild level of glenoid erosion. Because erosion in E2-type glenoids is apparent, but native glenoid bone remains, E2-type glenoids are good descriptors of the process of superior glenoid erosion (Figure 1-8). Patients requiring RTSA typically suffer from rotator cuff tears which can often lead to superior migration of the humeral head. In combination with glenohumeral arthritis, this results in an irregular articulation between the glenoid and humerus, and eventually leads to superior glenoid erosion.

In the previous chapter, FEA was performed to establish baseline levels of micromotion occurring in a standard RTSA baseplate in E2-type glenoid patients. We also identified potential areas that need to be addressed to improve fixation in these patients. With this baseline established, micromotion of commercially available implant designs can be evaluated.

The objective of this study was to quantify micromotion at the glenoid-baseplate interface as it pertains to commercially available implants. This includes a standard baseplate, a full-wedge baseplate, a half-wedge baseplate, and a 3mm and 6mm lateralized standard baseplate. It is hypothesized that the distribution of loads from the augmented baseplates to the glenoid differ between implants, and that this affects the overall baseplate micromotion. It is also believed that the wedge-type baseplates will demonstrate larger amounts of tangential micromotion, due to shearing, and will have lower load transfer area. Implants with a lateralized center of rotation will result in higher amounts of normal and tangential micromotion.

4.2 Methods and Materials

Seven patient CT scans, (mean age 68.8yrs ranging from 56 to 78yrs, with glenoid inclinations ranging from 10° to 19°) for patients with E2 glenoids scheduled to undergo RTSA, were used to create 3D scapula models.

4.2.1 Scapula Model Generation

Using Mimics imaging processing software (Materialise, Belgium), 3D scapula models were created, and noise from the CT images was eliminated. The scapula was exported as a stereolithography file (STL) and the number of faces in the model were reduced to 10,000 using MeshLab (Visual Computing Lab – ISTI – CNR, Italy). This a computational requirement for use of the scapula models in Solidworks (SOLIDWORKS Corp - Dassault Systemes, USA).

4.2.2 Implant Model Creation and Positioning

The coronal, sagittal, and transverse scapular planes were used to virtually implant each of the 5 RTSA baseplates tested (Figure 4-1). The glenoid baseplates used were either 25mm

or 29mm in diameter. They generally consisted of a Ti-6AL-4V-ELI “core”, and the backside and central peg were coated in 0.75mm of porous Ti-6AL-4V-ELI (Figure 4-2). Porosity of this coating was approximately 66%. No screw holes were created in the baseplates since screw fixation was not modeled in this study.

The full-wedge baseplate consisted of a 16mm long central peg and a 15° backside surface inclination, and the half-wedge baseplate had a central peg of 10mm in length with one half of the backside surface inclined at 30°. The standard and lateralized baseplates all contained the same peg length of 10mm, however the lateralization of each baseplate was achieved by adding an additional 3mm or 6mm of porous Ti-6AL-4V-ELI to the backside of the baseplate (Figure 4-1). All peg lengths were measured from the backside of the porous titanium alloy.

Each baseplate was positioned in neutral version and inclination. The baseplates were medialized in 0.25mm increments until full backside contact was achieved. Medialization required to achieve full backside contact was 11.79±1.14mm (10-13.75mm) for the full-wedge, 8.79±0.87mm (7.75-10.5mm) for the half-wedge, and 5.61±1.46mm (4.25-7.75mm) for the lateralized and standard baseplates.

The scapulae were trimmed at 50mm medially from the sagittal plane, and 50mm inferiorly from the transverse plane. This was to eliminate parts of the scapula that were particularly thin to prevent errors during meshing of the scapula models.

Scapulae were “reamed” using baseplate models with identical geometry but larger diameters. Once positioned, each implant was imported into ABAQUS (SIMULIA – Dassault Systemes, USA) as a STEP214 file which preserves implant positioning relative to the scapula, and the scapula was imported as a STL file.

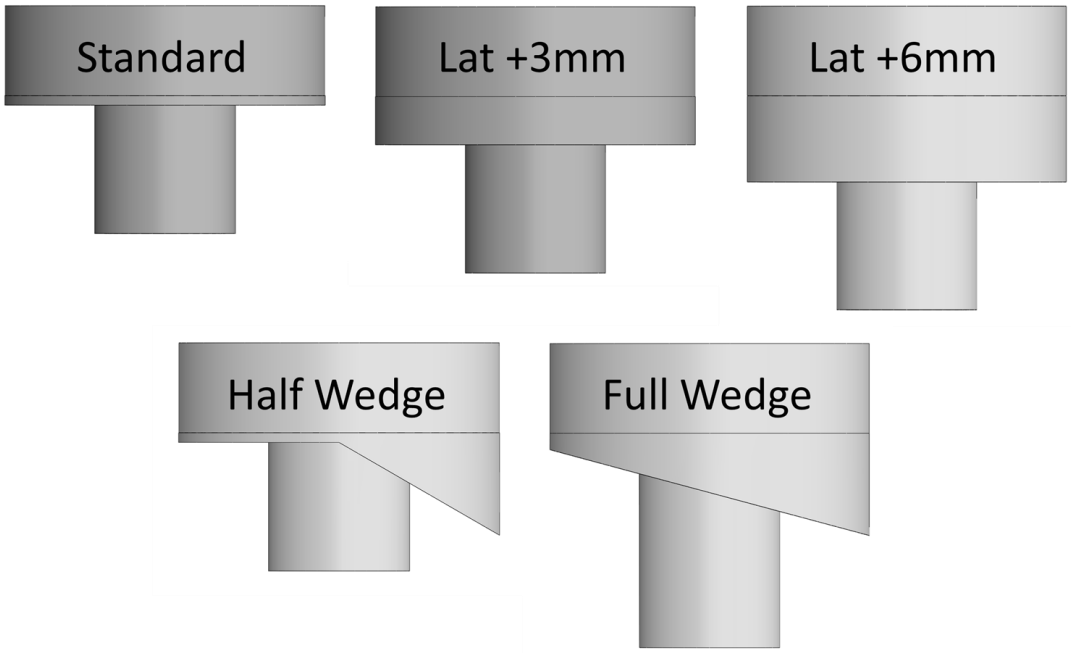

Figure 4-1 – CAD (Solidworks) models of the 5 implant models measured for implant fixation

Top (left to right): *Standard glenoid baseplate, 3mm lateralized baseplate (Lat+3mm), 6mm lateralized baseplate (Lat+6mm).*
Bottom (left to right): *Half wedge baseplate, full wedge baseplate*
Lateralization and wedge shapes were achieved by adding the corresponding thickness of porous titanium alloy.

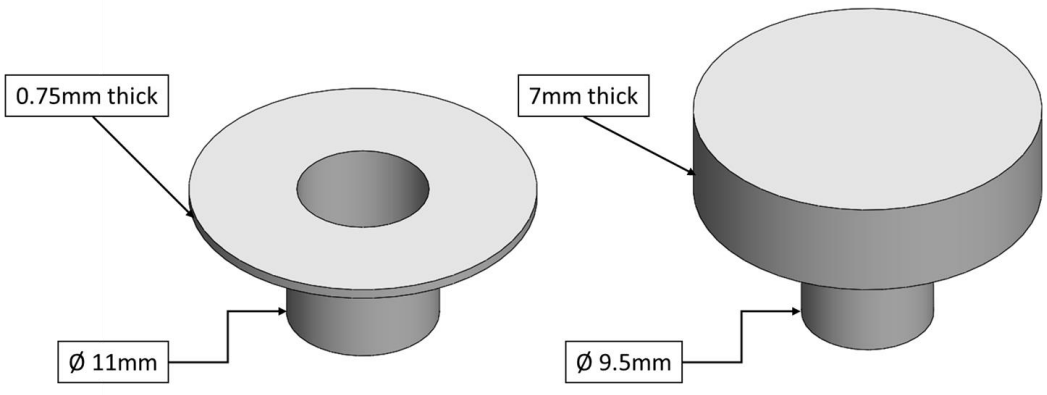

Figure 4-2 - Separate views and important dimensions for the titanium alloy core and porous backside

Left: *Porous titanium alloy backside and central peg coating. The entire coating is 0.75mm thick, except for lateralized baseplates, which have additional backside thickness.*
Right: *Ti-6AL-4V-ELI core of a 25mm standard baseplate*

4.2.3 Finite Element Modeling

Modeling was done using static, implicit analysis. The glenoid baseplates and scapula were meshed using linear solid tetrahedral elements (C3D4). The number of baseplate elements ranged from 75 000 to 130 000 elements based on implant size and type, and the number of scapula elements ranged from 282 000 to 359 000 elements based primarily on patient size. C3D4 elements were chosen to model the complex geometry of the scapula, and allowed for mesh congruency between the implant and scapular mesh.

A 0.75mm mesh size was used for the implant and for the baseplate-bone contact surfaces of the glenoid. From these surfaces, the mesh size was propagated up to 2mm at the medial border of the scapula. These mesh parameters were determined by performing a mesh convergence study. The scapular meshes were then exported to Mimics as ABAQUS input files, material properties were applied, and then brought back into ABAQUS. Each scapula model were assigned material properties based on Morgan et al.[19] (Equation 3-1) In ABAQUS, the baseplates were assigned material properties of Ti-6Al-4V-ELI and 66% porous Ti-6Al-4V-ELI, and a penalty contact model with a friction coefficient of 0.88 was modeled for a plasma coated baseplate backside on bone.[7] No gap was modeled between baseplate and bone. The scapula was bounded at the most medial edge, parallel to the sagittal plane, to simulate experimental test setup.

4.2.4 Loading Protocol and Outcome Variables

Loading was applied through location of the center of rotation of the glenosphere to simulate abduction in 15° intervals from 15° to 90°. These loads are based on a previous *in-vitro* cadaveric study, which used an instrumented implant to measure joint reaction forces.[17] The load profile of this simulation is illustrated via Figure 3-2 and Table 3-1.

Motion for each node on the baseplate backside surface, and the reamed surface of the scapula was collected from ABAQUS using python macros. Each node on the baseplate surface was then paired with the nearest point on the reamed scapular surface, and relative micromotion was calculated. After trimming the top and bottom 0.5% of results, results were processed using MATLAB (MathWorks, USA) for each combination of the 5 implants and 7 scapulae, for a total of 35 combinations. The total area of backside contact

under load was also retrieved from ABAQUS and the ELTA was calculated (see Equation 3-2) and analyzed in Microsoft Excel (Microsoft, USA).

The outcome variables for this study were maximum and mean, normal and tangential micromotion. Tangential micromotion was defined as motion of the baseplate in the plane of reaming, and normal micromotion was defined as motion of the baseplate perpendicular to the plane of reaming (Figure 3-3). Liftoff of the baseplate from the reamed surface defined the positive direction for normal micromotion. Maximum micromotion was defined as the peak micromotion recorded, after removing the top and bottom 0.5%, and mean micromotion was average relative motion of all nodes on the baseplate backside surface.

A three-way repeated-measures analysis of variance (RM-ANOVA) was performed to compare each implant, for micromotion in each of the anterior, inferior, posterior, and superior quadrants of the glenoid, at increasing levels of abduction. A two-way repeated-measures ANOVA was also performed to compare each implant at increasing levels of abduction for ELTA.

4.3 Results

The main effects of quadrants, abduction angle, and implant types were significant with regard to both normal and tangential micromotion, for mean and maximum micromotion ($p<0.004$). Observed power for all micromotion outcomes in this study was good, remaining above 0.95.

4.3.1 Normal Micromotion

4.3.1.1 Mean Normal Micromotion

Mean normal micromotion was found to be significantly less when using the standard baseplate (2.4±2.2μm), as opposed to the full-wedge (8.9±4.1μm, $p=0.006$), 3mm lateralized (4.9±3.2μm, $p=0.017$), and 6mm lateralized (8.1±4.2μm, $p=0.007$) baseplates (Figure 4-3). The half-wedge baseplate (5.7±3.7μm) also produced significantly less micromotion than the full-wedge ($p=0.002$), and the 3mm lateralized produced less micromotion than the full wedge ($p=0.018$) and 6mm lateralized ($p=0.017$).

The mean normal micromotion for the anterior, inferior, posterior, and superior quadrants was 9.9±6.4μm, 11.4±5.8μm, 2.0±1.1μm, and 0.7±0.6μm respectively. The inferior quadrant was found to have significantly more micromotion than the posterior ($p=0.021$) and superior ($p=0.015$) quadrants, and the anterior quadrant had significantly more micromotion than the superior quadrant ($p=0.046$). The superior quadrants contained significantly less micromotion than all other quadrants ($p<0.048$).

Micromotion was greatest at 30° (9.2±4.2) of abduction compared to 15° (5.5±2.5μm, $p=0.031$), 45° (8.6±4.4μm, $p=0.002$), 60° (7.0±4.1μm, $p<0.001$), 75° (4.108±3.268μm, $p=0.001$), and 90° (1.6±2.0μm, $p=0.006$) of abduction. The largest mean normal micromotion (25.2±8.9μm) occurred for the full-wedge baseplate in the inferior quadrant at 30° of abduction.

The standard baseplate resulted in the least micromotion overall compared to all other implants, with significance in all quadrants at 15°, 30°, 45°, and 60° ($p=0.001$ to $p=0.049$). Significance became less apparent with increasing abduction as higher levels of abduction tended to have low levels of micromotion in all baseplates. The full-wedge baseplate resulted in more micromotion than all baseplates with significance against the half-wedge, 3mm lateralized, and standard baseplates for all quadrants except the superior quadrant ($p=0.001$ to $p=0.049$). Once again, significance became less common with increasing abduction, with no significance occurring for any combinations at 90° abduction. The half-wedge baseplate demonstrated significantly less micromotion than the full-wedge ($p=0.001$ to $p=0.027$) in the inferior and posterior quadrants. Finally, the 3mm lateralized baseplate nearly always demonstrated significantly less micromotion than the 6mm lateralized baseplate, regionally and as a function of abduction ($p<0.001$ to $p=0.034$). As with most other trends, many significant findings were rendered insignificant with high (75°, 90°, and sometimes 60°) levels of abduction.

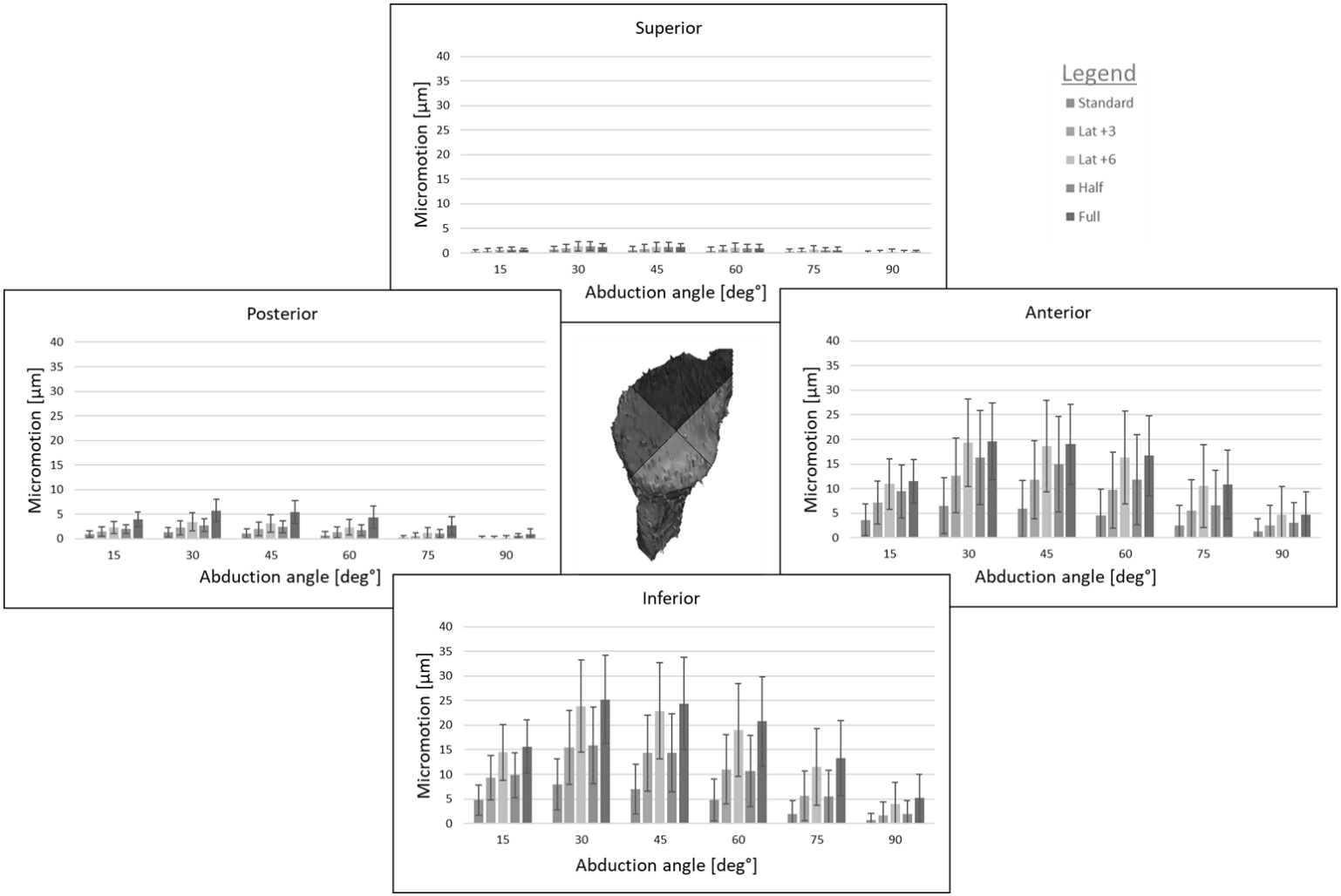

Figure 4-3 – Mean normal micromotion [µm] for various abduction angles [deg°], for each quadrant of the glenoid (Micromotion shown as mean±SD)

4.3.1.2 Maximum Normal Micromotion

Maximum normal micromotion was found to be significantly less when using the standard baseplate (5.2±4.3μm), as opposed to the full-wedge (16.2±7.2μm, p=0.004), 3mm lateralized (9.9±6.4μm, p=0.017), and 6mm lateralized (16.0±8.2μm, p=0.007) baseplates (Figure 4-4). The half-wedge baseplate (10.7±6.8μm) also produced significantly less micromotion than the full-wedge (p=0.003), and the 3mm lateralized produced less micromotion than the full wedge (p=0.026) and 6mm lateralized (p=0.003).

The maximum normal micromotion for the anterior, inferior, posterior, and superior quadrants was 16.8±9.4μm, 17.4±9.6μm, 7.2±3.3μm, and 5.0±3.7μm respectively. The inferior quadrant and anterior quadrants were found to have significantly more micromotion than the superior quadrant (p=0.016 and p=0.017 respectively).

Maximum normal micromotion was greatest at 30° (17.3±7.9μm) of abduction compared to 15° (10.3±4.6μm, p=0.03), 45° (16.3±8.1μm, p=0.002), 60° (13.4±7.8μm, p<0.001), 75° (8.3±6.2μm, p=0.001), and 90° (3.9±4.1μm, p=0.005) degrees of abduction. The largest maximum normal micromotion (35.3±14.6μm) occurred for the 6mm lateralized baseplate in the inferior quadrant at 30° of abduction.

The standard baseplate resulted in the least micromotion overall compared to all other implants, with significance in all quadrants at 15°, 30°, and 45° (p=0.001 to p=0.047). It was not significantly different than the half-wedge baseplate after 30° abduction, for the anterior and inferior quadrants. Significance became less apparent with increasing abduction as higher levels of abduction tended to have low levels of micromotion in all baseplates. The 6mm lateralized baseplate resulted in more micromotion than the 3mm lateralized and standard baseplates for all quadrants (p<0.001 to p=0.042). No significance was found for any combinations at 90° abduction. The half-wedge baseplate demonstrated significantly less micromotion than the full-wedge (p=0.002 to p=0.012) in the anterior, inferior, and posterior quadrants, across all levels of abduction. Finally, the 3mm lateralized baseplate demonstrated significantly less micromotion than the full-wedge baseplate (p=0.004 to p=0.043), except in the superior quadrant. As with most

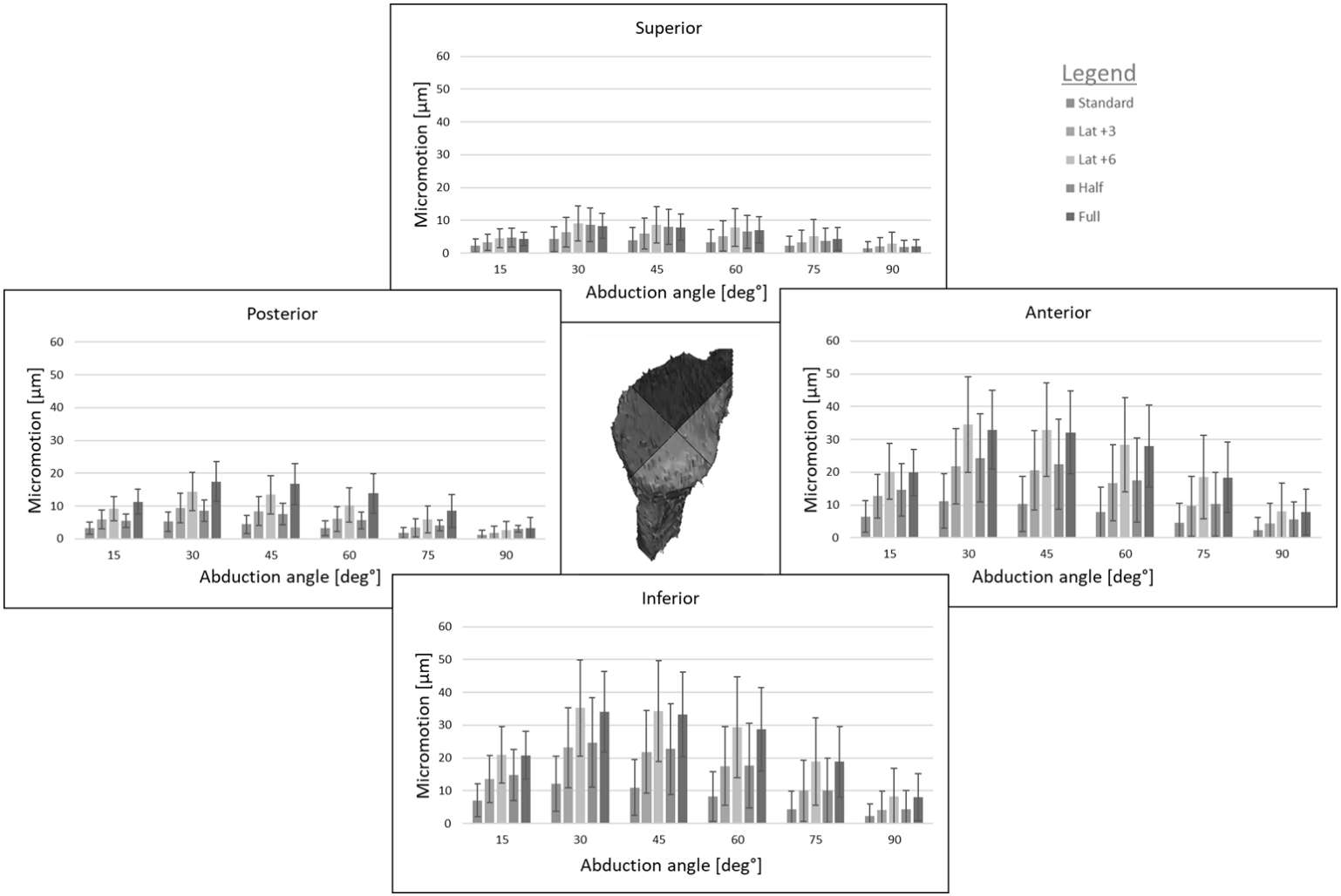

Figure 4-4 – Maximum normal micromotion [µm] for various abduction angles [deg°], for each quadrant of the glenoid (Micromotion shown as mean±SD)

other trends, many significant findings were rendered insignificant at 75° and 90° of abduction.

4.3.2 Tangential Micromotion

4.3.2.1 Mean Tangential Micromotion

Mean tangential micromotion was found to be significantly less when using the standard baseplate (5.0±2.5μm), as opposed to the full-wedge (7.8±2.2μm, p=0.012), half-wedge (8.6±3.2μm, p=0.006), 3mm lateralized (6.8±3.1μm, p=0.003), and 6mm lateralized (8.6±3.6μm, p=0.003) baseplates (Figure 4-5). The 3mm lateralized baseplate also produced significantly less micromotion than the 6mm lateralized (p=0.002).

The mean tangential micromotion for the anterior, inferior, posterior, and superior quadrants was 8.2±3.8μm, 11.2±4.6μm, 6.4±1.9μm, and 3.6±1.3μm respectively. The inferior quadrant was found to have significantly more micromotion than the anterior (p=0.007), posterior (p=0.029), and superior (p=0.009). The anterior and posterior quadrants had significantly more micromotion than the superior quadrant (p=0.027 and p=0.003 respectively).

Micromotion peaked at 30° (9.2±3.3μm) of abduction and decreased in both directions, with 90° (4.9±2.3μm) abduction resulting in the lowest amount of micromotion. Difference in micromotion was significant between almost all angles of abduction (p=0.001 to p=0.029). It was not significant between 15° (5.8±1.9μm) and 60° (8.4±3.4μm), 75° (6.6±2.9μm), and 90° abduction, as well as between 30° and 45° (9.2±3.4μm) degrees of abduction. The largest mean tangential micromotion (17.7±6.9μm) occurred for the 6mm lateralized baseplate in the inferior quadrant at 45° of abduction.

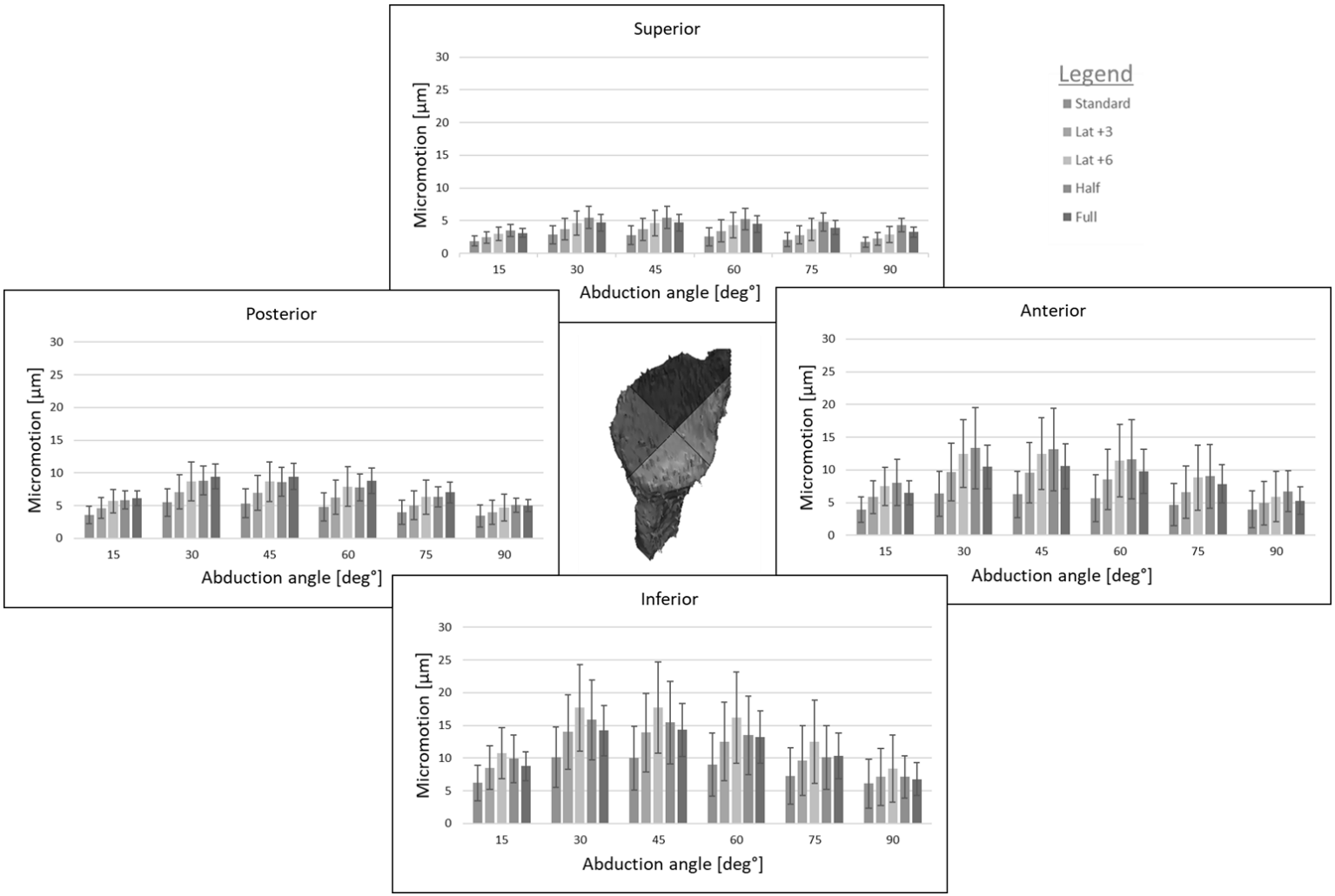

Figure 4-5 – Mean tangential micromotion [µm] for various abduction angles [deg°], for each quadrant of the glenoid (Micromotion shown as mean±SD

The standard baseplate resulted in the least micromotion overall compared to all other implants, with significance in all quadrants at most degrees of abduction ($p=0.001$ to $p=0.049$). The 6mm lateralized baseplate resulted in more micromotion than the 3mm lateralized and standard baseplates for all quadrants ($p<0.001$ to $p=0.023$) and levels of abduction. In the superior quadrant, the half-wedge baseplate demonstrated significantly more micromotion than the 3mm lateralized baseplate at low angles of abduction ($p<0.007$), and more micromotion than all baseplates at 90° abduction ($p<0.004$). Finally, the full-wedge baseplate was only significantly different than the standard baseplate as described above.

4.3.2.2 Maximum Tangential Micromotion

Maximum tangential micromotion was found to be significantly less when using the standard baseplate (7.4±3.9μm), as opposed to the half-wedge (11.6±4.9μm, $p=0.014$), 3mm lateralized (10.0±4.7μm, $p=0.003$), and 6mm lateralized (12.6±5.5μm, $p=0.003$) baseplates (Figure 4-6). The full-wedge (10.6±3.1μm), half-wedge, and 3mm lateralized baseplate also produced significantly less micromotion than the 6mm lateralized ($p=0.027$, $p=012$, $p=0.02$ respectively).

The maximum tangential micromotion for the anterior, inferior, posterior, and superior quadrants was 10.7±4.9μm, 12.5±5.2μm, 11.3±4.6μm, and 7.2±3.0μm respectively. The inferior quadrant was found to have significantly more micromotion than the anterior ($p=0.015$), posterior ($p=0.044$), and superior ($p=0.012$) quadrants, and the superior quadrant was found to have significantly less micromotion than all other quadrants ($p=0.012$ to $p=0.027$).

Micromotion peaked at 30° (13.1±5.0μm) of abduction and decreased in both directions, with 90° (7.1±3.6μm) abduction resulting in the lowest amount of micromotion. Difference in micromotion was significant between almost all angles of abduction ($p=0.001$ to $p=0.038$). However, it was not significant between 15° (8.0±2.9μm) and 60° (11.9±5.2μm), 75° (9.4±4.5μm), and 90° abduction, as well as between 30 and 45° (13.1±5.2μm) of abduction. The largest maximum tangential micromotion (19.3±7.4μm) occurred for the 6mm lateralized baseplate in the inferior quadrant at 45° of abduction.

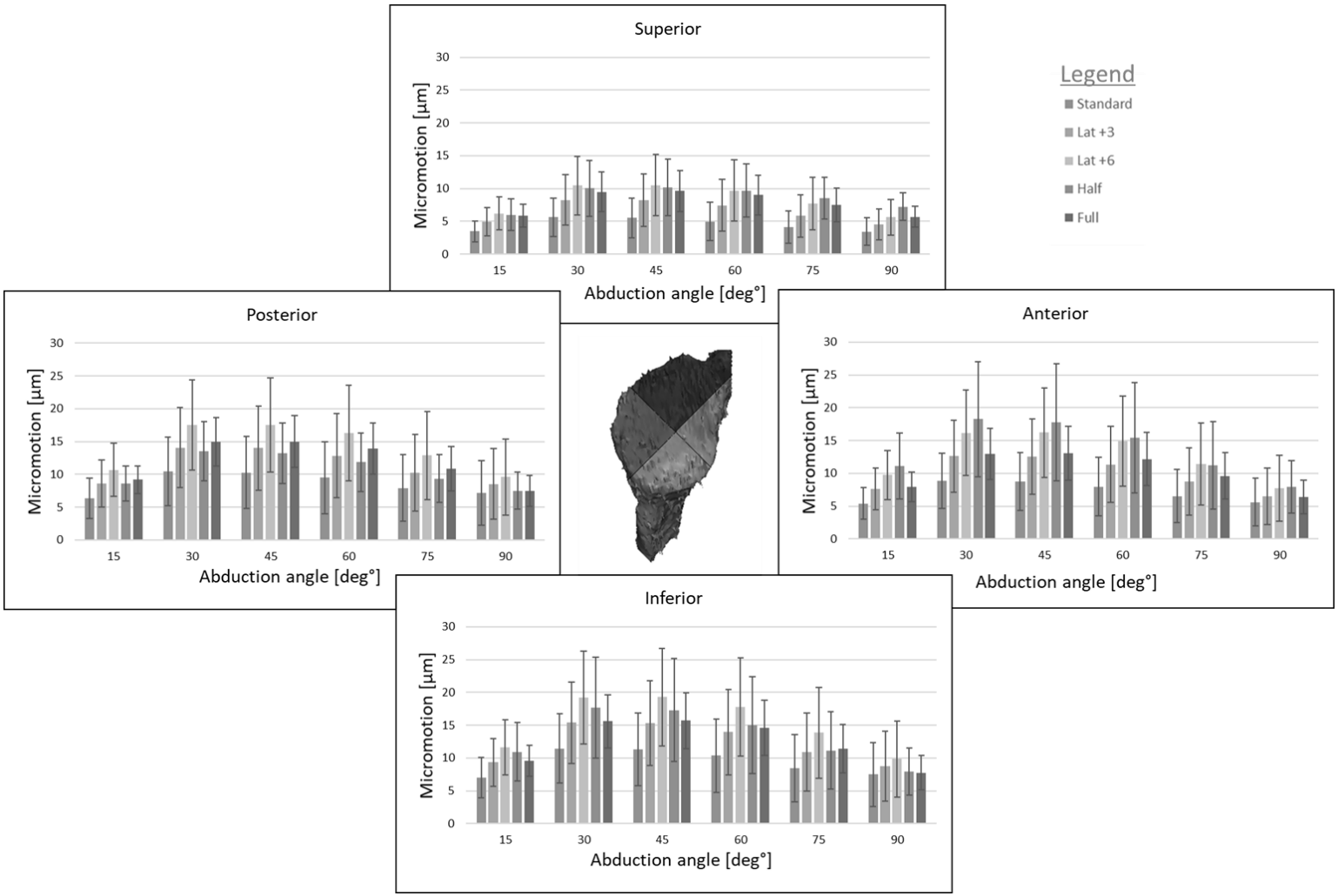

Figure 4-6 – Maximum tangential micromotion [µm] for various abduction angles [deg°], for each quadrant of the glenoid (Micromotion shown as mean±SD)

The standard baseplate resulted in the least micromotion overall compared to all other implants at low angles of abduction in the anterior and posterior quadrants. At higher angles of abduction, the standard baseplate only demonstrated significantly lower micromotion than the 3mm and 6mm lateralized baseplates, with significance in all quadrants ($p<0.001$ to $p=0.043$). The 6mm lateralized baseplate resulted in more micromotion than the 3mm lateralized and standard baseplates for all quadrants ($p=0.001$ to $p=0.026$) and levels of abduction. Other than the wedge baseplates being significantly different than the standard baseplate as mentioned above, the full-wedge and half-wedge baseplates did not result in significantly different amounts of micromotion than the other baseplates.

4.3.3 Effective Area of Load Transfer

The effective load transfer area (ELTA) was assessed by comparing the maximum possible baseplate backside contact area against the backside contact area under load for each angle of abduction. Angle of abduction and implant type were found to have significant main effects on ELTA ($p=0.033$ and $p=0.01$ respectively), but there was no significant interaction between any implants tested, nor between any angle of abduction.

However, the interaction between implant type and abduction angle also had a significant main effect on ELTA ($p=0.014$). At 15° and 30° abduction, the full-wedge baseplate had lower ELTA than the 6mm lateralized baseplate ($p<0.032$), and the half-wedge baseplate had lower ELTA than the 3mm lateralized baseplate ($p<0.046$). The half-wedge baseplate also had lower ELTA than the 6mm lateralized baseplate at abduction angles of 15° through 60° ($p<0.033$). Figure 4-7 shows the general trend of ELTA versus increasing abduction angle for each implant type.

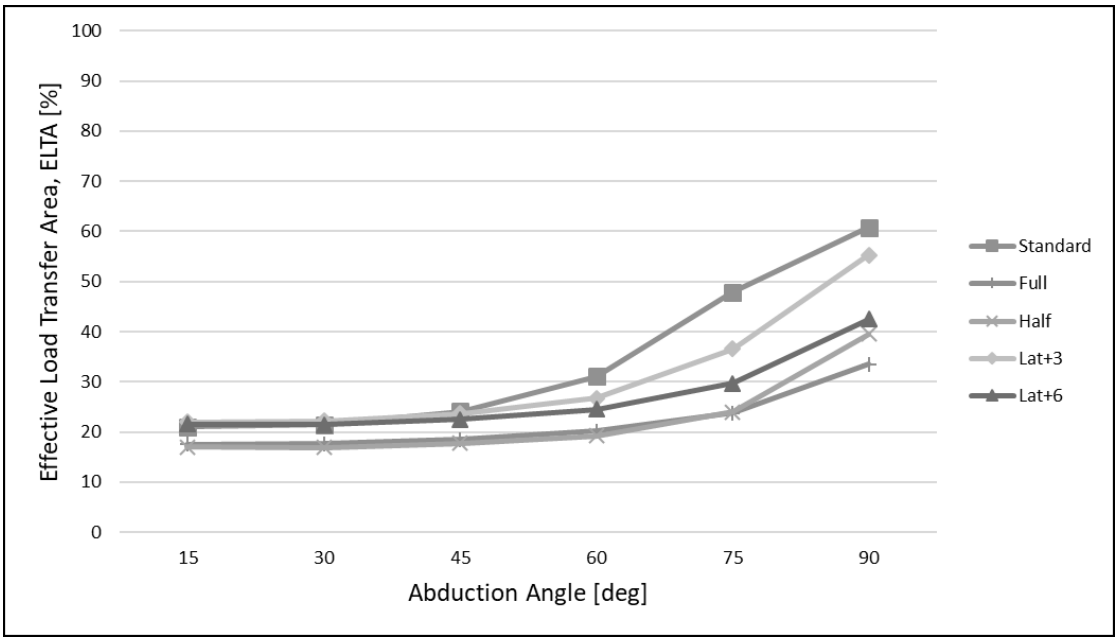

Figure 4-7 – Effective load transfer area, ELTA [%] for various abduction angles, for each of the 5 glenoid baseplates tested.

4.4 Discussion

In the previous chapter a baseline was established for implant performance by analyzing the micromotion and contact parameters of a standard baseplate in patients with E2-type glenoids. Micromotion has been identified as a key factor in implant fixation, therefore comparing implant types based on this parameter may allow us to predict which implants will perform better. Examining contact parameters is an important secondary objective that can provide insight into the mechanism behind each implants performance.

It was found that liftoff type micromotion peaks at about 30° of abduction and trails off significantly with higher and lower levels of abduction. For tangential micromotion, this trend stayed true. However, the micromotion at 45° of abduction was on par with the micromotion at 30°. For all types of micromotion, the inferior quadrant demonstrated the most amount of micromotion, while the superior quadrant demonstrated the least. It was also noted that most results became insignificant as abduction reached 75° and 90° of abduction. This is as expected since the loading vectors tend to produce a tilting of the

implant with compression towards the superior aspect (in the direction of load) and lift-off inferiorly.

In Chapter 2, we established that the superior and posterior quadrants contained the densest bone, as well as the highest volume of cortical bone. Regions of higher bone density can be shown to also contain increased bone stiffness,[1,15] therefore the bone in the superior and posterior quadrants can better resist the compressive loads caused by abduction of the arm. In turn, the reduction in motion is these quadrants lead to the result that there is more implant micromotion in the inferior and anterior quadrants. However, the mechanism of motion in the anterior and inferior quadrants is distraction in nature rather than compressive, and since our models excluded fasteners, such as bone screws, micromotion in the inferior and anterior quadrants is not being addressed to the same extent than it is in the superior and posterior quadrants. The only resistance against distraction motion is provided by the central peg, which prevents rotation of the implant in the direction of loading. In addition, we must consider these effects on tangential motion. An increase in compressive force in the superior and posterior quadrants will lead to higher forces of friction, reducing translational motion of the baseplate, and in the inferior and anterior quadrants, the opposite occurs.

Geometry of the baseplate also influences baseplate motion tangential to the reamed surface. The lowest amounts of micromotion were found in the standard and 3mm lateralized baseplates, both of which provide a neutral inclination at the baseplate-bone interface. Because the loads and wedge-type baseplates are both inclined superiorly in the scapular plane, there are no purely compressive forces and as such a larger portion of the joint loads affect tangential baseplate micromotion. This is shown by the lower levels of ELTA found in the full- and half-wedge baseplates. While this generally did seem to have an effect on micromotion, as the full and half wedge baseplate had higher amounts of micromotion, the trend in the data was not so clear cut. For liftoff micromotion, the half wedge had significantly less motion than the full wedge baseplate, showing that baseplate inclination angle is not the sole factor for increased motion, and that perhaps the flat portion of the half wedge contributed to stability. However, the flat portion of the half wedge baseplate did not contribute to translational stability as mean tangential micromotion

showed that the half wedge baseplate moved significantly more than all other baseplates at higher, more compressive angles of abduction. Some studies[8,9] have also shown that superior inclination of standard baseplates results in negative outcomes, and, in principle, the only difference between a wedge-type baseplate and a superiorly inclined baseplate is the correction of inclination of the glenoid.

In our results, higher levels of tangential micromotion in wedge-type baseplates was predicted. However, it was not expected that by nearly all measures, the 6mm lateralized baseplate would perform the worst. It resulted in the highest recorded values for maximum normal micromotion, and mean and maximum tangential micromotion, and it consistently resulted in more micromotion than the 3mm lateralized baseplate in all quadrants, for all levels of abduction. Interestingly however, the ELTA for the 6mm lateralized baseplate was lower than for the half-wedge and full-wedge baseplates.

Lateralization understandably produces larger amounts of liftoff micromotion due to the moment caused by the shear loads, and other studies have found that increasing lateralization of the center of rotation increase the potential for poor outcomes such as high levels of micromotion and glenoid component loosening.[2,10,24,26] Others however claim that lateralization did not affect micromotion, and remained within the boundaries of acceptable levels of micromotion.[25]

With respect to the relevance of these magnitudes of micromotion, Pilliar et al.[20] established that implants that promote bone growth using special backside coatings should be limited to no more than 150μm of baseplate-bone micromotion. Any micromotion larger than this results in the formation of dense fibrous tissue. However, Pilliar et al.[20] and Jasty et al.[11,12] found that fibrous tissue formed under less than approximately 60μm of micromotion still results in good bone ingrowth. None of the baseplate designs studied resulted in more than 40μm of relative motion between the baseplate and bone, indicating potential for acceptable bone ingrowth.

As with all studies, this one has its limitations. The loading protocol for this study varied from what is normally used in studies examining baseplate-bone interface micromotion. Typically, a 750N compressive load is applied to the baseplate followed by 750N of cyclic

shear loading. This results in much higher resultant loads than what was used in our study and is likely why the amount of micromotion found in our study was lower than what is found in the literature, and lower the 150μm threshold required for bony ingrowth. These low levels of micromotion may also be responsible for the lack of significance in some of our data. Significant results were almost never found at 75° and 90° of abduction, likely due to the decrease in shear forces with increasing abduction. This study also did not take into account variations in baseplate sizes and between patients. Baseplate size was chosen simply based on patient fit and was not considered a factor in our analysis. When looking at ELTA, some baseplates did not receive full coverage on the glenoid as a result of a reduced footprint due to reaming. This is not believed to have caused any issues since the portions of the baseplate with no glenoid coverage were not near the areas of load transfer, but we cannot be certain that it had no effect.

In this study, patient CT data was used to create accurate anatomical models with heterogeneous material properties. This strength is a rarity in that any FEA and experimental studies that have examined baseplate fixation in E-type glenoid have relied on bone foams with homogenous material properties. Our patient data provides the potential for follow-up on patient outcomes and comparison to results found in this study. Quasi-physiologic loading was used for this study, rather than the loads used in standard testing protocol for glenoid component loosening. The baseplate models used are very reflective of what is currently commercially available, which once again will allow for comparison with real patient follow ups. Testing on seven patient derived models allowed for the use of repeated-measures statistics to provide statistical conclusions, and is generally much higher than the typical number of specimens used in finite element studies, which is often as low as one.

It was established that baseplates with low levels of lateralization and flat backside geometries resulted in the best outcomes with regards to micromotion. However, these types of implants are not always feasible due to the required amount of bone removal, and medialization of the joint. Future directions would be to study acceptable levels of bone removal for patients with E-type glenoid erosion and required amounts of bone removal for these implants. The effect of these implants on joint mobility and other functional

patient outcomes, as well as the capability of bone-grafting as an alternative, specifically for E-type glenoids, should also be contemplated.

4.5 References

1. Anglin C, Tolhurst P, Wyss UP, Pichora DR. Glenoid cancellous bone strength and modulus. J. Biomech. 1999 Oct;32(10):1091–1097. doi:10.1016/S0021-9290(99)00087-1

2. Elwell J, Choi J, Willing R. Quantifying the competing relationship between adduction range of motion and baseplate micromotion with lateralization of reverse total shoulder arthroplasty. J. Biomech. 2017 Feb 8;52(Supplement C):24–30. doi:10.1016/j.jbiomech.2016.11.053

3. Frankle MA, Teramoto A, Luo Z-P, Levy JC, Pupello D. Glenoid morphology in reverse shoulder arthroplasty: Classification and surgical implications. J. Shoulder Elbow Surg. 2009 Nov;18(6):874–885. doi:10.1016/j.jse.2009.02.013

4. Friedman R, Stroud N, Glattke K, Flurin P-H, Wright TW, Zuckerman JD, et al. The Impact of Posterior Wear on Reverse Shoulder Glenoid Fixation. Bull. Hosp. Jt. Dis. 2013. 2015 Dec;73 Suppl 1:S15-20.

5. Friedman RJ, Hawthorne KB, Genez BM. The use of computerized tomography in the measurement of glenoid version. J. Bone Jt. Surg. 1992 Aug 1;74(7):1032–1037.

6. Gilot GJ. Addressing glenoid erosion in reverse total shoulder arthroplasty. Bull. Hosp. Jt. Dis. 2013. 2013;71 Suppl 2:S51-53.

7. Grant JA, Bishop NE, Götzen N, Sprecher C, Honl M, Morlock MM. Artificial composite bone as a model of human trabecular bone: The implant–bone interface. J. Biomech. 2007 Jan;40(5):1158–1164. doi:10.1016/j.jbiomech.2006.04.007

8. Gutiérrez S, Greiwe RM, Frankle MA, Siegal S, Lee III WE. Biomechanical comparison of component position and hardware failure in the reverse shoulder prosthesis. J. Shoulder Elbow Surg. 2007 May;16(3, Supplement):S9–S12. doi:10.1016/j.jse.2005.11.008

9. Gutiérrez S, Walker M, Willis M, Pupello DR, Frankle MA. Effects of tilt and glenosphere eccentricity on baseplate/bone interface forces in a computational model, validated by a mechanical model, of reverse shoulder arthroplasty. J. Shoulder Elbow Surg. 2011 Jul;20(5):732–739. doi:10.1016/j.jse.2010.10.035

10. Harman M, Frankle M, Vasey M, Banks S. Initial glenoid component fixation in “reverse” total shoulder arthroplasty: A biomechanical evaluation. J. Shoulder Elbow Surg. 2005 Jan;14(1, Supplement):S162–S167. doi:10.1016/j.jse.2004.09.030

11. Jasty M, Bragdon C, Burke D, O’Connor D, Lowenstein J, Harris WH. In vivo skeletal responses to porous-surfaced implants subjected to small induced motions. J. Bone Joint Surg. Am. 1997 May;79(5):707–714.

12. Jasty M, Bragdon CR, Zalenski E, O'Connor D, Page A, Harris WH. Enhanced stability of uncemented canine femoral components by bone ingrowth into the porous coatings. J. Arthroplasty. 1997 Jan;12(1):106–113.

13. Jones RB. Addressing glenoid erosion in anatomic total shoulder arthroplasty. Bull. Hosp. Joint Dis. 2013;71.

14. Jones RB, Wright TW, Roche CP. Bone Grafting the Glenoid Versus Use of Augmented Glenoid Baseplates with Reverse Shoulder Arthroplasty. Bull. Hosp. Jt. Dis. 2013. 2015 Dec;73 Suppl 1:S129-135.

15. Kalouche I, Crépin J, Abdelmoumen S, Mitton D, Guillot G, Gagey O. Mechanical properties of glenoid cancellous bone. Clin. Biomech. 2010 May;25(4):292–298. doi:10.1016/j.clinbiomech.2009.12.009

16. Klein SM, Dunning P, Mulieri P, Pupello D, Downes K, Frankle MA. Effects of Acquired Glenoid Bone Defects on Surgical Technique and Clinical Outcomes in Reverse Shoulder Arthroplasty. J Bone Jt. Surg Am. 2010 May 1;92(5):1144–1154. doi:10.2106/JBJS.I.00778

17. Langohr GDG, Giles JW, Athwal GS, Johnson JA. The effect of glenosphere diameter in reverse shoulder arthroplasty on muscle force, joint load, and range of motion. J. Shoulder Elbow Surg. 2015 Jun;24(6):972–979. doi:10.1016/j.jse.2014.10.018

18. Matsen FA, Boileau P, Walch G, Gerber C, Bicknell RT. The Reverse Total Shoulder Arthroplasty. J Bone Jt. Surg Am. 2007 Mar 1;89(3):660–667.

19. Morgan EF, Bayraktar HH, Keaveny TM. Trabecular bone modulus–density relationships depend on anatomic site. J. Biomech. 2003 Jul 1;36(7):897–904. doi:10.1016/S0021-9290(03)00071-X

20. Pilliar RM, Lee JM, Maniatopoulos C. Observations on the effect of movement on bone ingrowth into porous-surfaced implants. Clin. Orthop. 1986 Jul;(208):108–113.

21. Roche CP, Stroud NJ, Martin BL, Steiler CA, Flurin P-H, Wright TW, et al. Achieving fixation in glenoids with superior wear using reverse shoulder arthroplasty. J. Shoulder Elbow Surg. 2013 Dec;22(12):1695–1701. doi:10.1016/j.jse.2013.03.008

22. Schett G, Gravallese E. Bone erosion in rheumatoid arthritis: mechanisms, diagnosis and treatment. Nat. Rev. Rheumatol. 2012 Nov;8(11):656–664. doi:10.1038/nrrheum.2012.153

23. Sirveaux F, Favard L, Oudet D, Huquet D, Walch G, Mole D. Grammont inverted total shoulder arthroplasty in the treatment of glenohumeral osteoarthritis with massive rupture of the cuff RESULTS OF A MULTICENTRE STUDY OF 80 SHOULDERS. J. Bone Joint Surg. Br. 2004;86(3):388–395.

24. Stroud N, DiPaola MJ, Flurin P-H, Roche CP. Reverse shoulder glenoid loosening: an evaluation of the initial fixation associated with six different reverse shoulder designs. Bull. Hosp. Jt. Dis. 2013. 2013;71 Suppl 2:S12-17.

25. Virani NA, Harman M, Li K, Levy J, Pupello DR, Frankle MA. In vitro and finite element analysis of glenoid bone/baseplate interaction in the reverse shoulder design. J. Shoulder Elbow Surg. 2008 May;17(3):509–521. doi:10.1016/j.jse.2007.11.003

26. Wagner E, Houdek MT, Griffith T, Elhassan BT, Sanchez-Sotelo J, Sperling JW, et al. Glenoid Bone-Grafting in Revision to a Reverse Total Shoulder Arthroplasty. J Bone Jt. Surg Am. 2015 Oct 21;97(20):1653–1660. doi:10.2106/JBJS.N.00732

27. Wright TW, Roche CP, Wright L, Flurin P-H, Crosby LA, Zuckerman JD. Reverse Shoulder Arthroplasty Augments for Glenoid Wear. Comparison of Posterior Augments to Superior Augments. Bull. Hosp. Jt. Dis. 2013. 2015 Dec;73 Suppl 1:S124-128.

Chapter 5

5 Discussion

OVERVIEW

The final chapter of this thesis will summarize the results and discussions of the previous chapters, while re-visiting the objectives and hypotheses set out in Chapter 1. Strengths and limitations of this work will be discussed and future work will be suggested. To conclude, the significance of this work will be presented.

(Some aspects of this Discussion have been covered in Chapters 2, 3, & 4, but are repeated here due to the "Integrated Article" format of this thesis.)

5.1 Summary and Conclusions

In this thesis, the relevant background information pertaining to shoulder arthroplasty and the effect of osseous erosion in the glenoid was covered. In particular, literature on the effects of rotator cuff tears and their effects on the glenohumeral joint was studied.

Tears in the rotator cuff lead to decreased stability in the glenohumeral joint and subluxation of the humeral head. This eventually leads to irregular joint articulation and can create erosion in the superior portion of the glenoid. A variety of approaches have been presented to address these issues. However, the impact that osseous foundation and implant design have on implant fixation has been sparse in the literature. Therefore, the goal of this thesis was to establish a knowledge base upon which proper implant designs can be created for patients suffering from superior glenoid erosions (specifically type E2 glenoids).

The first objective of this thesis was to examine the quality of bone in patients with E2 glenoids, and attempt to distinguish any variations in region or depth within the glenoid (Chapter 2). This was done by retrieving patient CT data and examining difference in cortical and cancellous bone density for the anterior, inferior, posterior, and superior regions of the glenoid. Differences in bone density with increasing depth were also examined. It was found that for cortical bone, the quadrants of the glenoid did not differ significantly in bone density, and cortical bone density was highest at the surface of the glenoid. Cortical bone density was also highest deeper than 6mm into the glenoid. For cancellous bone, the inferior quadrant contained significantly less bone density. This is likely caused by bone adaptation due reduced stresses in that region. The eroded region (superior, and sometimes posterior), demonstrated the densest cancellous bone, again likely due to bone adaptation. This region also contained the highest volume of cortical bone relative to cancellous bone. A comparison with the literature showed that these trends are often similar in normal glenoids, and the magnitudes of bone density found fell within the range of what is reported in the literature. These results indicate that perhaps the bone properties of the E2 glenoid do not differ markedly from regular glenoids. However, the morphology is certainly different. While our hypotheses were supported overall, we found that bone density deep into the eroded part of the glenoid did not differ greatly from bone at the same depth in other regions.

The second objective of this project served as a stepping stone in determining the effects of RTSA baseplate design on implant fixation in patients with E2-type glenoids. For the Chapter 3, we established a baseline for performance of a standard RTSA baseplate in E2 glenoids. Using a loading protocol developed *in-vitro* to simulate abduction of the arm, standard RTSA baseplates were virtually implanted into E2 glenoids and tested for fixation and load transfer parameters. It was found that liftoff of the baseplate from the glenoid surface was larger in magnitude than tangential micromotion. Liftoff micromotion likely had a significant impact on tangential micromotion. With increased liftoff, there is a decrease in contact, and therefore friction resisting tangential motion. This resulted in higher overall relative motion between the bone and baseplate. The largest amounts of micromotion were found in the inferior quadrant of the glenoid, and the least in the superior quadrant. The inferior quadrant is at risk of liftoff due to the direction of the load vector, and therefore it follows that the inferior quadrant is more likely to result in tangential micromotion. In addition, Chapter 2 established that the superior quadrant contained the densest bone, so even in the event that the entire baseplate was under pure compressive or tensile stress the lack of density in the inferior quadrant would likely always cause higher levels of micromotion in this region. Micromotion peaked at 30° of simulated abduction. Factors likely contributing to the peak in micromotion were the load transfer contact area and the direction and magnitudes of the joint load vector. Larger loads, non-compressive loads, and lower levels of contact area, which increased with increasing abduction, seemed to have a combined effect on the magnitudes of micromotion. Overall levels of micromotion found did not exceed what is considered permissible for bony ingrowth into the implant.

With this baseline performance established, the third and final objective was to examine the effect of any geometric differences in baseplate design (Chapter 4). The baseplates examined were a full-wedge, half-wedge, 3mm lateralized, 6mm lateralized, and a standard baseplate. The wedge-shaped baseplates are likely to be used to avoid excess removal of bone, whereas lateralized baseplates may be used in cases where joint lateralization is required, bone grafts are performed, or there is ample bone volume. Each baseplate was subjected to the same protocol as in Chapter 3 and were compared to each other, as well as

the standard baseplate. It was found that the standard baseplate performed the best (resulted in the least amount of micromotion), followed by the 3mm lateralized baseplate. The full-wedge and half-wedge baseplates both performed similarly. However, the half-wedge baseplate resulted in less liftoff micromotion, likely because the aggressive slope of the half-wedge baseplate allowed for distribution of the compressive load to the flat portion of the baseplate. The 6mm lateralized baseplate resulted in the worst performance. Although the neutral baseplate inclination generally resulted in good micromotion outcomes, the level of lateralization likely resulted in excessive moments at the baseplate-bone interface, and therefore higher overall micromotion. It was found that the wedge-type baseplates resulted in the lowest amounts of load transfer area, indicating that increasing conformity between the inclination angle of the baseplate backside and the joint load vector negatively impacts load transfer mechanics. These results confirm the stated hypotheses that extreme lateralization or backside inclination result in poor baseplate fixation mechanics.

5.2 Limitations and Strengths

As with most studies, the studies presented in Chapters 2,3 and 4 have some limitations. In Chapter 2, we did not to account for the differences in sizes for each patient. While this likely would not have affected the bone density measurements made for each quadrant of the glenoid, it may have affected the measurements at each depth in the glenoid. We chose to measure up to 10mm into the glenoid, however each individual has a different sized glenoid and 10mm may account for a different percentage of an individual's glenoid. We also chose to report our data in Hounsfield units, rather than apparent density which appears more often in the literature due to the number of experimental studies. This is problematic because the conversion between Hounsfield units and apparent density can vary depending on the settings of the CT scanner at the time of use. Limitations in Chapter 3 were also related to the inability to generalize data with respect to other studies. Our simplified baseplate model, which did not model fixation screws or glenosphere attachment, is uncommon with what is found in the literature. We also used a unique *in-vitro* loading protocol which resulted in lower joint load magnitudes, and may have been the reason for our lower micromotion values. We also did not account for all proper surgical guidelines (*i.e.* we accounted for inferior placement of the baseplate to avoid scapular notching, but

did not account for excessive medialization of the baseplate causing reduced deltoid tensioning). The limitations from Chapter 3 also apply to Chapter 4. In addition, we did not account for variations in baseplate size as a factor influencing levels of micromotion. Finally, regarding the effective load transfer area, the data was normalized to the backside area of the baseplate used, and not to the available contact area between the baseplate and glenoid (some baseplates had slight overhang from the glenoid while others did not).

These studies also had strengths. Throughout this thesis, patient data was used rather than performing cadaveric studies, as is common in the literature. This provides a more accurate idea of what is occurring in these patients *in-vivo*. Since we used patient data, records of the treatments that these patients received can also be compared to proposed treatments and the theoretical results and suggestions made in these studies. In Chapter 2, although our depth measurements were not standardized to the size of each patient's glenoid, our region of measurement extended deeper than what is generally reported. The data was also found to fall within the range of reported bone densities. In Chapters 3 and 4, simplification of the baseplate models was performed. While excluding fixation screws and glenosphere attachment may not accurately depict an *in-vivo* scenario, comparisons can still be made between implant designs. However, it is important to note that micromotion trends may change with increased model complexity. The baseplate models still closely reflect commercially available implants, potentially allowing for the generalization of these results onto existing implants. Where FEA study design is concerned, anatomically correct scapulae are somewhat of a rarity in shoulder modeling, as is the use of multiple specimens. Our loading protocol did not allow us to generalize data, as mentioned in our limitations. However, it is believed that the *in-vitro* loads used in these studies much more accurately represent *in-vivo* loads of humeral abduction. Finally, this work is one of the first to examine any issues relating to superior glenoid erosion and E2-type glenoids.

5.3 Future Directions

The work herein is one of the first to examine the issue of superior glenoid erosion in shoulder arthroplasty, and therefore, potential directions for this work are numerous. To expand upon this work, replication studies can and should be performed, and the limitations discussed for each chapter should be addressed. An important area of study lies in implant

micromotion as a function of abduction. We did not establish a relationship between peak micromotion and load magnitudes, directions, and effective load transfer area. However, it is believed that there are important interactions at play. Examining augmented baseplate fixation using standard surgical guidelines, including screw fixation, is also important to determine whether our knowledge of regular RTSA can be applied to augmented RTSA. Experimental studies can be performed to validate the FEA studies, and short-term surgical outcomes of *in-vivo* use of augmented implants should be made available as soon as possible.

5.4 Significance

The use of RTSA is predicted to become more common as the total percentage of the population aged >65years increases. With this increase, there will inevitably be an increase in variety of osseous morphologies and surgical complexities, and learning to address these issues before they arise may save in health costs and procedure times, and increase the functional life of implants, as well as provide greater patient relief and satisfaction. In addition, the frequency of literature on superior glenoid erosion is alarmingly low considering that implants are commercially available. This body of work will prompt an increase in research for implant design as they relate to specific patient complications, as well as accelerate the improvement of augmented RTSA baseplates for E2-type glenoid erosions.

Appendix A Scapular Meshing and Mesh Convergence

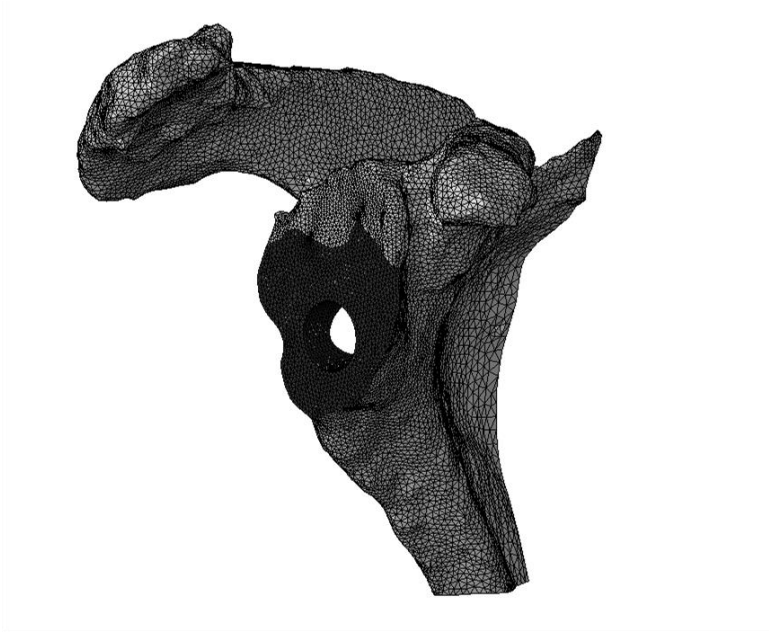

Figure A-1 – Reamed glenoid surface (dark)/location of smallest mesh elements (0.75mm)

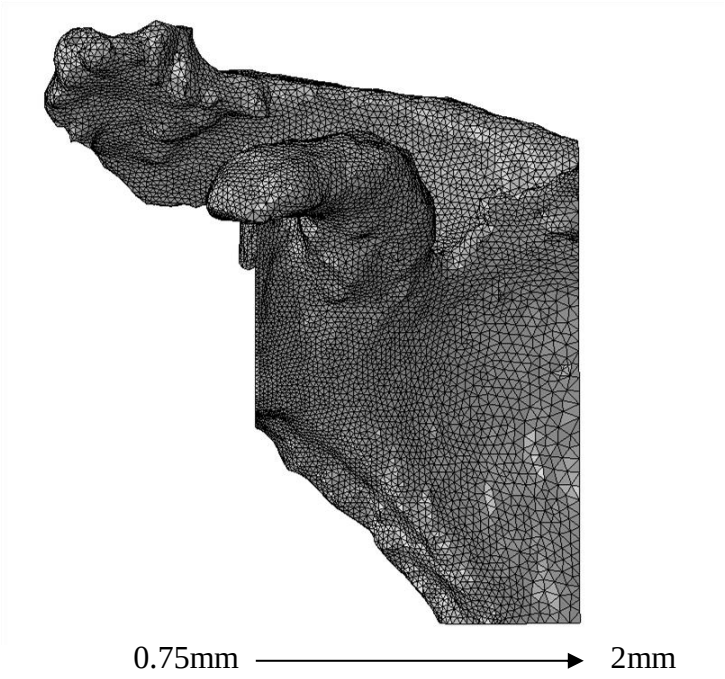

Figure A-2 – Mesh element size increasing from 0.75mm (left) to 2mm (right)

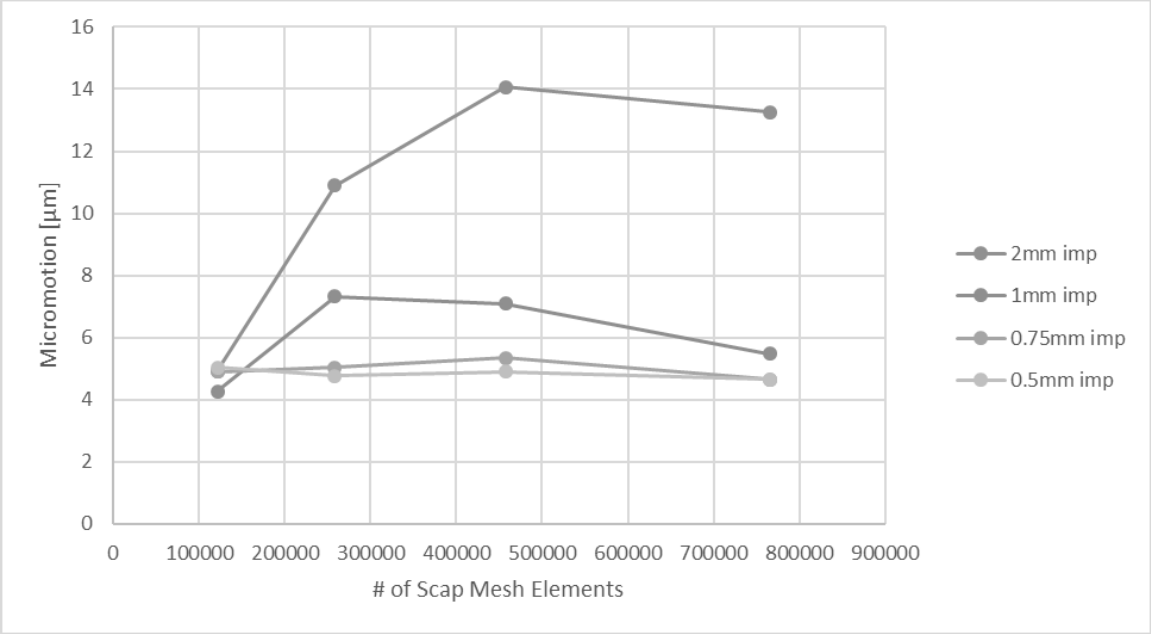

Figure A-3 - Graph of micromotion as a function of the number of scapular mesh elements

Implants with 0.75mm and 0.5mm mesh elements sizes both resulted in stable micromotion outcomes.

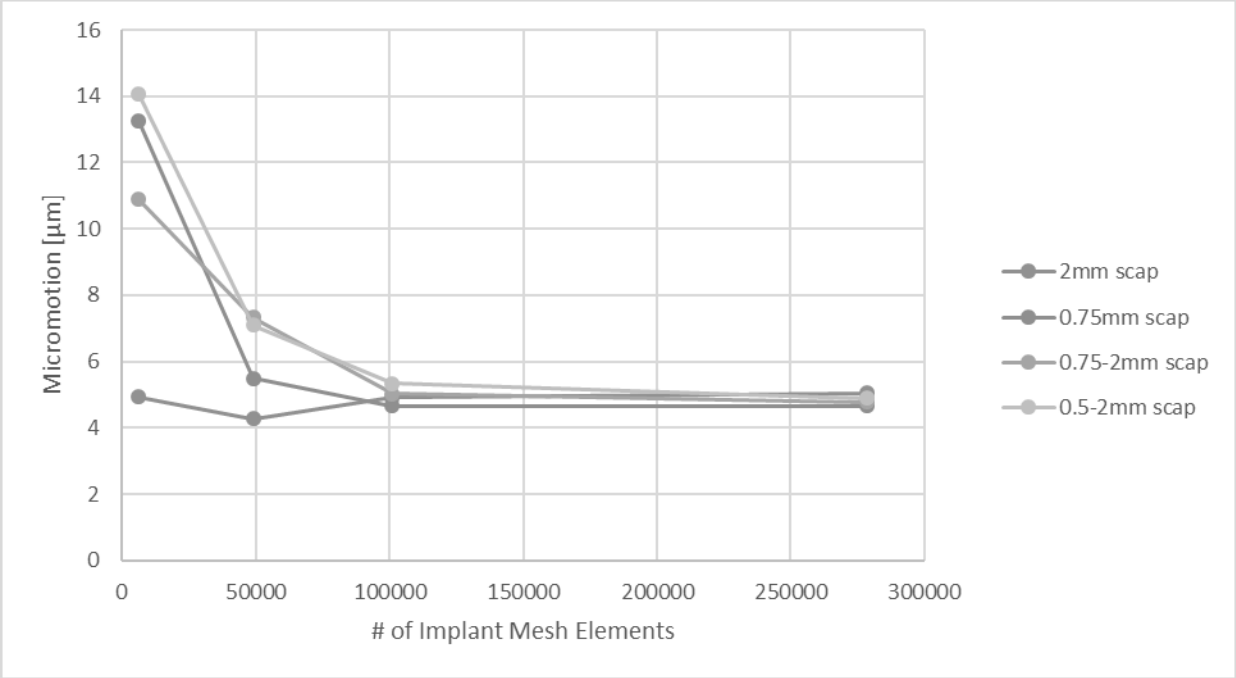

Figure A-4 – Graph of micromotion as a function of the number of implant mesh elements

All scapular mesh type resulted in convergence of micromotion for higher implant mesh densities. The last two data points on this graph correspond with the 0.75mm and 0.5mm implant mesh sizes respectively.

Table A-1 – Computational run time and differences from expected values for each implant/scapula mesh combination

Mesh size (implant/scapula) [mm]	%Difference from average	%Difference from median	Computational Run Time [s]
0.75/2	0.2	0.1	208
0.75/0.75s-2	2.4	2.7	365
0.5/0.75s-2	2.8	2.5	800
0.5/0.5	0.4	0.1	1151

Appendix B Example of Load Transfer Area Plot

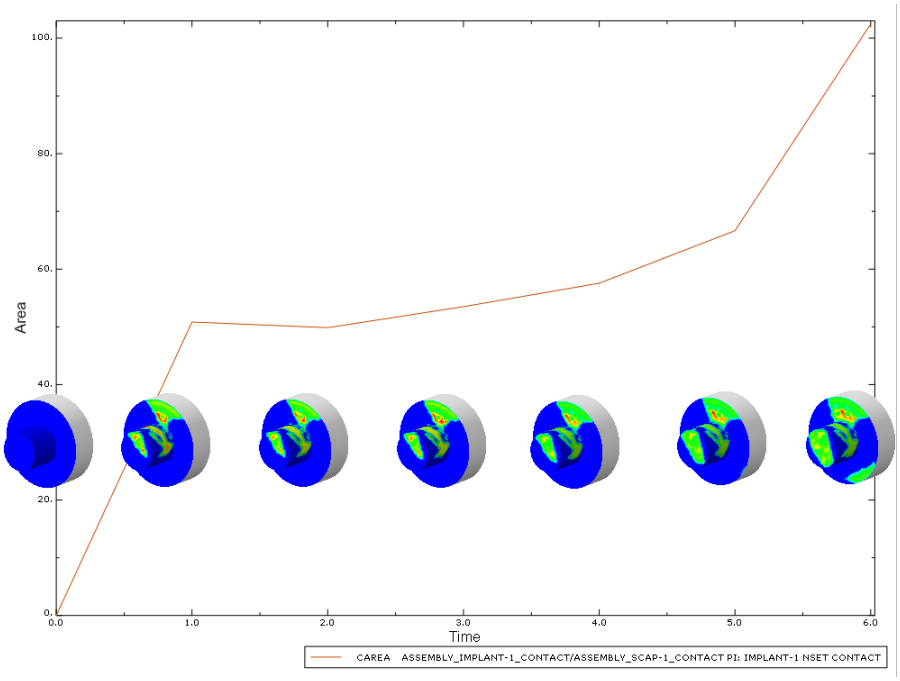

Figure B-1 – Load transfer area of the baseplate backside with area vs. abduction angle graph

Curriculum Vitae

Name: Matthew Mahaffy

Education

The University of Western Ontario
1151 Richmond St, London, ON N6A 3K7 **Expected 2017**
Master's Degree in Engineering Science (MESc) – Biomedical Engineering, Specialization in Biomechanics

The University of Western Ontario
1151 Richmond St, London, ON N6A 3K7 **Sept 2011-2015**
Bachelor's Degree in Engineering Science (BESc) – Mechanical and Materials Engineering

Recognitions and Award

Dean's Honour List
The University of Western Ontario
1151 Richmond St, London, ON N6A 3K7 **2013-2014 and 2014-2015**
Maintain an 80% average or greater

Western Graduate Research Scholarship
The University of Western Ontario
1151 Richmond St, London, ON N6A 3K7 **Sept 2015-Aug 2017**
$14,532/year + tuition

Research Experience

Graduate Research Assistantship
The University of Western Ontario
1151 Richmond St, London, ON N6A 3K7 **Sept 2015-Present**
Supervisor: Dr. James Johnson

Summer Research Assistant
The University of Western Ontario
1151 Richmond St, London, ON N6A 3K7 **June 2015-Aug 2015**
Supervisor: Dr. James Johnson

Thesis

Title: A Biomechanical Assessment of Bone Models Used for Upper Limb Prostheses Testing
Supervisor: Dr. James Johnson

Publications

Chan K, Langohr GDG, **Mahaffy M**, Johnson JA, Athwal GS (June 2017)
Does Humeral Component Lateralization in Reverse Shoulder Arthroplasty Affect Rotator Cuff Torque? Evaluation in a Cadaver Model. Clincal Orthopaedics and Related Research (CORR)

Teaching Experience

Graduate Teaching Assistant
The University of Western Ontario
1151 Richmond St, London, ON N6A 3K7 **Sept-Apr 2015/17**

Volunteering

Lab Assistant
The University of Western Ontario
1151 Richmond St, London, ON N6A 3K7 **Jan-Apr 2014**